PNNL-27846
RPT-DVZ-CHPRC 0005, Rev 0

Pacific Northwest
NATIONAL LABORATORY

Physical and Hydraulic Properties of Sediments from the 200-DV-1 Operable Unit

September 2018

ML Rockhold
FA Spane
TW Wietsma
DR Newcomer
RE Clayton
I Demirkanli
DL Saunders
MJ Truex
MM Valenta-Snyder
CJ Thompson

U.S. DEPARTMENT OF ENERGY

Prepared for the U.S. Department of Energy
under Contract DE-AC05-76RL01830

PACIFIC NORTHWEST NATIONAL LABORATORY
operated by
BATTELLE
for the
UNITED STATES DEPARTMENT OF ENERGY
under Contract DE-AC05-76RL01830

Printed in the United States of America

Available to DOE and DOE contractors from the
Office of Scientific and Technical Information,
P.O. Box 62, Oak Ridge, TN 37831-0062;
ph: (865) 576-8401
fax: (865) 576-5728
email: reports@adonis.osti.gov

Available to the public from the National Technical Information Service
5301 Shawnee Rd., Alexandria, VA 22312
ph: (800) 553-NTIS (6847)
email: orders@ntis.gov <http://www.ntis.gov/about/form.aspx>
Online ordering: http://www.ntis.gov

This document was printed on recycled paper.
(8/2010)

PNNL-27846
RPT-DVZ-CHPRC-0005 Rev 0

Physical and Hydraulic Properties of Sediments from the 200-DV-1 Operable Unit

September 2018

ML Rockhold
FA Spane
TW Wietsma
DR Newcomer
RE Clayton
I Demirkanli
DL Saunders
MJ Truex
MM Valenta-Snyder
CJ Thompson

Prepared for
the U.S. Department of Energy
under Contract DE-AC05-76RL01830

Pacific Northwest National Laboratory
Richland, Washington 99352

Executive Summary

This report summarizes physical and hydraulic property measurements of sediments from selected waste sites in the B-, S- and T-Complexes of the 200-DV-1 OU. Combined with related characterization studies published by the Deep Vadose Zone Applied Field Research Initiative, this work supports a remedial investigation and feasibility study for the 200-DV-1 OU. The results of this study also support the updating of conceptual site models for these and other waste sites on the Hanford Central Plateau.

The characterization efforts described herein, together with results presented in other 200-DV-1 OU attenuation and transport process characterization reports, provide data and associated interpretation to support the following three objectives, which are elements of the framework identified in U.S. Environmental Protection Agency guidance for evaluating monitored natural attenuation of inorganic contaminants:

- Define the contaminant distribution and the hydrologic and biogeochemical setting
- Identify attenuation processes and describe the associated attenuation mechanisms
- Quantify attenuation and transport parameters for use in evaluating remedies

Importantly, the information provided in this report is needed to define parameters for evaluating contaminant transport through the vadose zone and to the groundwater, to be conducted in support of a coupled analysis of groundwater and vadose zone contamination.

The specific 200-DV-1 OU waste sites from which samples were collected were selected through a data quality objective process to evaluate attenuation and transport processes for the known mobile uranium, technetium-99 (Tc-99), iodine-129 (I-129), chromium, and nitrate contaminants. Sampling locations were selected through joint meetings between Pacific Northwest National Laboratory (PNNL) and CH2M Hill Plateau Remediation Company (CHPRC) per a characterization sampling and analysis plan (Attenuation SAP Addendum, DOE 2017). Core samples of Ringold Formation and Cold Creek Unit sediments from five boreholes (C9497, C9555, C9498, C9503, C9507, and C9513), including samples from the perched water zone in the B-Complex, were collected and analyzed.

Core samples were analyzed for physical properties, including bulk and particle densities and particle size distributions, and for hydraulic properties, including moisture retention characteristics and saturated hydraulic conductivity. Hydraulic properties were obtained on intact sediment cores using the multistep outflow method. Parameters representing the van Genuchten and Brooks-Corey water retention models were fit to the experimental data. In addition, operational data from the B-Complex perched water removal action in the 200-DV-1 OU were analyzed to quantify the in situ hydraulic properties of the perched water zone.

For the core samples that were characterized, samples from the Ringold Formation, Rwie unit, and the CCU gravel (CCUg) had larger bulk densities, smaller porosities, and larger hydraulic conductivities relative to the Ringold Formation Taylor Flats unit, Rtf, and the CCU silts (CCUz). Laboratory-measured saturated hydraulic conductivity values for these samples vary by three orders-of-magnitude, ranging from high values of 4.48e-03 and 2.5e-03 cm/s for samples of the Rwie and CCUg units, respectively, to low values of 3.03e-06 and 3.36e-6 cm/s for samples of the CCUz unit. The lowest hydraulic conductivity values measured were on two CCUz samples of the “perching silt” unit that creates a flux-limiting layer underlying the B-Complex.

Hydraulic and storage properties were also characterized for a sandy subunit of the CCU silts that lies above the CCUg and forms a perched water aquifer above the CCUz perching silt in the B-Complex. Pump test results provide information on storage capacity, saturated hydraulic conductivity and anisotropy. The hydraulic boundary assessment described herein is qualitative in nature, but the analysis suggests that it will take ~1000 days before predicted well drawdown starts to deviate from the simulated no-boundary condition (i.e., infinite extent aquifer). This implies that it will take significantly long periods of time to meaningfully assess the current perched water aquifer dewatering activities given the existing operational scheme used for the current pumping system. As such, the extent of the boundary cannot fully be determined without incorporation of additional PWA extraction well centers and monitoring wells that could enhance the ability to detect a hydrologic boundary and accelerate PWA dewatering activities.

In summary, the physical and hydraulic property information provided in this report complements the information on attenuation and transport processes described in other characterization reports for the 200-DV-1 OU. This study provides both direct measurements and quantitative estimates of physical and hydraulic properties of vadose zone sediment cores to support parameterization of models for fate and transport assessment for vadose zone sites on the Hanford Central Plateau. The 200-DV-1 OU RI/FS effort, associated conceptual site model, and fate and transport models require the type of information contained in this report on subsurface hydraulic properties as a technical basis to describe the contaminant conditions and estimate future transport. Notably, the site-specific nature of the information contained in this report improves our understanding of controlling features and processes for transport of contaminants through the vadose zone to groundwater and enhances the technical defensibility of the assessment and its use to support remedy evaluation. In conjunction with transport analyses, the results from this study helps provide a technical basis for remedial investigation/feasibility study (RI/FS) efforts for the 200-DV-1 OU.

Acknowledgments

This work was funded by CH2M Hill Plateau Remediation Company (CHPRC) as part of the 200-DV-1 operable unit activities at the Hanford Site. Pacific Northwest National Laboratory (PNNL) is operated by Battelle Memorial Institute for the DOE under Contract DE-AC05-76RL01830.

We thank Mark Byrnes (CHPRC) for project oversight, Kathy Leonard, Sunil Mehta, Sarah Springer, and Virginia Rohay (all CHPRC), and Mart Oostrom (Intera) for independent technical reviews, and Mike Fayer (PNNL) for internal technical review. Finally, we thank Matt Wilburn (PNNL) for editorial review and text-processing assistance.

Acronyms and Abbreviations

bgs	below ground surface
BRF	barometric response function
CCU	Cold Creek Unit
CCUc	Cold Creek unit – carbonate
CCUg	Cold Creek unit – gravel-dominated
CCUz	Cold Creek unit – silt-dominated
CF	constant flux
CHPRC	CH2M Hill Plateau Remediation Company
CSM	conceptual site model
EMSL	Environmental Molecular Sciences Laboratory
EPA	U.S. Environmental Protection Agency
FH	falling head
FIO	For Information Only
FY	fiscal year
KGS	Kansas Geological Survey
OU	operable unit
PNNL	Pacific Northwest National Laboratory
PWA	perched-water aquifer
QA	quality assurance
Rwie	Ringold Formation member Wooded Island unit E
SAP	sampling and analysis plan
SSE	sum-of-squared error
STOMP	Subsurface Transport Over Multiple Phases
XMT	X-ray micro-tomography

Contents

Figures

Tables

1.0 Introduction

Contaminants disposed of at the land surface must migrate through the vadose zone before entering groundwater. Processes that occur in the vadose zone can attenuate contaminant concentrations during transport through the vadose zone. Thus, quantifying contaminant attenuation and contaminant transport processes in the vadose zone, and the resulting temporal profile of contaminant discharge to the underlying groundwater, is important for assessing the need for, and type of, remediation in the vadose zone and groundwater. This type of information will enhance the existing conceptual site models (CSMs) for the 200-DV-1 operable unit (OU) (Serne et al. 2010; CHPRC 2015a,b) in support of fate and transport analysis and remedy evaluation.

Contaminant transport through the vadose zone beneath aqueous waste disposal sites is affected by two types of attenuation processes: (1) attenuation caused by advective and dispersive mechanisms related to unsaturated water flow and (2) attenuation caused by biogeochemical reactions and/or physical/chemical interaction with sediments (e.g., phenomena such as sorption, solubility control, and decay/degradation that slow contaminant movement relative to water movement). Hydraulic property estimates are important inputs to assess attenuation caused by advection and dispersion.

A framework to characterize these attenuation and transport processes is provided by U.S. Environmental Protection Agency (EPA) guidance document *Use of Monitored Natural Attenuation for Inorganic Contaminants in Groundwater at Superfund Sites* (EPA 2015). Additional information about vadose zone attenuation processes reported by Truex and Carroll (2013) and Truex et al. (2015) is also relevant for characterization of the vadose zone. These documents point to approaches that can be applied to identify and describe transport parameters for a vadose zone site.

The 200-DV-1 OU project is in the process of characterizing the vadose zone to support a remedial investigation and feasibility study (DOE 2012, 2016a). Through a data quality objectives process (DOE 2017), specific 200-DV-1 OU waste sites were selected for evaluation of attenuation and transport processes for the known mobile uranium, technetium-99 (Tc-99), iodine-129 (I-129), chromium, and nitrate contaminants.

The 200-DV-1 OU includes variably-saturated vadose zone sediments that lie between the elevations of the ground surface and the regional water table in the Hanford Central Plateau. Intact core samples were collected from selected depth intervals in Cold Creek Unit (CCU) and Ringold Formation sediments during well drilling in the T-, S-, and B-complexes (Figure 1). Physical and hydraulic property data from these 200-DV-1 OU sediment samples were needed to improve the understanding of flow and transport behavior in the vadose zone and provide parameter estimates for subsurface flow and contaminant transport modeling.

Numerical models of subsurface flow and transport require parameters describing the physical, hydraulic, and transport properties of contaminants of concern for vadose zone sediments and underlying aquifer materials. Physical properties include bulk and particle densities, porosities, and grain size distributions. Hydraulic properties include pressure-saturation relations (a.k.a. water-retention characteristics) and hydraulic conductivity as a function of aqueous saturation or pressure head. This report describes results of physical and hydraulic property characterization for selected core samples from the 200-DV-1 OU, and perched-water aquifer test results from the B-Complex in the Hanford 200 East Area.

The hydraulic and physical sediment property information herein complements the information about attenuation and transport processes described in other characterization reports for the 200-DV-1 OU (Truex et al. 2017; Szecsody et al. 2017; Demirkanli et al. 2018). This characterization information will be used to refine CSMs by enhancing the understanding of controlling features and processes for transport of contaminants through the vadose zone to the groundwater. Collectively, the 200-DV-1 OU attenuation and transport process information supports the upcoming remedy evaluation in the 200-DV-1 OU feasibility study.

This report is organized as follows. Section 2.0 describes the methods used for drilling, core sampling, and physical and hydraulic property characterization in both the laboratory and field. Results of the physical and hydraulic property measurements are presented and discussed in Section 3.0. Conclusions are presented in Section 4.0. Quality assurance procedures are discussed in Section 5.0, followed a list of cited references in Section 6.0. Appendix A contains a table of quasi-static water retention data obtained from the multi-step outflow experiments on intact core samples. Appendix B provides a more detailed discussion of the perched-water aquifer testing that was performed in the B-Complex.

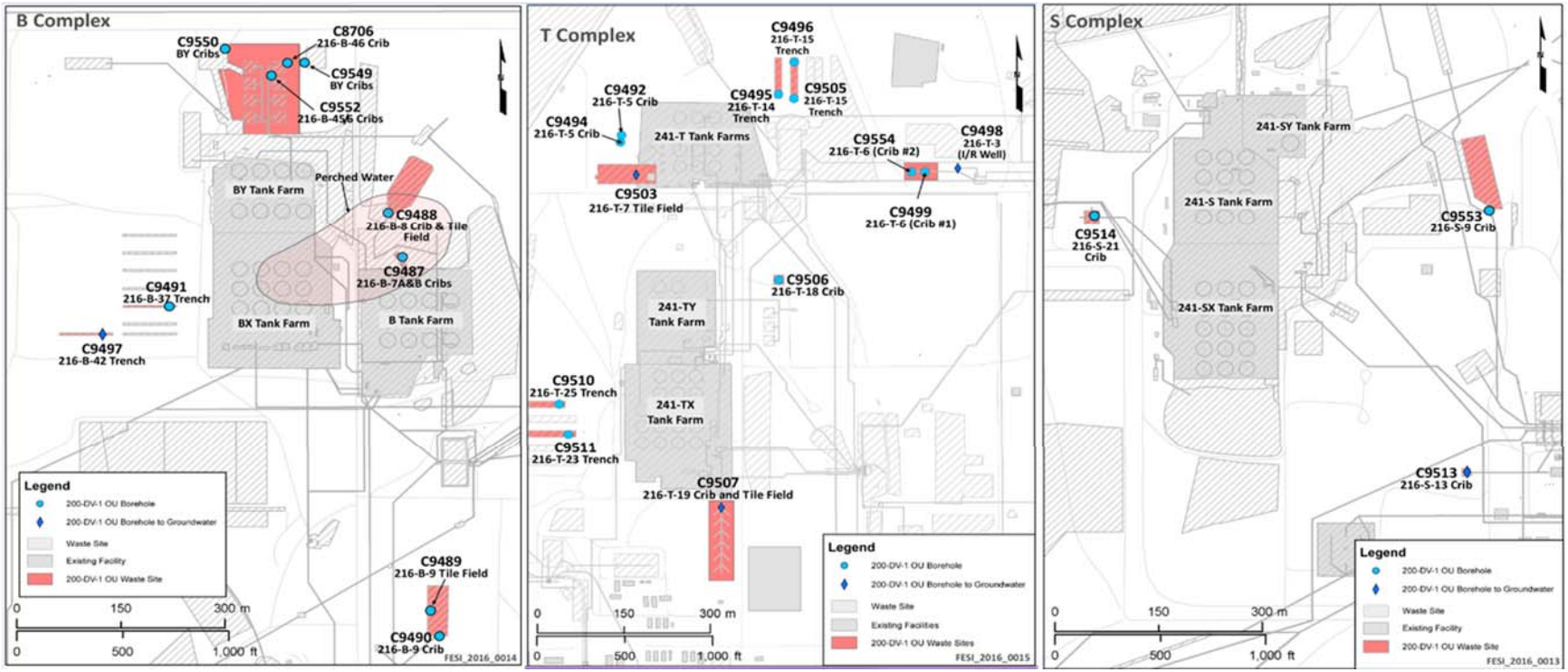

Figure 1. Location of 200-DV-1 OU waste sites in Central Plateau inner area (Source: DOE 2016b).

2.0 Materials and Methods

This section describes core sampling sites, steps involved in core sampling, selection and processing of specific cores used for physical and hydraulic property characterization in the laboratory, and methods that were used. Perched aquifer field testing sites and associated methods are also discussed.

2.1 Sampling and Test Sites

Samples for laboratory analyses were collected by CH2M Hill Plateau Remediation Company (CHPRC) as part of the drilling campaign for the 200-DV-1 OU remedial investigation. Sampling details are provided in Table 1. Multiple sets of samples were collected from each borehole for potential characterization. The handling procedures used upon sample delivery to the laboratory are described below. This section also describes the process of selecting specific samples for hydraulic property testing on the intact cores.

Table 1. Locations, geologic formations, and sampling information for 200-DV-1 OU characterization.

Complex	Waste Site	Borehole	Sample ID	Geologic Formation	Depth Interval [ft bgs]	Liner Length Used for Testing	Drill Date
B-Complex	216-B-8 Crib And Tile Field	C9488	B355M0	CCU Perched Zone	223.5-224.5	15 cm	FY 2016
		C9488	B355M1	CCU Perched Zone	224.5-225.5	15 cm	FY 2016
	216-B-42 Trench	C9497	B39M11	CCUg	248-249	30 cm	FY 2017
S-Complex	216-S-13 Crib	C9513	B39X68	Rtf	162.7-163.7	30 cm	FY 2017
			B39X53**	CCUc	153.7-154.7	30 cm	FY 2017
T-Complex	216-T-7 Tile Field	C9503	B39VY9	Rwie	155-156	24 cm	FY 2017
			B39VV7	CCUc	102-103	30 cm	FY 2017
	216-T-19 Crib & Tile Field	C9507	B35435	CCUz	95.1-96.1	10.6 cm	FY 2016
			B35463*	Rwie	142.6-147.7	23 cm	FY 2016

FY = fiscal year.

*Sample was split in half and both the upper and lower portions underwent hydraulic properties analysis separately.

**Liner was significantly damaged; measurement could not be completed.

In addition to core sampling for sediment characterization in the laboratory, this report also summarizes field characterization efforts for a perched-water aquifer (PWA) in the B-Complex of the Hanford 200

East Area. The results described later in this report were obtained from recently performed hydraulic tests (i.e., single-well slug tests and single/multi-well pumping tests) conducted at PWA extraction wells 299-E33-350 and 299-E33-351, and observation well 299-E33-344.

2.2 Drilling and Core Selection

Drilling at the field sites for 200-DV-1 sediment characterization was performed using a combination of Becker-hammer and resonant sonic drilling methods. The resonant sonic method was used during the first 15 ft of drilling, continuing with a Becker-hammer to penetrate the high-contamination zone, and returning to sonic drilling for sample collection. The resonant sonic method was chosen because of its speed and ability to reach depths greater than 200 ft. However, this method also generates a lot of heat. Thermal monitoring was used during drilling to identify cores with potential heat damage. The split-spoon sampler was lined with five 1-ft-long Lexan liner segments, placed end-to-end, to hold the sediment samples. After drilling through the target sampling horizon, the drill string was pulled to the surface, and the split spoon sampler was opened. The Lexan core liners were removed from the sampler, end caps were placed on the ends of the cores, and the endcaps were taped shut to prevent loss of sediment or moisture from the core samples. The cores were then labeled, cooled to ≤6 °C and transferred to the Pacific Northwest National Laboratory (PNNL) 331 Building for further analyses. At PNNL, cores were inspected for defects and heat damage and were stored at ≤6 °C until they were used for project needs. PNNL and CH2M Hill Plateau Remediation Company (CHPRC) jointly selected samples for testing based on core quality observed after completion of drilling and conditions outlined in the sampling and analysis plan (SAP). Photos taken of cores were presented at PNNL/CHPRC project team meetings and with SAP target geologic units in mind a subset of samples was identified for potential hydraulic property characterization.

2.2.1 X-Ray Micro-Tomography (XMT)

A subset of intact cores from particular hydrostratigraphic units of interest were selected and imaged using an XMT system. The imaging results were used to help guide selection of specific core samples that were used for physical and hydraulic property characterization in the laboratory. The XMT system that was used is housed in the Environmental Molecular Sciences Laboratory (EMSL) on PNNL's Richland, WA campus.

The nominal resolution of the XMT system is ~1/1000 of the largest sample dimension. Whole core imaging was performed for screening purposes to determine when cores contained excessive amounts of gravel and cobbles that could make measurements more difficult, as opposed to performing higher-resolution scans over smaller regions to quantify porosity and pore topology (Wildenschild and Sheppard 2013). The intact cores from 200-DV-1 OU were nominally ~300-mm long, so the resolution of the whole core XMT images was ~0.3 mm. This resolution was sufficient for non-destructive imaging of individual gravel and larger-sized particles, as well as defects and voids, within the intact core samples. Selected XMT images for core samples that were characterized are presented below.

Figure 2 shows a series of vertical and horizontal XMT image slices through a 300-mm-long and 88.9-mm- (3.5-in-) diameter core sample of unit CCUg (sample B39M11). The larger gravel and cobble particles are the lighter-colored regions in the images. Similar images for core samples from units Rwie (sample B39VY9), Rtf (sample B39X68), and CCUc (sample B39X53) are shown in Figure 3, Figure 4, and Figure 5, respectively. Samples B39X68 and B39X53 from the Rtf and CCUc units, respectively, both appear to be much more fine-grained and uniform, relative to samples B39M11 and B39VY9. Figure 6 shows XMT image slices for another core sample of the CCUc unit (sample B39VV7). Sample B39VV7 appears to have coarser texture than B39X53.

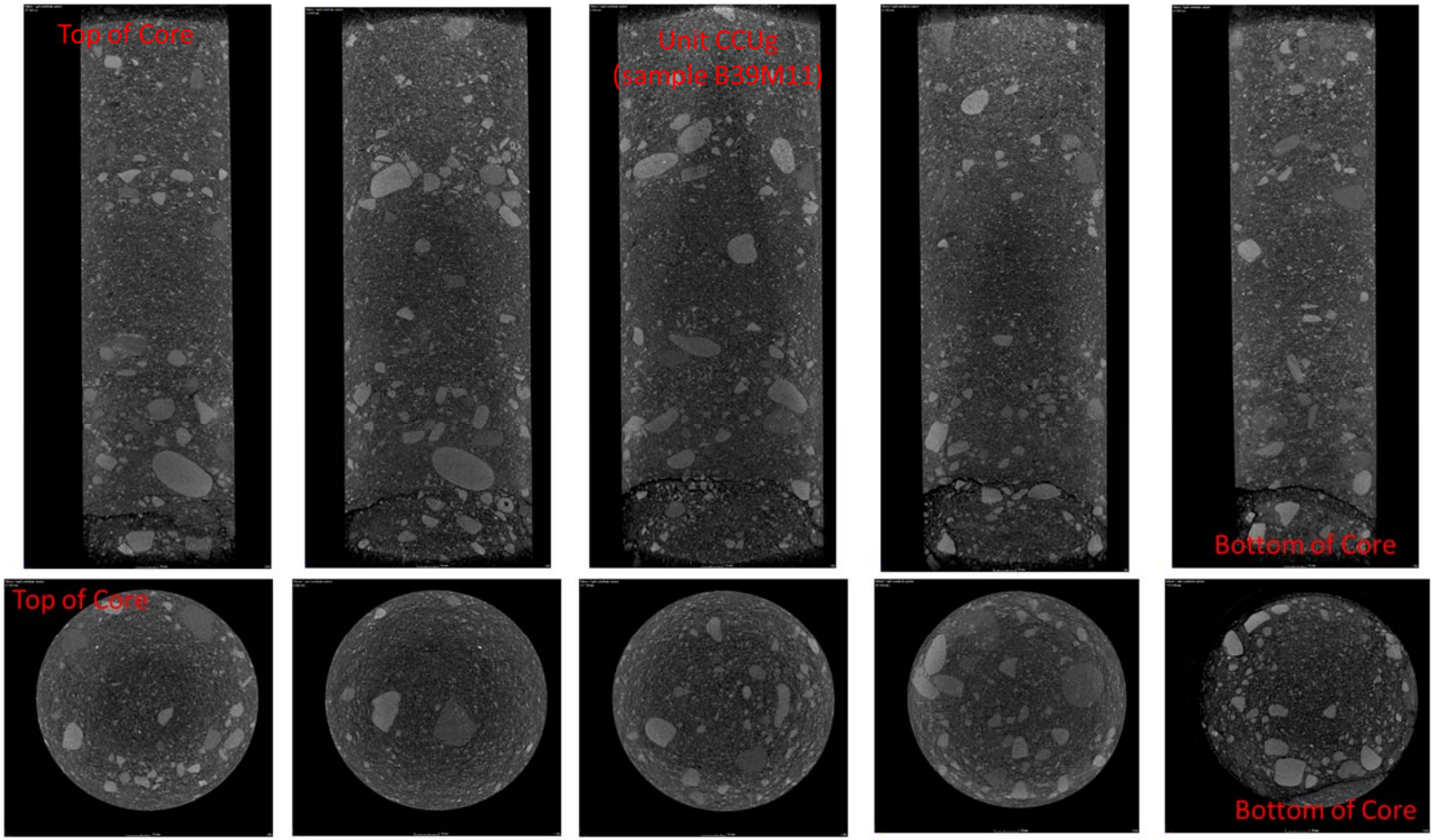

Figure 2. Vertical (top row) and horizontal (bottom row) XMT image slices through 300-mm-long and 88.9-mm-diameter core sample from unit CCUg (sample B39M11).

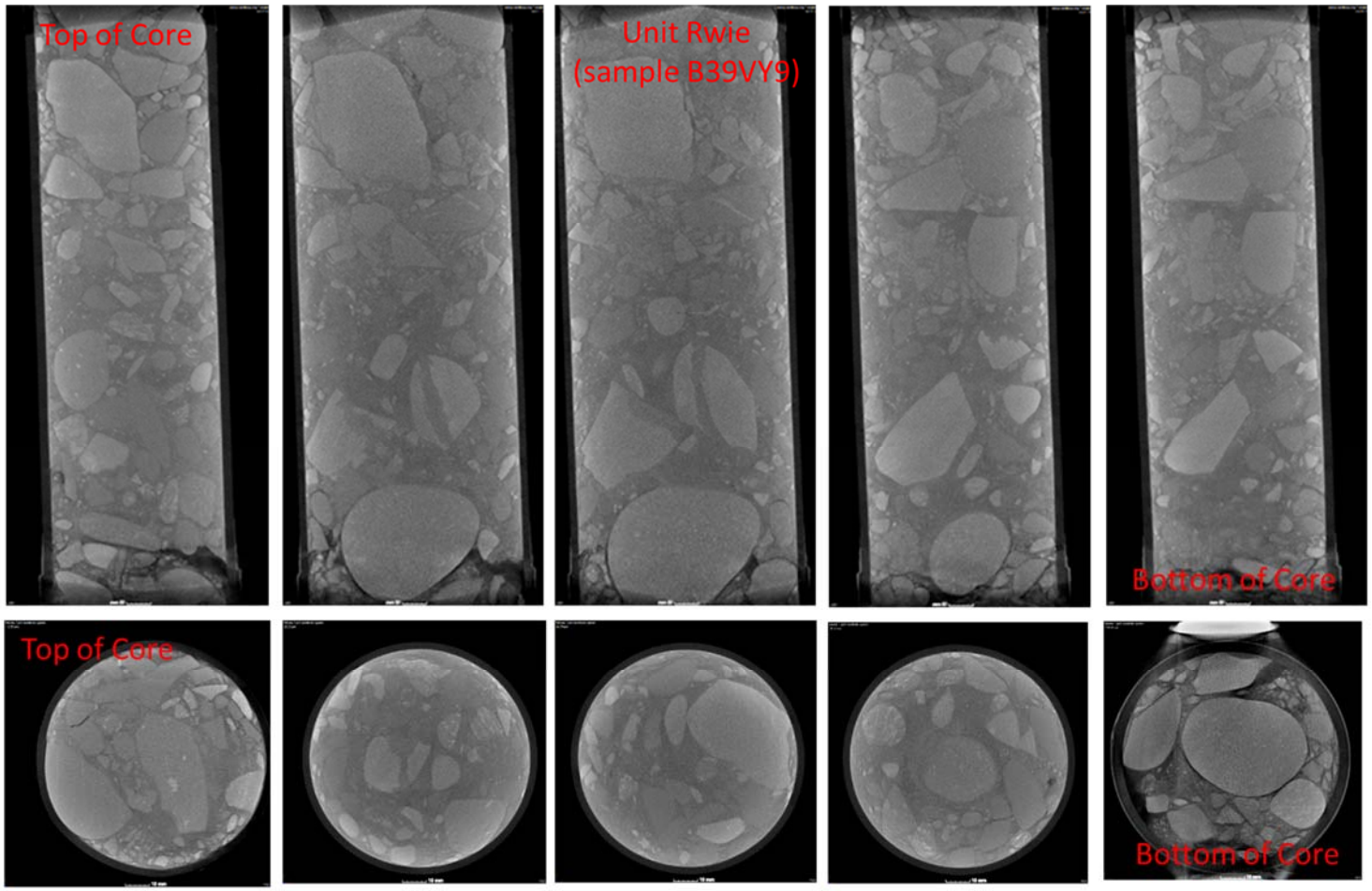

Figure 3. Vertical (top row) and horizontal (bottom row) XMT image slices through 300-mm-long and 88.9-mm-diameter core sample from unit Rwie (sample B39VY9).

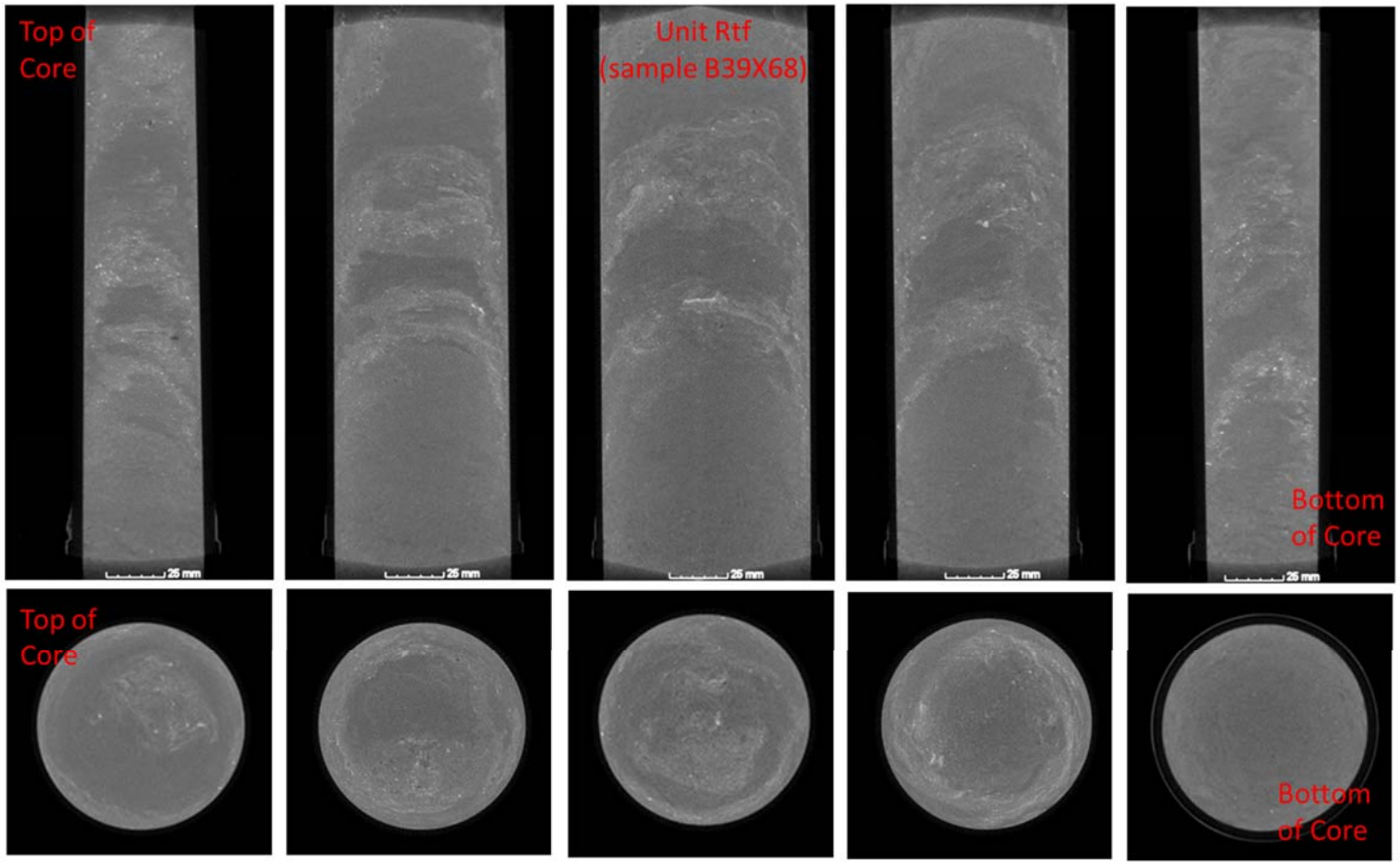

Figure 4. Vertical (top row) and horizontal (bottom row) XMT image slices through 300-mm-long and 88.9-mm-diameter core sample from unit Rtf (sample B39X68).

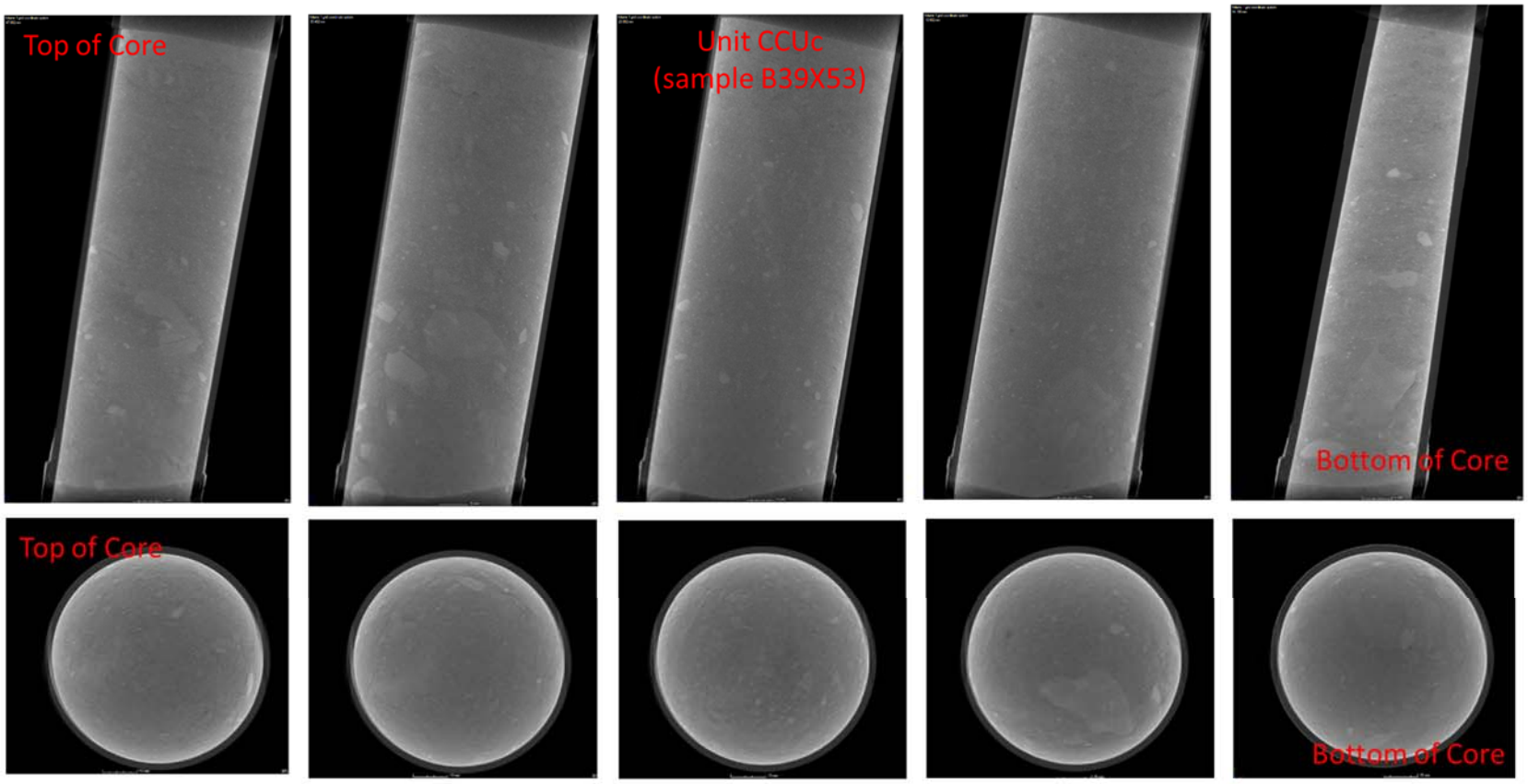

Figure 5. Vertical (top row) and horizontal (bottom row) XMT image slices through 300-mm-long and 88.9-mm-diameter core sample from unit CCUc (sample B39X53).

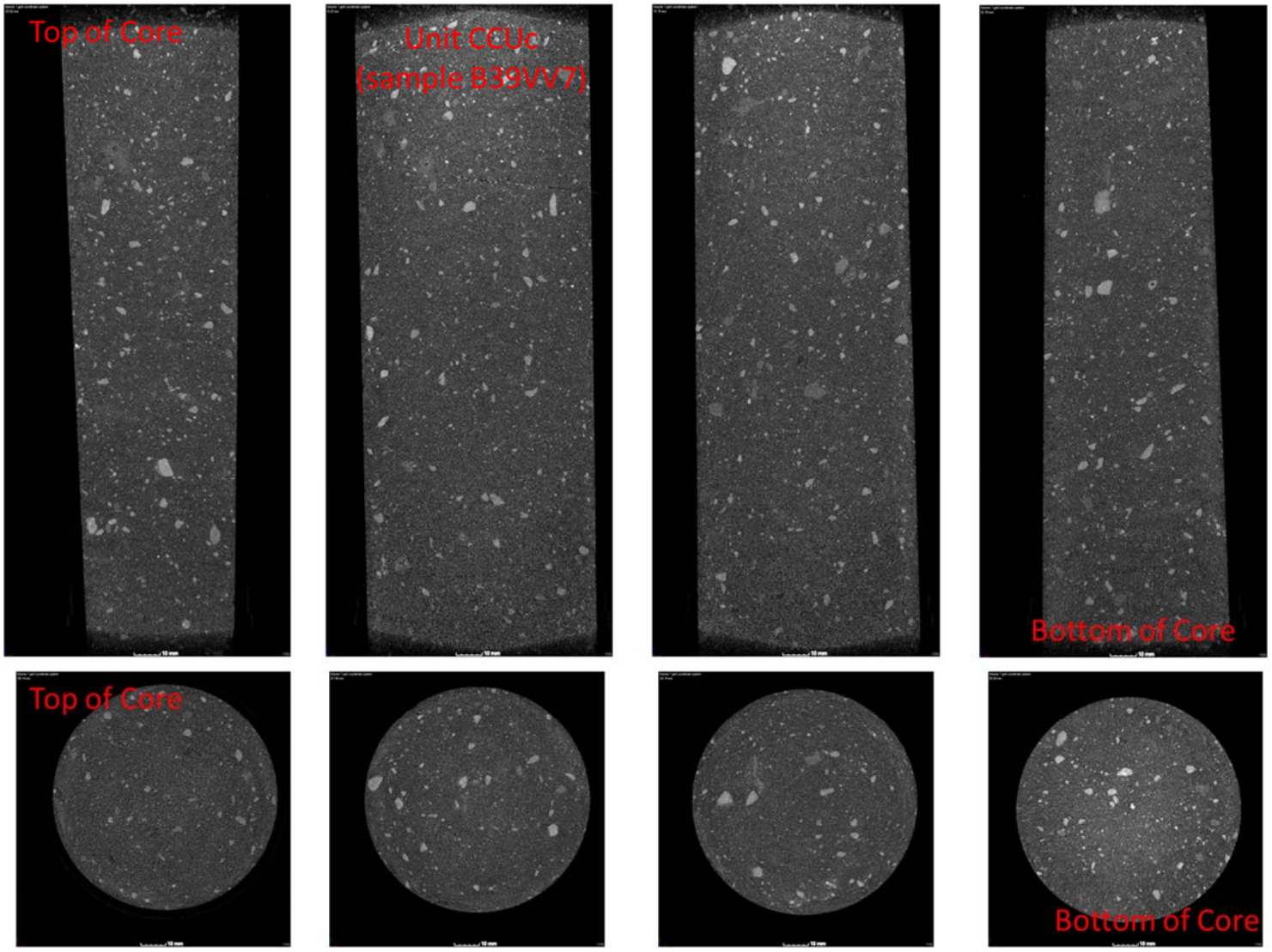

Figure 6. Vertical (top row) and horizontal (bottom row) XMT image slices through 300-mm-long and 88.9-mm-diameter core sample from unit CCUc (sample B39VV7).

Figure 7 shows vertical and horizontal XMT image slices through two halves of a 300-mm-long by 88.9-mm-diameter core sample of unit CCUz (sample B35435). Sample B35435 was cut into two nominally 150-mm-long lengths, and each was used separately for hydraulic property analysis. Figure 8 shows vertical and horizontal XMT image slices through a core sample of unit Rwie (sample B35463). This sample was also trimmed, to a length of 24 cm, for hydraulic property testing.

Samples B355M0 and B355M1 from the CCUz unit were not initially imaged using XMT owing to their fine texture, but visual inspection of these cores found material consistent with the CCUz silt of the perched zone in the B-Complex. The 88.9-mm- diameter, 300-mm-long core samples were cut in half (to 150 mm) to accommodate multiple analytical requirements. The upper portions of the samples were designated for geochemical analysis. For example, the sample named B355M0-G was designated for geochemical characterization (not part of this task.) The lower portion of this core was designated for hydraulic properties analysis and named B355M0-H. The upper portion of sample B355M1 was designated for hydraulic properties analysis, B355M1-H, and the lower portion was designated B355M1-G for geochemical analysis. Both B355M0-H and B355M1-H were later imaged after they had undergone multistep outflow experiments. Post-experiment XMT images for the perched zone cores are shown later in the results section of this report.

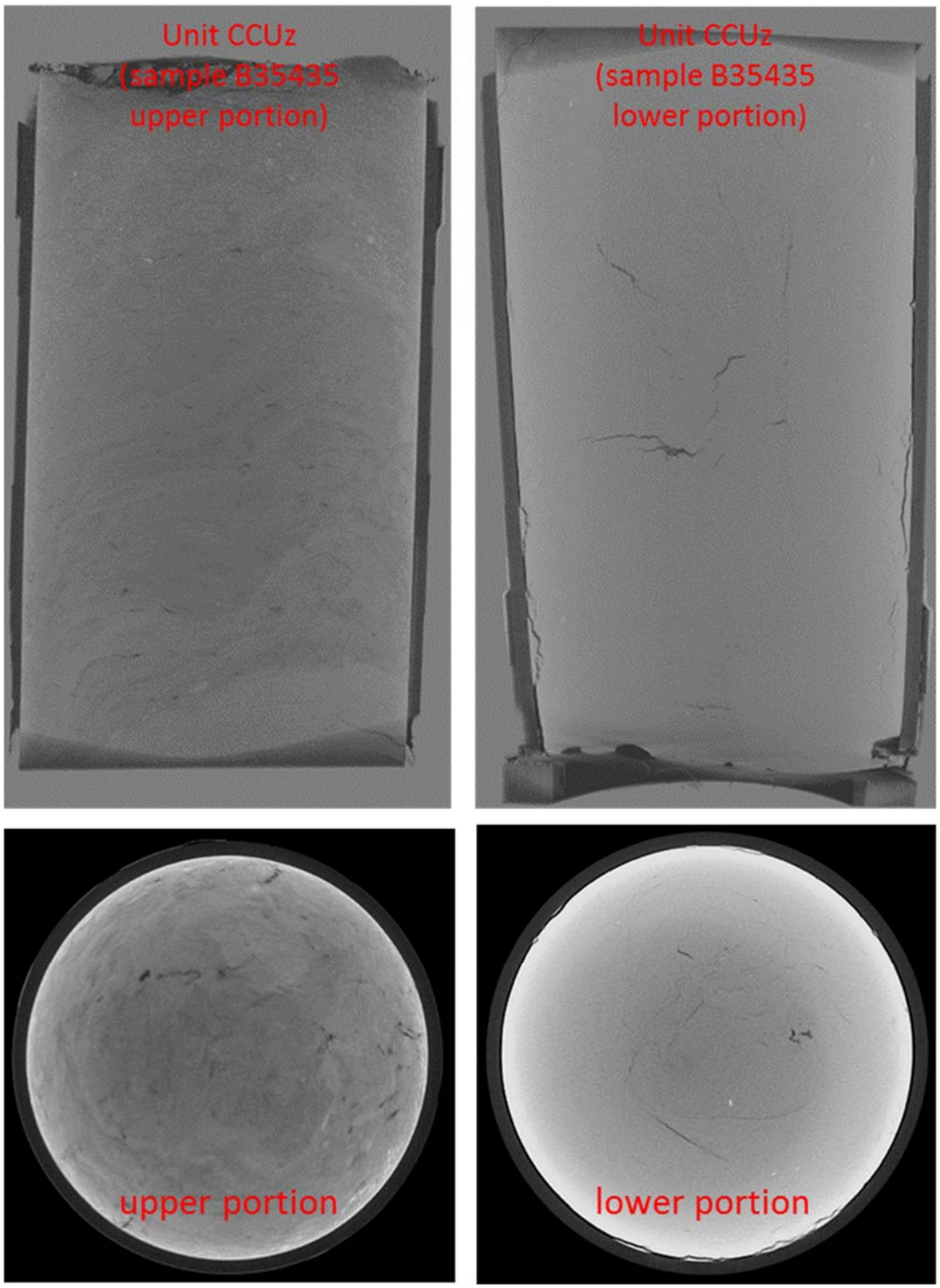

Figure 7. Vertical and horizontal XMT image slices through a core sample of unit CCUz (sample B35435).

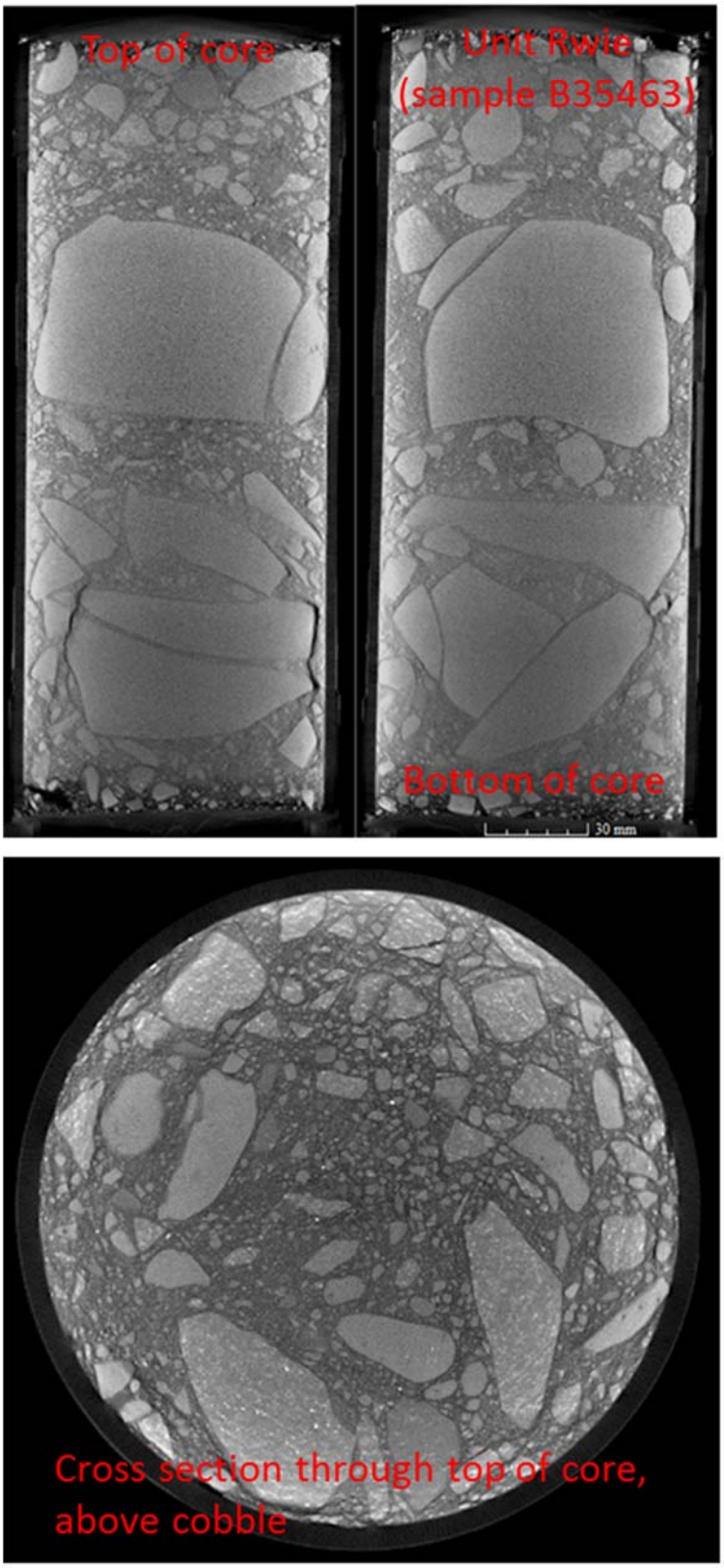

Figure 8. Vertical and horizontal XMT image slices through a core sample of unit Rwie (sample B35463).

2.3 Hydraulic Properties – Laboratory Testing

Hydraulic property characterization was performed on core samples in the laboratory under both water-saturated and unsaturated conditions. Owing to the potentially contaminated nature of some of the sediment cores, hydraulic property characterization was performed in a laboratory in PNNL's 331 Building, which is equipped and authorized for work with radioactive materials. The experimental apparatus used for hydraulic property characterization was originally developed and housed in the EMSL Subsurface Flow and Transport Experimental Laboratory, but was moved to the 331 Building for this characterization effort.

2.3.1 Saturated Hydraulic Conductivity

The saturated hydraulic conductivity, K_s, of a porous medium can be determined in the laboratory using constant head, falling head, and constant flux (a.k.a. steady flow) methods. Wietsma at al. (2009) developed an experimental apparatus for automated measurement of K_s using any or all of these methods (Figure 9). According to Reynolds and Elrick (2002), the range of K_s that can be determined using the constant head method is about 10^0 to 10^{-5} cm s^{-1}, and the range of K_s that can be determined using the falling head method is about 10^{-4} to 10^{-7} cm s^{-1}. In theory, the constant flux method is applicable for any value of K_s.

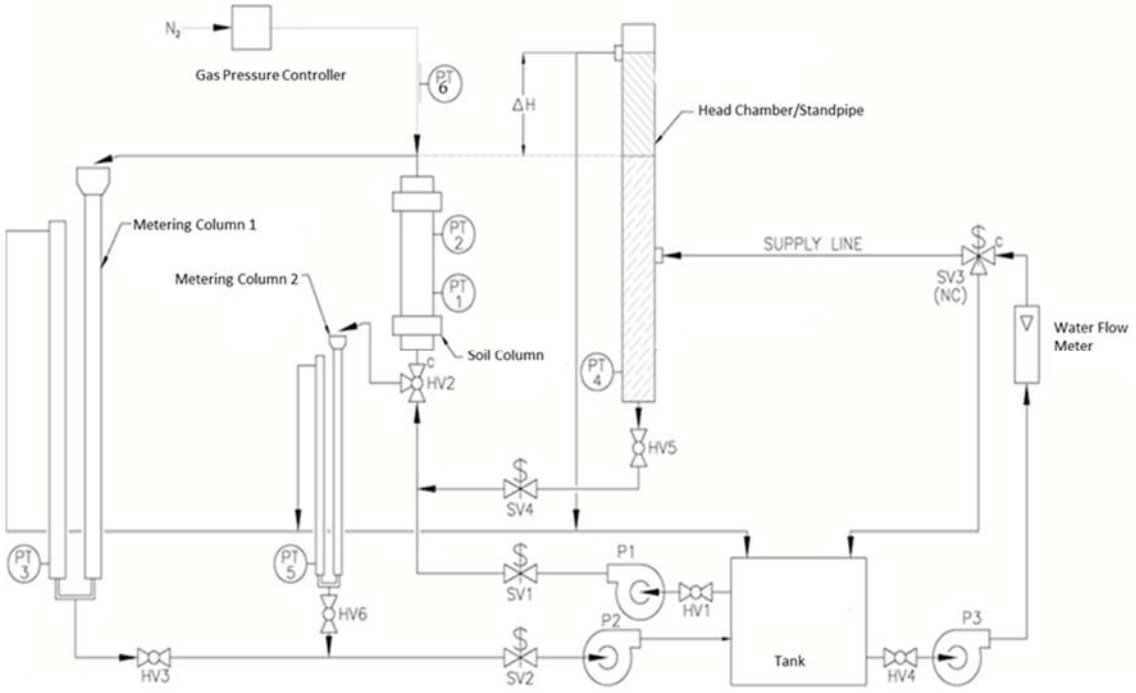

Figure 9. Schematic drawing of the experimental system used for determining saturated hydraulic conductivity with pressure transducers (PT1-PT6), pumps (P1-P5), solenoid valves (SV1-SV2), and manual valves (HV1-HV5).

The constant flux and falling head methods were used for characterization of the 200-DV-1 OU sediment samples reported here. The constant head method was not used because it usually requires the use of larger volumes of water, which would have to be treated as radioactive waste for the 200-DV-1 OU cores. The following sections describe the measurements and calculations used to determine K_s using these methods.

2.3.1.1 Falling Head Method

For the falling head method, the column conducts water according to a decreasing head in a standpipe with cross-sectional area A_s [L^2]. The parameter K_s is computed according to the following equation:

$$K_s = \left(\frac{A_s L_c}{A_c \Delta t}\right) ln\left(\frac{H_1}{H_2}\right) \quad (1)$$

where L_c [L] is the length of the porous media in the column, Δt [T] is the time for the hydraulic head to fall from level H_1 to level H_2 [L], and A_c [L^2] is the cross-sectional area. With reference to Figure 9, H_1 and H_2 are the logged, time-stamped, digital pressure (head) readings of PT4 at two different times whose difference is Δt. The parameters A_s, L_c, and A_c were all measured using a steel tape measure.

2.3.1.2 Constant Flux Method

For the constant flux method, a 0.01 M $CaCl_2$ solution is injected at a specified rate while hydraulic head measurements are obtained by pressure transducers connected to tensiometers at two or more internal locations. The K_s values obtained using this method represent the zone between the two locations where the hydraulic heads are measured, according to the following equation:

$$K_s = \frac{Q L_p}{A_c \Delta H_p} \quad (2)$$

where L_p [L] and ΔH_p [L] are the distance and hydraulic head difference, respectively, between the two locations where the hydraulic head data are obtained, Q [L^3 T^{-1}] is the observed flow rate, and A_c is the column cross-sectional area [L^2]. With reference to Figure 9, pump P1 imposes a flow rate and time-stamped pressure date are logged from pressure transducers PT1, PT2, and PT3. The observed flow rate Q is the logged digital pressure reading from PT3, converted to volume, as a function of time. Again, the volume, $V = (\pi r^2 h)*2$, where r is the radius of Metering Column 1, h is the pressure reading of PT3 in units of cm of water, and the value is multiplied by 2 because Metering Column 1 is made of two standpipes with identical radius. The volume conversion method was validated with a Type A graduated cylinder, and the parameters L_p and A_c were measured with a steel tape measure.

2.3.2 Water Retention and Transmission Properties

Several laboratory methods are available for determining water retention characteristics of variably saturated porous media. These include the hanging water column and pressure plate extraction methods (Dane and Hopmans 2002a,b). The hanging water column method is usually applicable to soil moisture tensions up to ~300 cm of water, while the pressure plate extraction methods are typically used for much higher soil moisture tensions, up to ~15,000 cm of water, depending on the bubbling pressures of the porous plates. Water retention and transmission properties for variably-saturated conditions can also be obtained simultaneously using the multistep outflow method (Hopmans et al. 2002) that was used in the current study.

Figure 10 shows a more detailed schematic of a soil-filled column, or intact core sample. For determination of K_s, acrylic endcaps are typically fitted with perforated support plates. For multistep outflow experiments, a porous ceramic plate is typically used on the bottom end of the core. The core is also instrumented with tensiometers attached to pressure transducers for measurement of aqueous pressures.

Placement of tensiometers in intact cores can be problematic. If the cores contain large fractions of coarse material, the porous ceramic cups on the tensiometers may have poor contact with the sediment (or rocks) and can be cracked during emplacement. Once installed, the tensiometer tubes are sealed to the core liner using marine-grade epoxy. The bubbling pressure of the porous ceramic cups and porous plates used in the multistep outflow experiments for the 200-DV-1 OU cores was ~1000 cm of water.

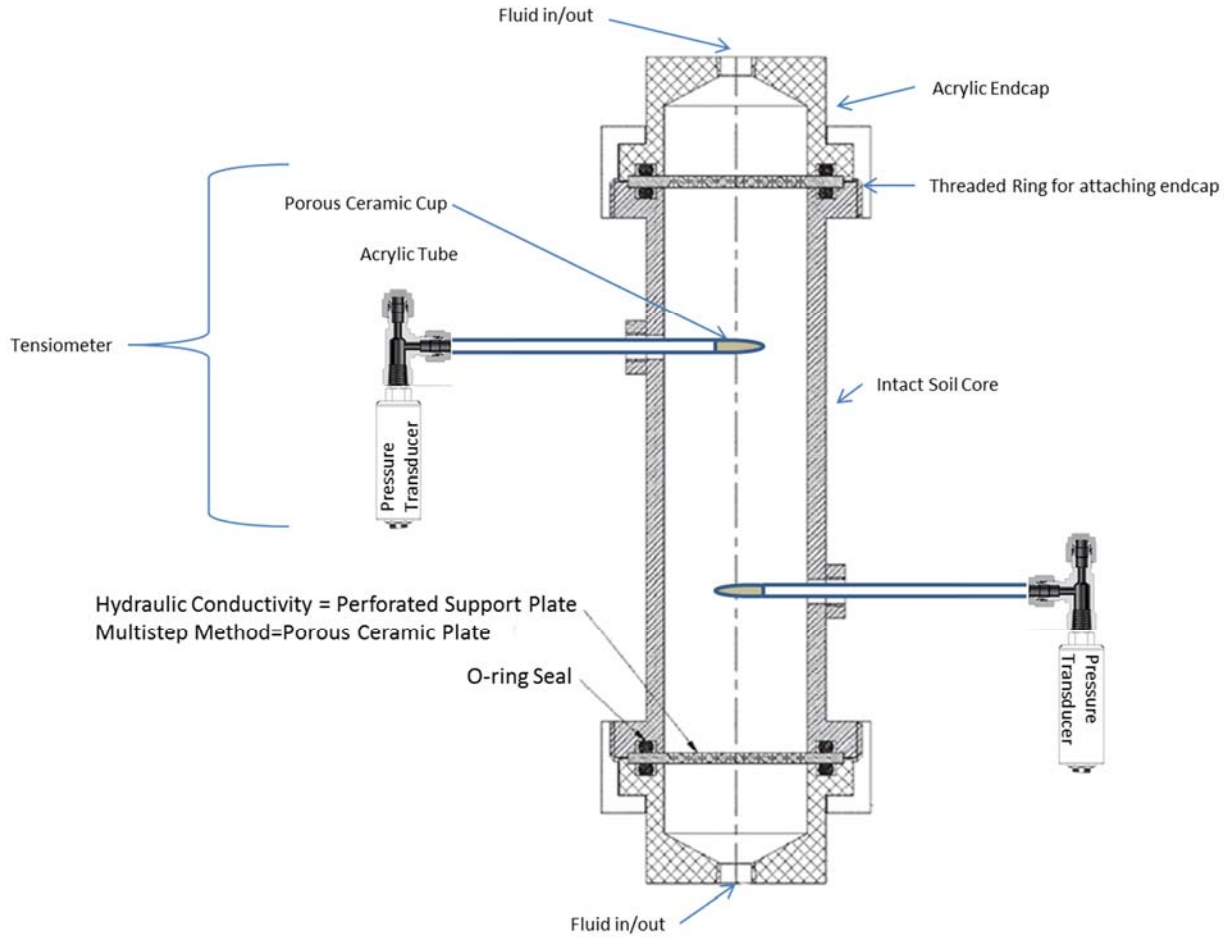

Figure 10. Schematic of a column or sediment-filled core sample used for multistep outflow experiments.

2.3.2.1 Multistep Outflow Method

The multistep outflow procedure is performed as follows. After the intact core sample is mounted in the experimental apparatus, the core is initially saturated with de-aired water from the bottom up, to minimize entrapped air. The porous plate at the bottom of the core and the bottom endcap are completely water-filled and are attached to a water-filled outflow line. The end of the outflow line is positioned so that the drip point is at the same elevation as the top of the sediment in the column. The top endcap is then attached and connected to a gas flow line. At this point the core should be gas-tight.

With the outflow line positioned as described, the lower boundary condition for the soil column is a fixed aqueous pressure, equal to the height of the sediment-filled column. The upper boundary condition is set to a prescribed gas pressure (initially atmospheric) using a gas pressure controller. With reference to 0, gas pressure is measured at PT6, and aqueous pressures are measured at PT1 and PT2. Gas pressure is increased incrementally, and the cumulative water outflow volume and changes in aqueous pressures are

measured as a function of time. Gas pressure is typically increased when the water outflow has ceased and the aqueous pressures have stabilized for the current gas pressure step. A multistep outflow experiment is terminated when negligible outflow is observed after a prolonged period at relatively higher gas pressure.

The air-entry pressure of the porous plate at the bottom of the core is nominally ~1000 cm, so this is the maximum gas pressure that could theoretically be applied before the system was no longer gas-tight. However, pressures this high are rarely used in order to maintain a safety factor, in case the bubbling pressure of the plates is lower than advertised. In practice, the maximum air pressure applied to the top of the columns is ~700 cm. Multistep outflow experiments on intact cores are often terminated earlier than planned, however, owing to air leaks. Air leaks did occur during some of the multistep outflow experiments that were performed for this project, and further details on this and other experimental issues are provided in the results section of this report. Air leaks are not uncommon when multistep outflow experiments are performed on intact sediment cores, due to the stresses experienced by the Lexan core liners during drilling. The high temperature and pressure conditions that develop during drilling can make the Lexan liners susceptible to cracking, and the cracks may open when the core liner is pressurized. When obvious air leaks do occur, attempts are usually made to seal the leak with marine-grade epoxy. The core is then resaturated and the experiment is repeated.

2.3.2.2 Parameter Estimation

Hydraulic parameters can be estimated from multistep outflow experimental data in several different ways. The most common approach is to numerically simulate the experiment and to use non-linear parameter estimation to determine hydraulic parameters, using measured outflow and pressure data as observations (Eching and Hopmans 1993a; Eching et al. 1994). In this inverse parameter estimation approach, the experiment is simulated repeatedly as parameters are adjusted iteratively to minimize the differences between measured and simulated outflow volumes and water pressures. Most inverse parameter estimation methods used for estimating hydraulic parameters from multistep outflow data have used a single-phase flow equation, known as the Richards equation (Richards 1931), for solving the forward flow problem (Kool and Parker 1988; Eching and Hopmans 1993a,b; Eching et al. 1994; Tuli et al. 2001).

For the current study, the water-air operational mode of the STOMP (Subsurface Transport Over Multiple Phases) simulator (White and Oostrom 2006) was used in conjunction with the parameter estimation software PEST (Doherty 2016). The water-air operational mode of STOMP, referred to as STOMP-WA, solves coupled mass conservation equations for both aqueous (water) and gas (air) phases under isothermal conditions. PEST is a well-known parameter estimation software package that can use several different parameter estimation algorithms, including the Levenberg-Marquardt method (Levenberg 1944; Marquardt 1963) that was used in the current study.

STOMP-WA is well suited for simulating the type of multistep outflow experiment described here since the boundary conditions used in the experiment can be accurately prescribed for the simulator. No liquid water moves across the top boundary of the core sample, and the bottom of the core sample sits on a water-saturated porous plate through which air cannot pass, unless the air-entry pressure of the plate is exceeded. Therefore, Dirichlet-type boundary conditions of fixed aqueous pressure and prescribed gas pressures are specified for the bottom and top of the model domain, respectively. Neumann-type zero-flux boundary conditions are specified for the aqueous and gas phases at the top and bottom of the domain, respectively.

Nonuniformities in a core sample, and/or poor contact between the porous cups of the tensiometers and sediments contained within the intact core, can make pressure data unreliable. Use of only outflow data for observation in inverse parameter estimation may be necessary if tensiometers fail or exhibit spurious

or unexpected behavior during a multistep outflow experiment. However, owing to the well-constrained boundary conditions used in the experimental setup, and the use of a two-phase flow simulator, outflow data alone are expected to yield reliable parameter estimates.

An alternative to using inverse modeling for parameter estimation is to use the prescribed gas pressures and measured aqueous pressures from the multistep experiment to calculate capillary pressures, and the measured outflow volumes and volume of water remaining at the end of the experiment to calculate average water contents as a function of time. The average water contents and capillary pressures at selected times can then be paired and fitted to estimate parameters for any water retention model of interest.

2.3.2.3 Water Retention Functions and Unsaturated Hydraulic Conductivity Models

Many different functions and models have been proposed for representing the water retention characteristics and unsaturated hydraulic conductivity of porous media. The water retention functions of van Genuchten (1980) and Brooks and Corey (1964) are the most popular owing to their relative simplicity and accuracy in representing measured water retention characteristics. The van Genuchten (1980) model can be written as

$$S_e(h) = [1 + (\alpha h)^n]^{-m} \tag{3}$$

where:

S_e = effective saturation = $\frac{\theta - \theta_r}{\theta_s - \theta_r}$; $0 \leq S_e \leq 1$
h = soil-moisture tension [L]
α = curve-fitting parameter related to the inverse of the air-entry pressure [L^{-1}]
n, m = curve-fitting parameters related to the pore size distribution; $m = 1\text{-}1/n$ is often assumed [-]
θ_r = residual water content [-]
θ_s = saturated water content [-].

The van Genuchten hydraulic conductivity relationship, based on the Mualem (1976) hydraulic conductivity model with the restriction that $m = 1 - 1/n$, can be written as

$$K(S_e) = K_s S_e^l \left[1 - \left(1 - S_e^{1/m}\right)^m\right]^2 \tag{4}$$

where K_s is the saturated hydraulic conductivity and l is a pore-interaction term that is equal to 1/2.

The Brooks-Corey model may be written as

$$S_e(h) = \left(\frac{h_b}{h}\right)^{\lambda} \; if \; h \geq h_b$$
$$S_e(h) = 1 \; otherwise. \tag{5}$$

where λ is a pore-size distribution parameter that affects the slope of the water retention function, and h_b is the air-entry (a.k.a. bubbling) pressure. The Brooks-Corey function can be combined with the Burdine (1953) or Mualem (1976) relative permeability models to yield

$$K(S_e) = K_s S_e^{2+l+2/\lambda} \tag{6}$$

where the pore-interaction term l = ½ and 1 for the Mualem and Burdine models, respectively.

Eqs. (3) and (4) are the most commonly used hydraulic property functions for vadose zone materials, followed by Eqs. (5) and (6). Note that the Brook-Corey water retention model [Eq. (5)] is sometimes preferred over the van Genuchten model [Eq. (3)] if a porous medium has relatively uniform particle and pore sizes that result in a sharp or abrupt decrease in aqueous saturation from a fully water-saturated condition after a distinct air-entry pressure is exceeded.

Porous media can also have multi-modal pore size distributions that manifest multi-modal water retention characteristics. Such characteristics can be represented using multiple, van Genuchten-type subcurves, S_{e_i}

$$S_e = \frac{\theta - \theta_r}{\theta_s - \theta_r} = \sum_{i=1}^{k} w_i S_{e_i} \tag{7}$$

where

$$S_{e_i} = [1 + (\alpha_i h)^{n_i}]^{-m_i} \tag{8}$$

and where i denotes a subcurve, k is the number of subcurves, w_i are weighting factors with $0 < w_i < 1$, and $\sum w_i = 1$ (Durner 1992, 1994). Priesack and Durner (2006) developed closed-form expressions for multi-modal unsaturated hydraulic conductivity functions based on the van Genuchten-Mualem relationships.

2.4 Hydraulic Properties – Field Testing

Hydraulic property characterization was also performed in the field for a perched-water aquifer site in the B-Complex of the 200 East Area. Details regarding field methods are described in references cited in Section 3.0 of this report, and in Appendix B.

2.5 Physical Properties

After laboratory multistep outflow experiments were terminated, the acrylic endcaps on the intact core samples were removed and the sediment contained in the cores was removed and oven dried in a convection oven for 24 hours at 105 °C. Physical properties, including porosity, dry bulk density, particle density, and particle size distribution, were then determined as described below. Some exceptions to this processing protocol for the CCU perched zone cores (Table 1) are described in Section 3.0 of this report.

2.5.1 Total Porosity

The total porosity of the intact cores was estimated by converting the mass of water remaining in the sediments at the end of the multistep outflow experiment to a volume, and then adding the volume of water that flowed out of the column during the experiment. This calculation assumes that the sediment is fully water-saturated at the beginning of a multistep outflow experiment, with no excess water ponded on top of the sediment. The porosity calculated in this way is an *apparent* total porosity, rather than the true total porosity that exists in situ, owing to potential sample disturbance during core sampling.

The XMT images for most of the intact cores indicate some degree of sample disturbance that resulted in creation of small cracks or a small amount of void space around the walls of the Lexan liner and sometimes around the ends of the columns. Outflow data from nearly all of the analyzed cores also show evidence of "wall effects," wherein a relatively small volume of water drained from the cores in the first pressure step, even for relatively fine-textured materials. Although the cores were collected intact, some degree of sample disturbance inevitably occurs during drilling and sampling, and this is expected.

Total porosity, ϕ, can also be estimated from bulk and particle densities using

$$\phi = 1 - \frac{\rho_b}{\rho_s} \tag{9}$$

where ρ_b and ρ_s are the dry bulk density [M L^{-3}] and particle density [M L^{-3}], respectively. Bulk density was determined for the whole cores, while particle density was determined on subsamples of the <2 mm size fraction, as described below. Differences between porosity calculated using Eq. (9) and porosity calculated as the sum of the water volume drained plus water volume remaining in the column at the end of a multistep experiment divided by core volume can be attributed, in part, to differences in the particle density of the bulk sediment, versus the measured particle density for the subsample from the < 2mm size fraction.

2.5.2 Dry Bulk Density

The dry bulk density, ρ_b [M L^{-3}], is defined as

$$\rho_b = \frac{M_s}{V_b} \tag{10}$$

where M_s is the dry mass of solids and V_b is the bulk volume occupied by the solids. Particle density was calculated as the total mass of dry sediment contained in the Lexan core liner, divided by the volume of core liner. For all samples used in this study, the inside diameter of the Lexan core liners was 8.89 cm. The nominal length of the core liners was 30 cm, but several samples were cut down to shorter lengths to avoid sections with large cobbles.

2.5.3 Particle Density

Particle density, ρ_s [M L^{-3}], is defined as

$$\rho_s = \frac{M_s}{V_s} \tag{11}$$

where M_s is the dry mass of solid particles and V_s is the volume of the particles. Particle density was determined on subsamples of the <2 mm size fraction of sediments from the core samples using the pycnometer method (Flint and Flint 2002).

2.5.4 Particle Size Distribution

Particle size distribution was determined using two methods: mechanical sieving (Gee and Or 2002) and laser light scattering (ASTM D4464-15). Sieving was performed on the dried, bulk sediment that was removed from Lexan core liners after completion of the multistep outflow experiments, using standard

sieve sizes of 2.5 in., 1.25 in., 5/85 in., and #5 and #10 sieves. These correspond to sizes of 64, 32, 16, 8, and 2 mm, respectively. The laser light scattering method was used on subsamples of the <2 mm size fraction that were collected from the catch pan at the bottom of the sieve stack. The <2 mm size fraction contains particles that are sand-sized and smaller. The data generated by the sieve and laser light scattering methods were combined to determine the complete particle size distributions for the bulk sediments.

3.0 Results and Discussion

This section presents the results from 200-DV-1 core sample characterization and perched zone aquifer testing performed in the B-Complex. Results for hydraulic property characterization are discussed first, followed by physical properties.

3.1 Hydraulic Properties – Laboratory Testing

3.1.1 Saturated Hydraulic Conductivity

Measurements to determine the vertical saturated hydraulic conductivity, K_s, of the intact core samples were made primarily using the falling head (FH) method. Measurements with the FH method were typically performed in triplicate, with each replicate done at two different starting hydraulic head differences. Therefore reported K_s values (Table 2) obtained using the FH method typically represent an average for six sets of measurements. The calculated K_s value for any given replicate is also the average of all calculated K_s values for the set of measurements collected during that run, excluding any initial spurious values that occurred at the start of a set of measurements. The K_s values vary by three orders-of-magnitude, ranging from high values of 4.48e-03 and 2.5e-03 cm/s for samples of the Rwie and CCUg units, respectively, to low values of 3.03e-06 and 3.36e-6 cm/s for samples of the CCU perching silt zone underlying the B-Complex.

Figure 11 shows an example of calculated K_s values for one replicate set of measurements obtained using the FH method at two starting hydraulic head differences for a core sample of the CCUg unit (HEIS sample B39M11). Figure 11 also illustrates the excellent reproducibility of measurements obtained using the FH method.

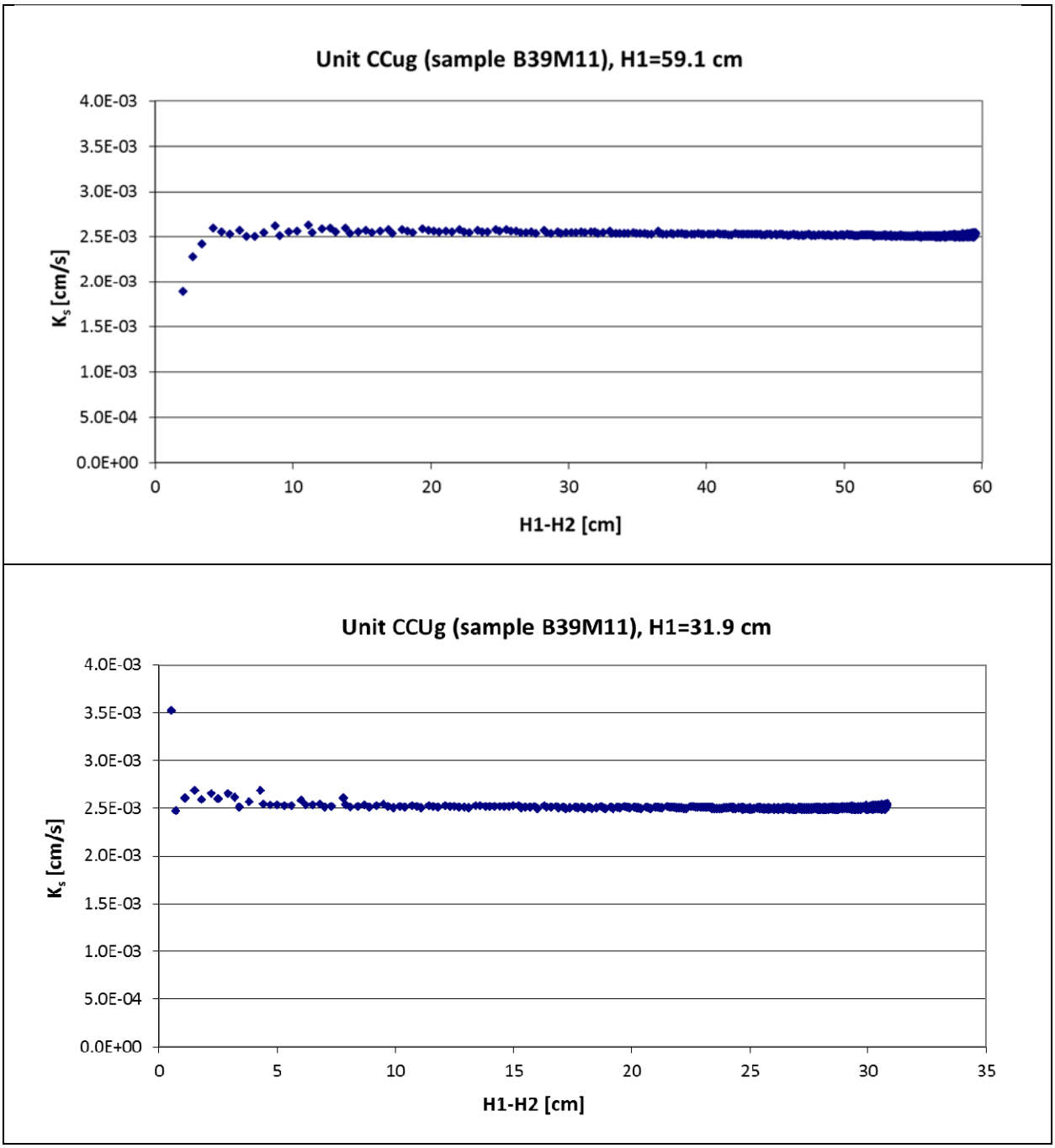

Figure 11. Calculated K_s values generated using the FH method for one replicate set of measurements obtained for two different starting hydraulic head differences on a core sample of the CCUg unit (HEIS sample B39M11).

The constant flux (CF) method was used for two CCUz samples. In the CF method, a 0.01 M $CaCl_2$ solution is injected at known rates while hydraulic head measurements are obtained by pressure transducers connected to tensiometers at two or more locations. Figure 12 shows the head gradient versus volumetric flow rate for two replicate sets of measurements using the CF method for a core sample of the CCUz unit (sample B35435, top). Values of K_s are calculated from the applied flow rate and head

gradient, *H*, using Eq. (3). Figure 12 also illustrates the excellent reproducibility of measurements obtained using the CF method.

A summary of the K_s values determined on intact cores from the 200-DV-1 OU is shown in Table 2. The K_s values vary by three orders-of-magnitude, ranging from high values of 4.48e-03 and 2.5e-03 cm/s for samples of the Rwie and CCUg units, respectively, to low values of 3.03e-06 and 3.36e-6 cm/s for samples of the CCU perching silt zone underlying the B-Complex.

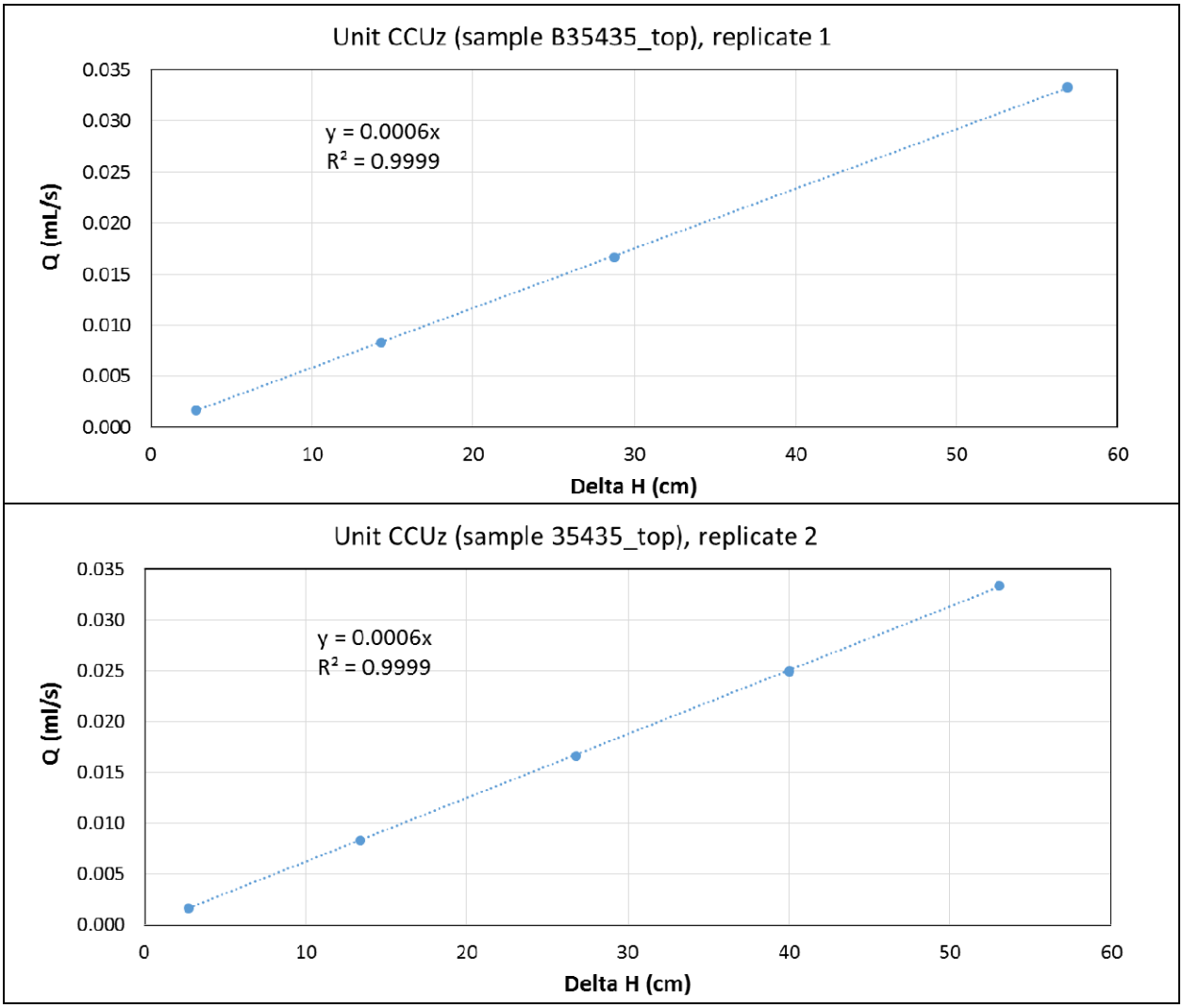

Figure 12. Calculated K_s values generated using the constant flux method.

Table 2. Summary of calculated K_s values determined on intact core samples from 200-DV-1 OU.

Formation	Sample ID	Complex	Method[(a)]	Average K_s[(b)] [cm/s]
Rwie	B35463	T	FH	4.48e-03 ± 4.28e-04 (8)
	B39VY9	T	FH	1.47e-05 ± 3.93e-07 (6)
Rtf	B39X68	S	FH	6.99e-05 ± 1.13e-06 (6)
CCUz	B35435 (top)	T	CF	1.03e-04 ± 5.09e-06 (2)
	B35435 (bottom)	T	CF	5.01e-05 ± 5.14e-06 (5)
CCUz (perching silt)	B355M1 (top)	B	FH	3.03e-06 ± 2.66e-07 (6)
	B355M0 (bottom)	B	FH	3.69e-06 ± 6.55e-07 (6)
CCUc	B39X53	S	FH	1.02e-05 ± 1.62e-06 (8)
	B39VV7	T	FH	2.24e-04 ± 3.10e-06 (6)
CCUg	B39M11	B	FH	2.53e-03 ± 3.99e-05 (6)

(a) FH and CF refer to falling head and constant flux methods, respectively.

(b) Numbers represent average ± one standard deviation, with the number of measurement sets listed in parentheses.

3.1.2 Water Retention and Transmission Properties

Data obtained from the multistep outflow experiments consist of time-series of air pressures applied to the tops of core samples, water pressures measured via pressure transducers attached to tensiometers that are installed at multiple locations within the cores, and water outflow volumes. For a 30-cm-long core, tensiometers were typically installed at three locations: approximately 5, 15, and 25 cm from the top of the core. If a core was trimmed down to a shorter length, owing, for example, to the presence of large cobbles that would obstruct flow, then tensiometers might be installed at two locations instead of three, depending on the length of the core. In some cases, gravel or cobble within a core prevented the installation of tensiometers at target measurement locations, so those locations were abandoned and the access holes were sealed.

Post-processing of data from multistep outflow experiments consisted of the following steps.

1. The total volume of water that flowed out of a column during an experiment was added to the volume of water left in the column at the end of the experiment, as determined by oven drying of the sediments after the experiment was terminated. This total water volume divided by the core volume provides an estimate of total porosity.

2. Capillary pressures, P_c, (equivalent here to soil moisture tensions, h) were calculated by subtracting the aqueous pressure, P_a, recorded by the pressure transducer at each tensiometer measurement location from the applied air pressure, P_g

$$P_c = P_g - P_a \tag{12}$$

3. Average volumetric water content values from step 1 were paired with capillary pressures from step 2 and were plotted to determine if/when tensiometers failed, and to identify wall effects.

4. Selected values of average capillary pressures and average volumetric water contents were fitted using the Solver in Excel to estimate parameters for the van Genuchten (1980) and Brooks-Corey (1964) water retention functions. The values used for fitting were typically chosen to be the last set of measurements from the time series made just prior to each step change (increase) in gas pressure.

5. Time-series of air and water pressures and water outflow volumes were reformatted to generate boundary conditions and observational data sets for inverse parameter estimation.

6. Inverse modeling was performed using STOMP (White and Oostrom 2006) and PEST (Doherty 2016).

3.1.2.1 Parameter Estimation from Average Water Content and Pressure Data

Figure 13 shows average volumetric water content versus capillary pressure from a multistep outflow experiment performed on a sample from CCUg (HEIS sample ID B39M11). For this experiment, failure of the middle tensiometer occurred at a capillary pressure corresponding to a volumetric water content of ~0.12, as evidenced by the abrupt drop in capillary pressure at this point. Failure of the upper tensiometer occurred later, at a pressure corresponding to a volumetric water content of ~0.1. The lower tensiometer continued to perform well through the rest of the experiment. For this sample, the average volumetric water content was paired with the average capillary pressure for the upper and lower tensiometers if the calculated water content was greater than or equal to 0.11, and with the capillary pressure for just the lower tensiometer when the water content was less than 0.11.

Figure 13 also shows calculated capillary pressures of less than zero at water contents greater than ~0.222, and an inflection in the curvature of the trend of the data after this point. This behavior is attributed to "wall effects," wherein water contained in void space between the sediments and the wall of the Lexan liner, and/or in cracks or fissures in the cores, drains freely under little to no applied gas pressure. The potential influence of wall effects on estimated water retention parameters was minimized by not using data with negative values of calculated capillary pressure.

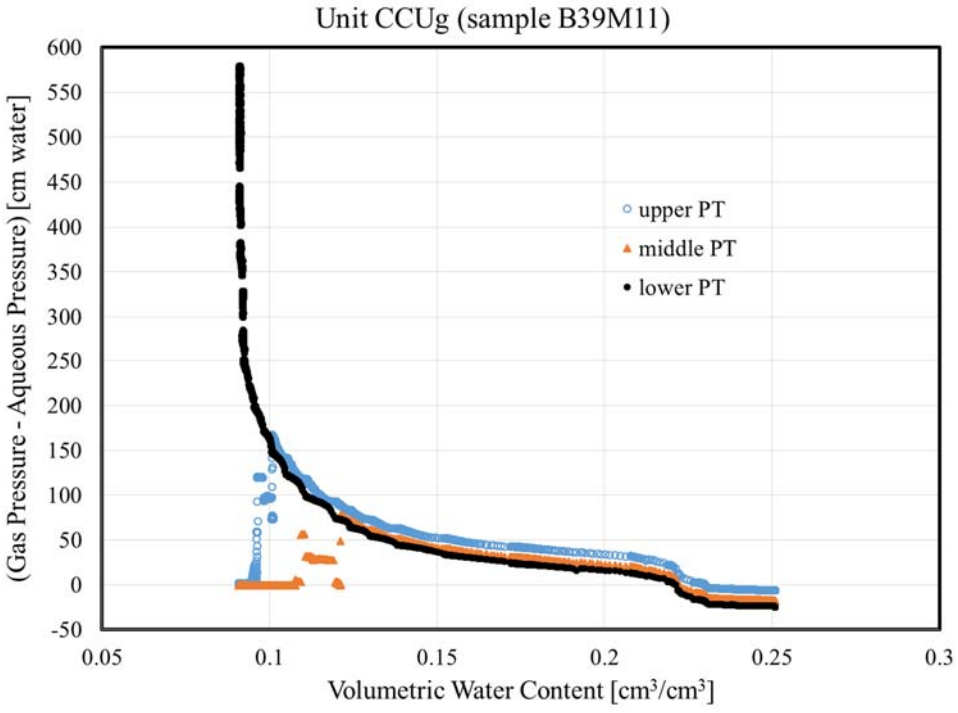

Figure 13. Average volumetric water content versus capillary pressures determined from multistep outflow experiment on a sample of the CCUg unit (HEIS sample B39M11).

Figure 14 to Figure 265 show selected values of average water content and average capillary pressure fit to the standard van Genuchten (1980) and Brooks-Corey (1964) models for the multistep outflow experiments that were successful. Fitted model parameters are summarized in Table 3. In general, both models provide excellent fits to the water retention data. One exception is the sample from unit Rwie (HEIS sample B39VY9), that has multi-modal water retention characteristics that were not fit well by either of the standard van Genuchten (vG) or Brooks-Corey (BC) model (Figure 19 and Figure 20).

Figure 27 shows the water retention data from sample B39VY9 fit with a bimodal van Genuchten-type water retention function, based on Eqs. (7) and (8). The bimodal function provides a significantly improved fit to the water retention data relative to the standard van Genuchten or Brooks-Corey functions. The fitted parameters of the bimodal van Genuchten water retention function for this data set are: θ_s = 0.157, θ_r = 0.082, w_1 = 0.5537, α_1 = 0.2689, n_1 = 3.1975, α_2 = 0.0073, and n_2 = 18.7654, with SSE = 0.00018. Note that the water retention data for sample B35435 could probably also be fit better using a multimodal function. It should be noted that multimodal water retention and unsaturated hydraulic conductivity functions are not typically used to describe the hydraulic properties of sediments from the Hanford Site, and the STOMP simulator does not currently have this option. However, this option could be added to the code, if needed.

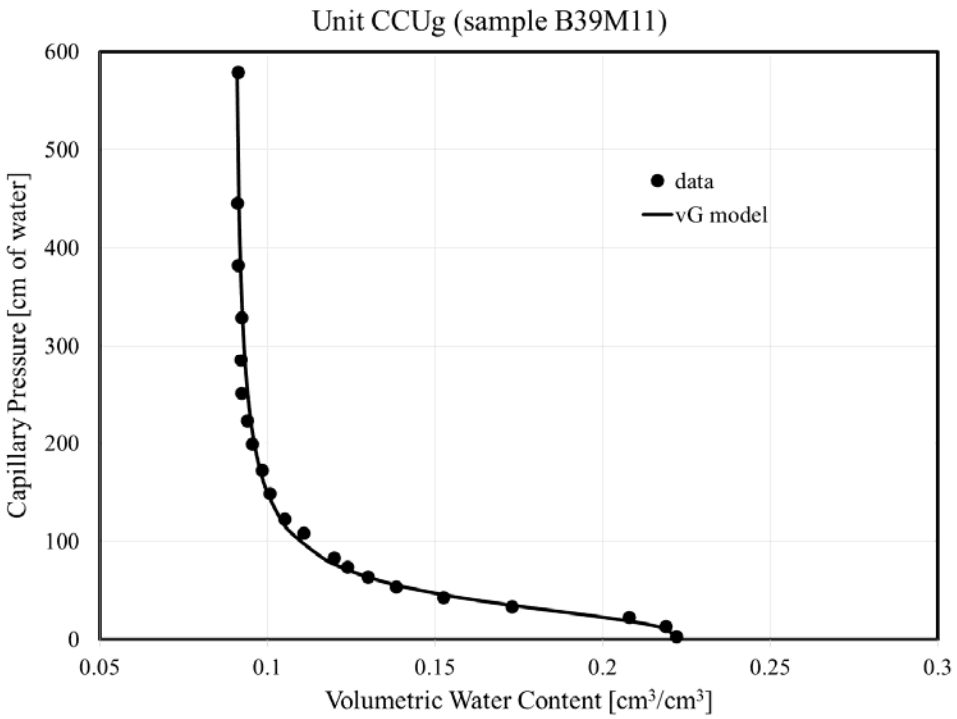

Figure 14. Selected values of average water content and capillary pressure fit to the van Genuchten (1980) model for a sample of the CCUg unit (HEIS sample B39M11).

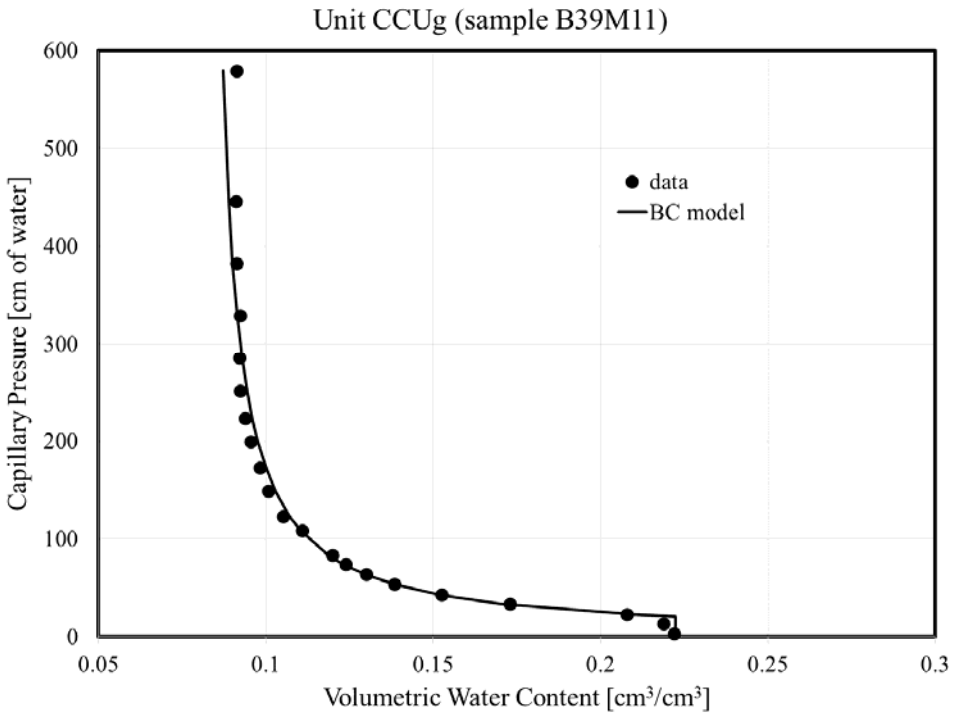

Figure 15. Selected values of average water content and capillary pressure fit to the Brooks-Corey (1964) model for a sample of the CCUg unit (HEIS sample B39M11).

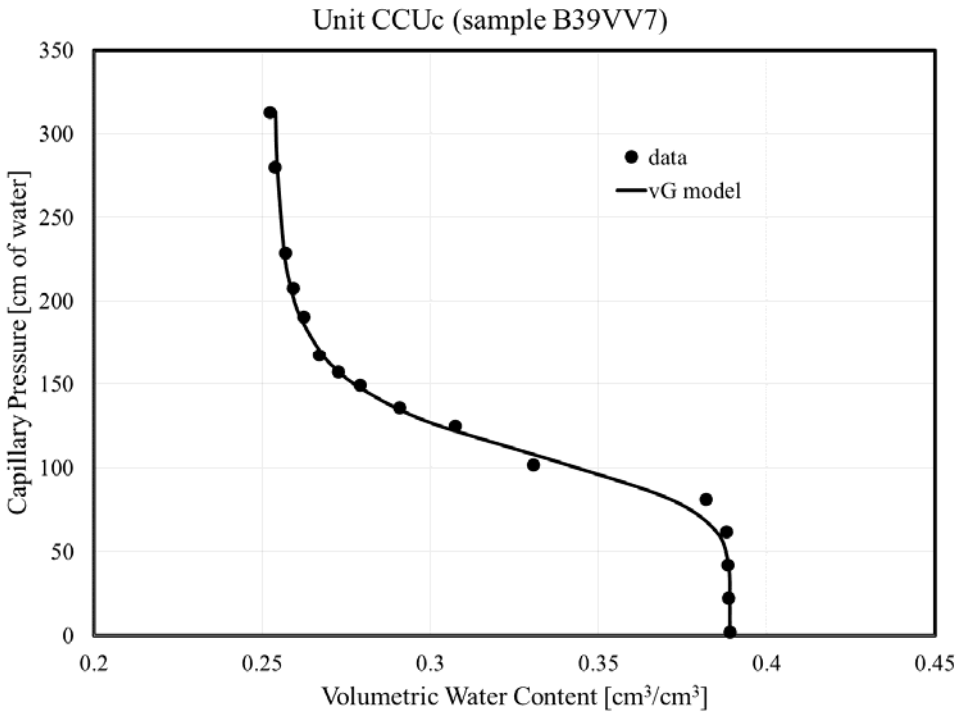

Figure 16. Selected values of average water content and capillary pressure fit to the van Genuchten (1980) model for a sample of the CCUc unit (HEIS sample B39VV7).

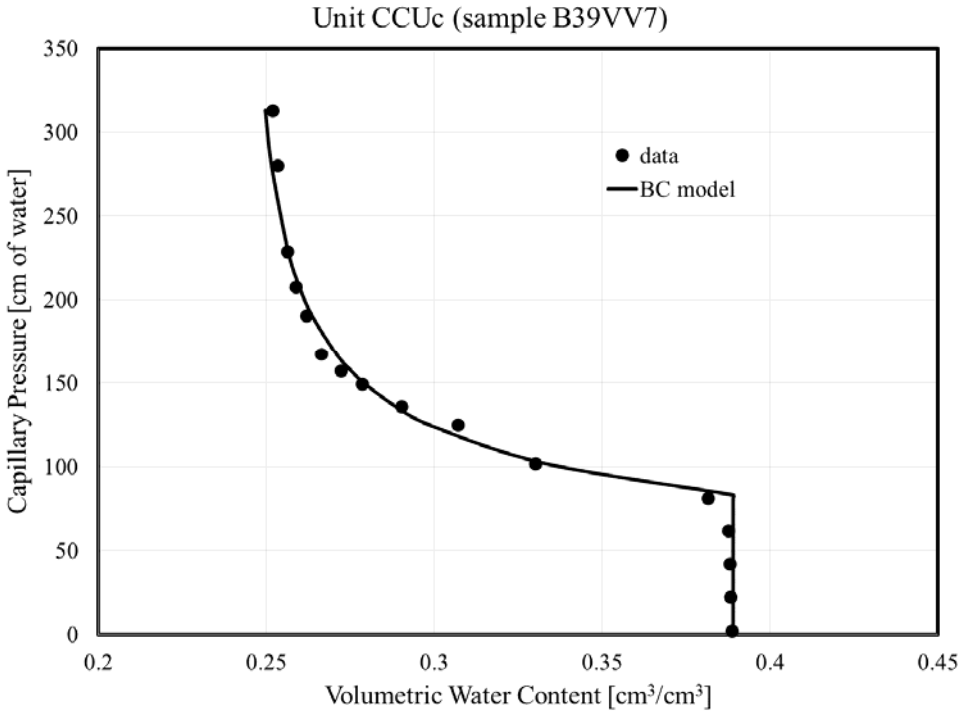

Figure 17. Selected values of average water content and capillary pressure fit to the Brooks-Corey (1964) model for a sample of the CCUc unit (HEIS sample B39VV7).

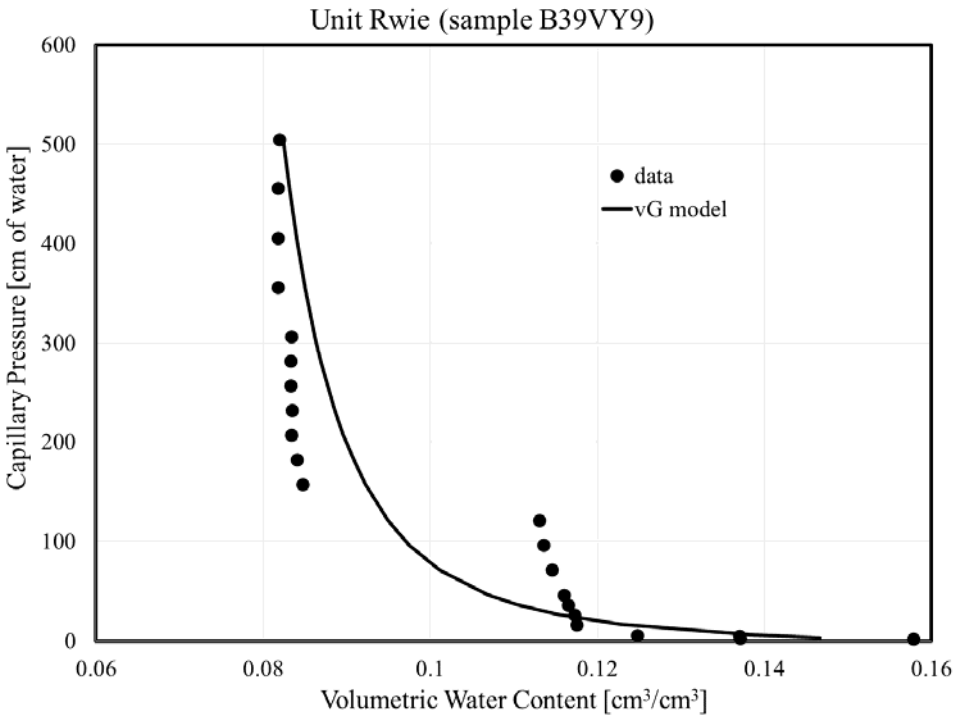

Figure 18. Selected values of average water content and capillary pressure fit to the van Genuchten (1980) model for a sample of the Rwie unit (HEIS sample B39VY9).

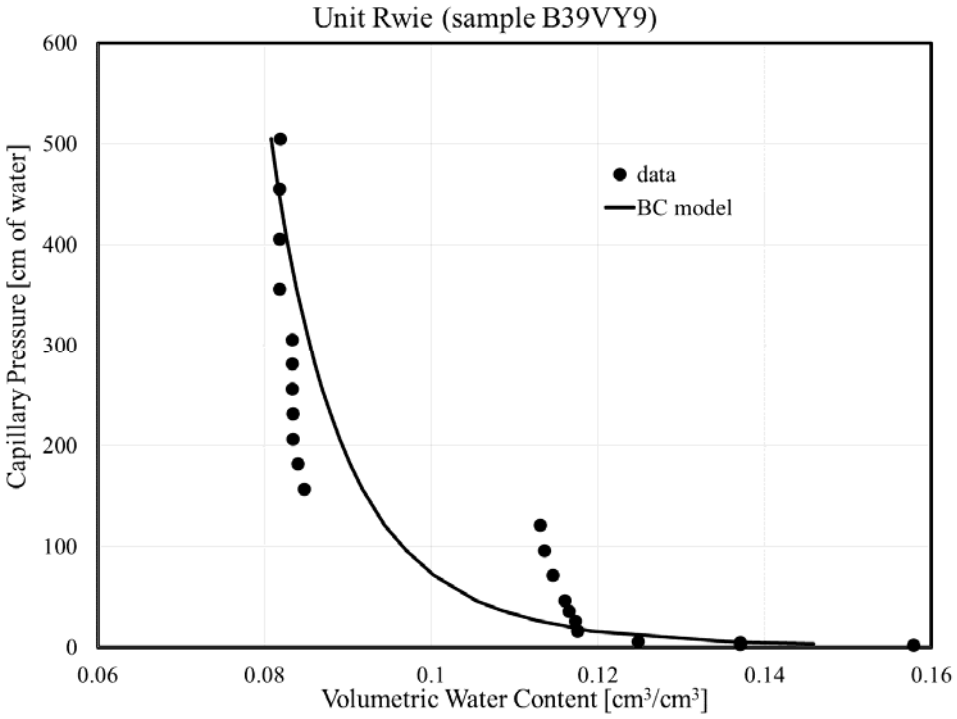

Figure 19. Selected values of average water content and capillary pressure fit to the Brooks-Corey (1964) model for a sample of the Rwie unit (HEIS sample B39VY9).

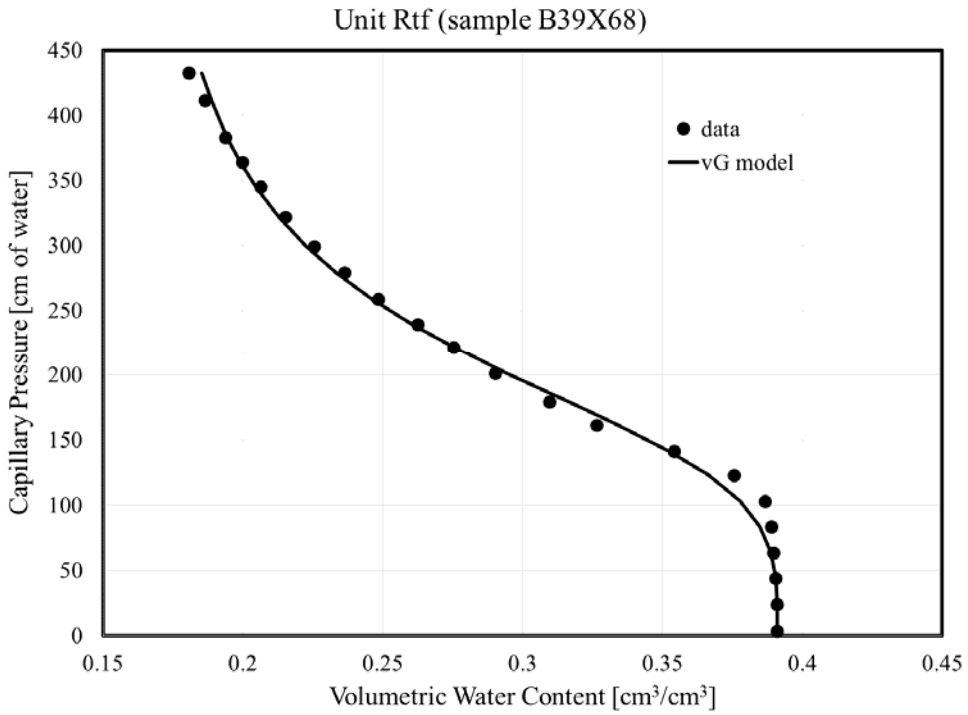

Figure 20. Selected values of average water content and capillary pressure fit to the van Genuchten (1980) model for a sample of the Rtf unit (HEIS sample B39X68).

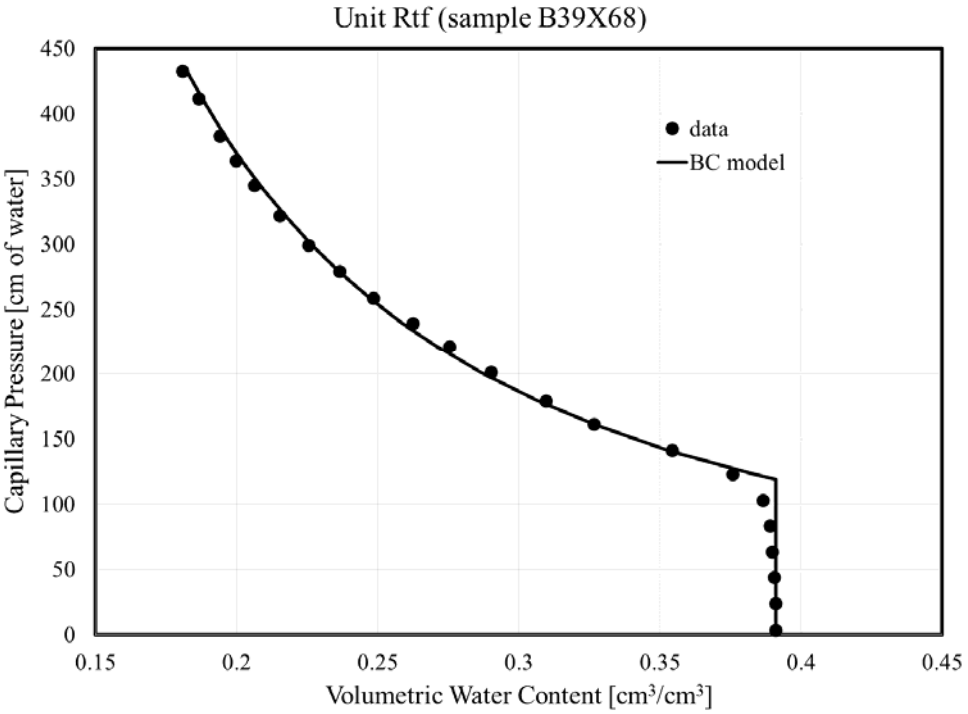

Figure 21. Selected values of average water content and capillary pressure fit to the Brooks-Corey (1964) model for a sample of the Rtf unit (HEIS sample B39X68).

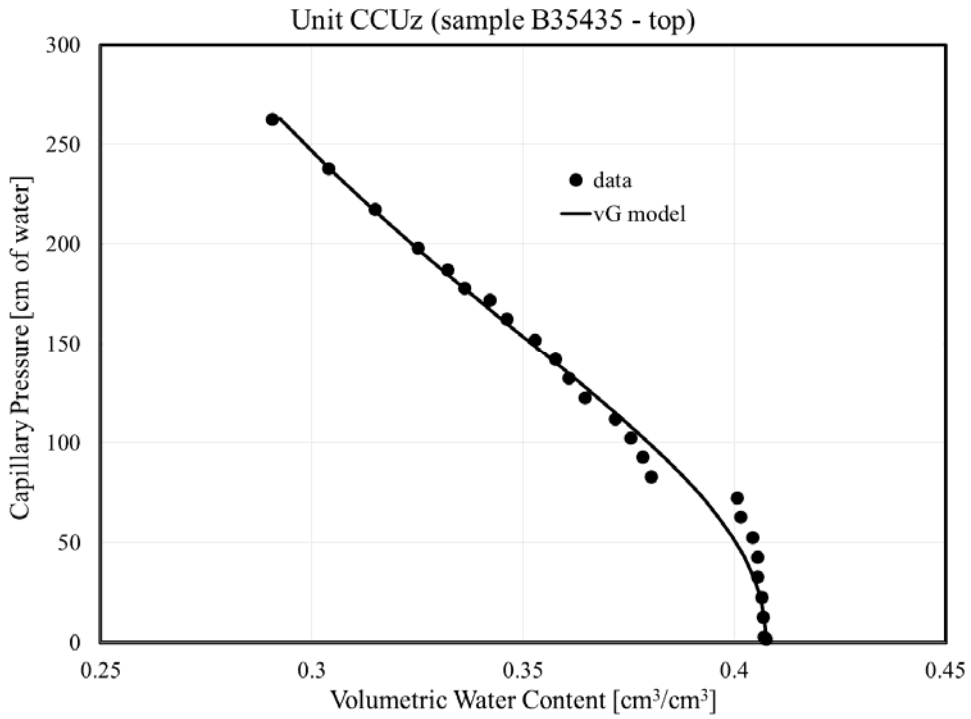

Figure 22. Selected values of average water content and capillary pressure fit to the van Genuchten (1980) model for a sample of the CCUz unit (HEIS sample B35435).

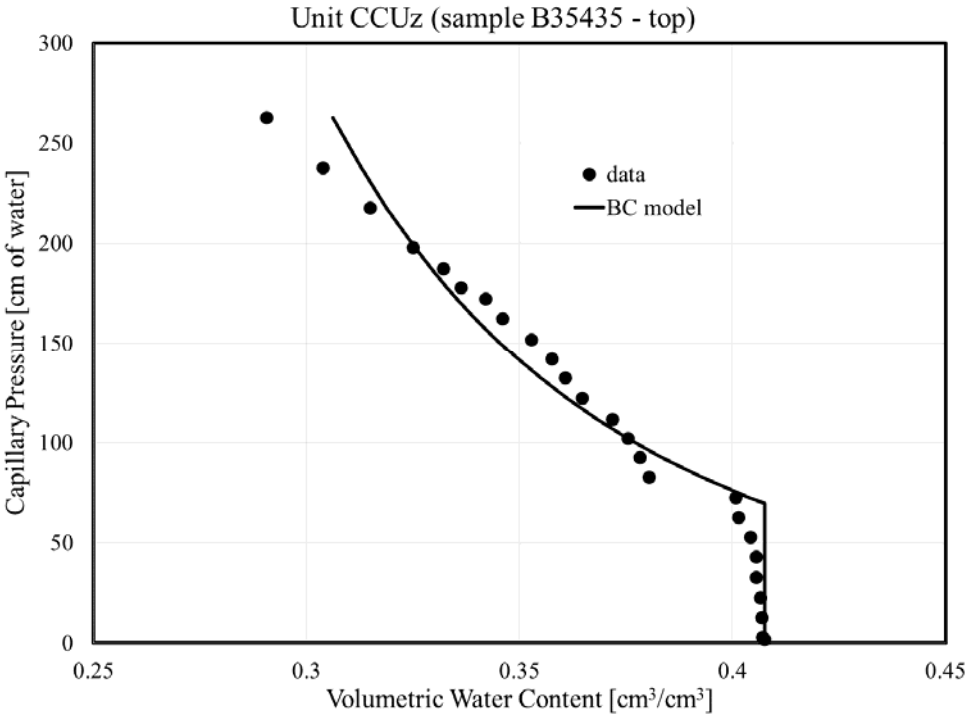

Figure 23. Selected values of average water content and capillary pressure fit to the Brooks-Corey (1964) model for a sample of the CCUz unit (HEIS sample B35435).

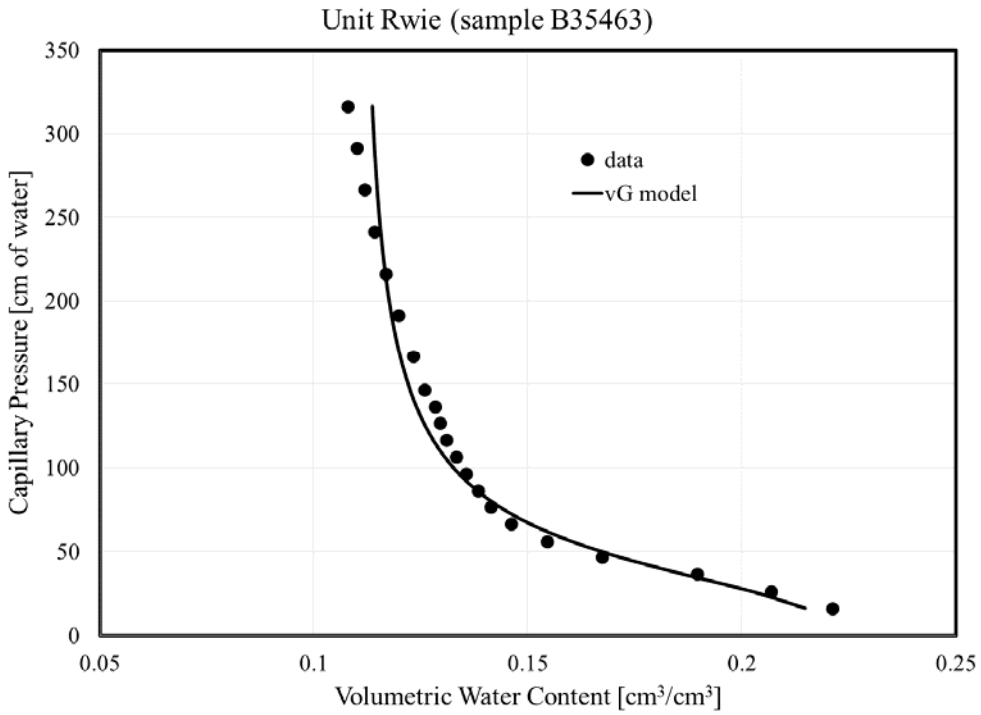

Figure 24. Selected values of average water content and capillary pressure fit to the van Genuchten (1980) model for a sample of the Rwie unit (HEIS sample B35463).

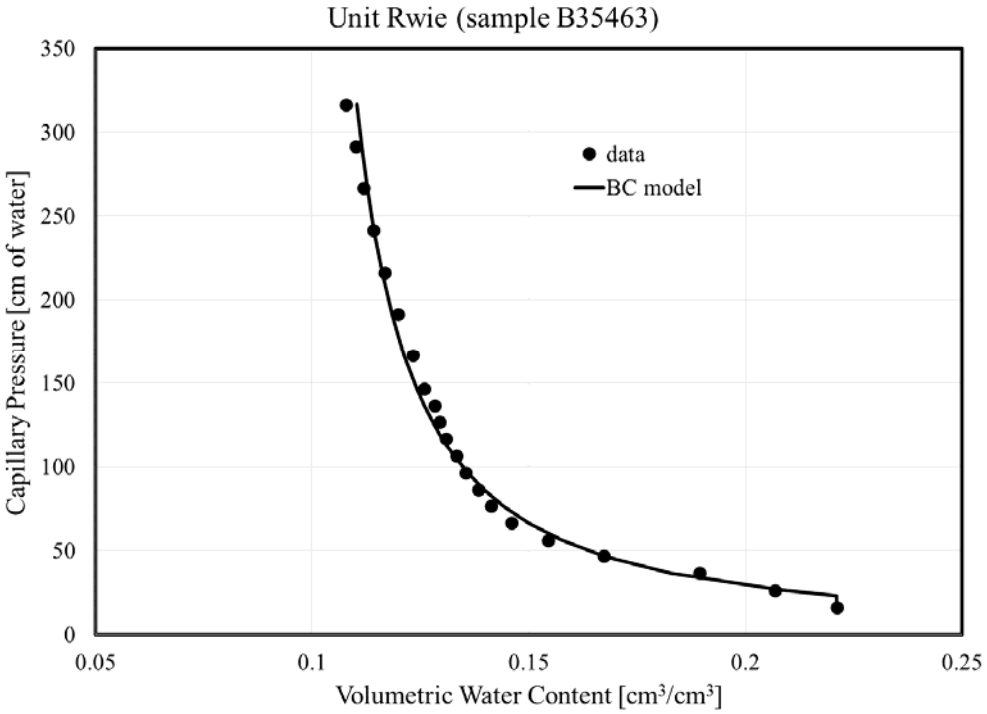

Figure 25. Selected values of average water content and capillary pressure fit to the Brooks-Corey (1964) model for a sample of the Rwie unit (HEIS sample B35463).

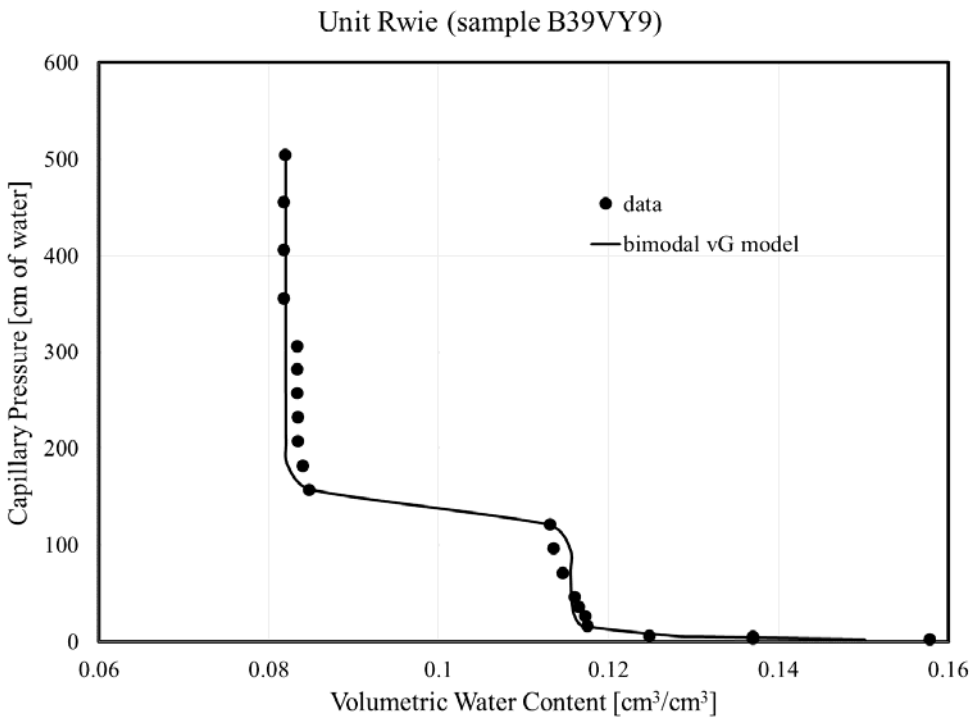

Figure 26. Selected values of average water content and capillary pressure fit to a bimodal van Genuchten-type model for a sample of the Rwie unit (HEIS sample B39VY9).

Table 3 lists the van Genuchten (1980) and Brooks-Corey (1964) model water retention parameters determined using selected average capillary pressure and volumetric water data from the multistep outflow experiments. Saturated water contents, θ_s, were fixed at water content values corresponding to near-zero capillary pressure, while the θ_r, α, and n parameters were fit. The residual saturation parameter, $S_r = \theta_r/\theta_s$, is tabulated because it is an input parameter for the STOMP simulator (White and Oostrom 2006). The θ_s parameters in Table 3 are equivalent to the "diffusive" porosity used by STOMP. Note that the parameters for the bimodal van Genuchten model fit to the data from sample B39VY9 (Figure 27) are not listed in Table 3 due to the increased number of parameters, but are provided in the text with the discussion for Figure 27.

Table 3. van Genuchten (1980) and Brooks-Corey (1964) model water retention parameters estimated using selected capillary pressure and water content data from multistep outflow experiments performed on intact core samples from 200-DV-1.

van Genuchten model							
Formation	Sample ID	θ_s[(a)]	θ_r	S_r[(b)]	α [1/cm]	n	SSE[(c)]
Rwie	B35463	0.221	0.1102	0.4984	0.0254	2.6566	0.0003
	B39VY9	0.157	0.06	0.3821	0.212	1.3136	0.0017
Rtf	B39X68	0.391	0.1616	0.4133	0.0051	3.831	0.0004
CCUz	B35435 (top)	0.4075	0.1265	0.3104	0.0049	2.1334	0.0003
	B35435 (bottom)	NA	NA	NA	NA	NA	NA
CCUz (perching silt)	B355M1 (top)	NA	NA	NA	NA	NA	NA
	B355M0 (bottom)	NA	NA	NA	NA	NA	NA
CCUc	B39X53	NA	NA	NA	NA	NA	NA
	B39VV7	0.389	0.2533	0.6512	0.0092	5.9423	0.0003
CCUg	B39M11	0.2224	0.09	0.4047	0.0296	2.7272	0.0001
Brooks-Corey model							
Formation	Sample ID	θ_s	θ_r	S_r	h_b [cm]	λ	SSE
Rwie	B35463	0.221	0.0931	0.4213	23.07	0.7667	0.0001
	B39VY9	0.157	0.0244	0.1554	1.8	0.1515	0.0021
Rtf	B39X68	0.391	0	0	118.77	0.59	0.0002
CCUz	B35435 (top)	0.4075	0	0	69.72	0.2156	0.0009
	B35435 (bottom)	NA	NA	NA	NA	NA	NA
CCUz (perching silt)	B355M1 (top)	NA	NA	NA	NA	NA	NA
	B355M0 (bottom)	NA	NA	NA	NA	NA	NA
CCUc	B39X53	NA	NA	NA	NA	NA	NA
	B39VV7	0.389	0.2436	0.6262	83.26	2.3951	0.0002
CCUg	B39M11	0.2224	0.0814	0.3360	20.55	0.9514	0.0001

(a) θs values were fixed at water contents corresponding to near-zero capillary pressure.
(b) $Sr = \theta r/\theta s$
(c) SSE = sum-of-squared error
NA = Not available; experiment was either not performed or was unsuccessful due to air leaks or other problems.

A notable observation from Table 3 is that significantly different values of S_r were obtained for some of the same samples when using the van Genuchten versus Brooks-Corey models. For example, the fitted S_r values for Rtf (B39X68) and CCUz (B35435 (top) samples are equal to zero for the Brooks-Corey model and greater than 0.3 for the van Genuchten model. These differences are attributed primarily to the lack of water retention data for higher capillary pressures. The character of the water retention data, combined with the differences in the functional forms of the van Genuchten and Brooks-Corey models, are such that significantly different estimates of the S_r parameters were obtained for these samples. Some of the parameters in these water retention functions also tend to be correlated so that a low value of S_r may be offset by a change in the h_b and λ parameters, or in the α and n parameters, for the Brooks-Corey and van Genuchten models, respectively. If additional water retention data for higher capillary pressures were available, the fitted values of the S_r parameters for the Brooks-Corey and van Genuchten would likely be more similar. The fitted S_r values for the van Genuchten and Brooks-Corey models could be forced to be more similar by giving increased weight to the lowest water content data points, but this was not done here. Another observation from Table 3 is that significantly different values of all water retention

parameters were obtained for samples B35463 and B39VY9, which are both from unit Rwie. This result is presumably due to the natural spatial variability and nonuniformity of the sediments.

Multistep outflow experiments were not performed on all of the intact cores selected for characterization. For example, a multistep outflow experiment was not performed on sample B35435 (bottom) because XMT imaging suggested that it was very similar to sample B35435 (top), so results were not expected to differ substantially. Experiments were not performed on sample B38X53 because it was contaminated with methyl isobutyl ketone (MIBK), a solvent that was used in the REDOX process for Pu separation. MIBK is corrosive to plastics and active corrosion and associated cracking of the Lexan liner for core B38X53 was observed in the laboratory. A multistep outflow experiment was not performed on this sample out of concern that the cracked liner would leak under pressure.

Two of the multistep outflow experiments were also unsuccessful. Multistep outflow experiments were initiated on the CCU perching zone silt samples (B355M0, B355M1), but very little water could be removed from these samples after a prolonged period at relatively high air pressures (>300 cm water equivalent), so the experiments on these samples were discontinued after consultation with CHPRC. Saturated hydraulic conductivity measurements were repeated on these cores after the multistep experiments were stopped, at the request of CHPRC/Intera, because the original saturated hydraulic conductivity values determined for these cores were thought to be too large, based on calculations reported by Oostrom et al. (2013). The repeated Ksat measurements were, however, approximately one-order-of-magnitude greater than the original measurements, so results from the repeated measurements are not shown in Table 2. XMT images of the CCU perching zone silt samples were collected after termination of the multistep outflow experiments in an attempt to determine why larger volumes of water could not be removed from these core samples during the multistep outflow experiments, and why the Ksat values increased.

Figure 27 and Figure 28 show a series of XMT image slices through CCUz unit samples B355M0 and B355M1, respectively. Small cracks can be seen in the sediments of both cores. We speculate that the CCUz perching silt has a metastable structure (Tadepalli et al. 1992) that compressed slightly at higher gas pressures, leading to the formation of cracks and subsequent bypassing of water flow around some of the soil matrix when the Ksat measurements were repeated. The specific causes for the inability to remove more water from these cores during the multistep outflow experiments are unknown, but may have been due to unidentified air leaks and/or partial clogging of the porous plates at the bottom of the cores.

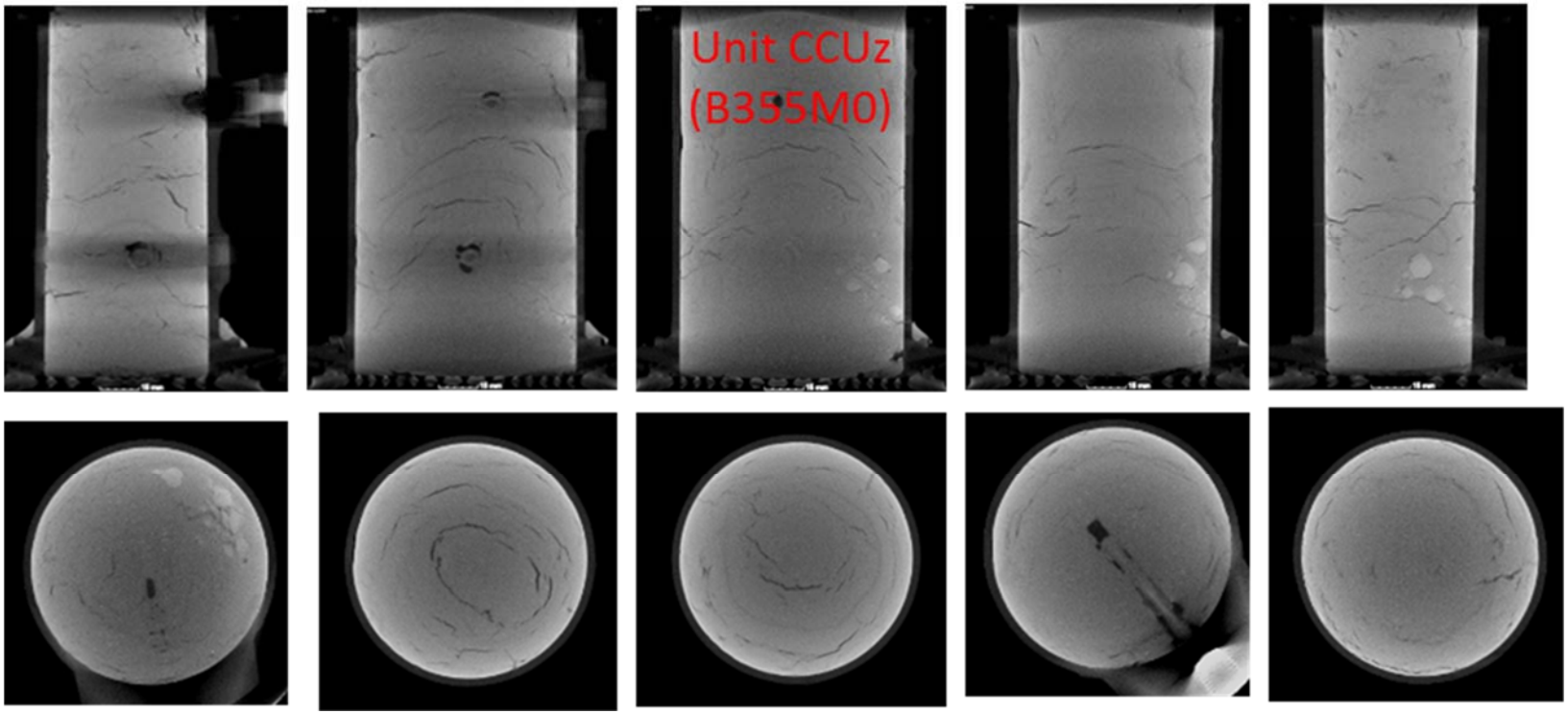

Figure 27. XMT images showing vertical and horizontal slices through a core sample of unit CCUz (sample B355MO).

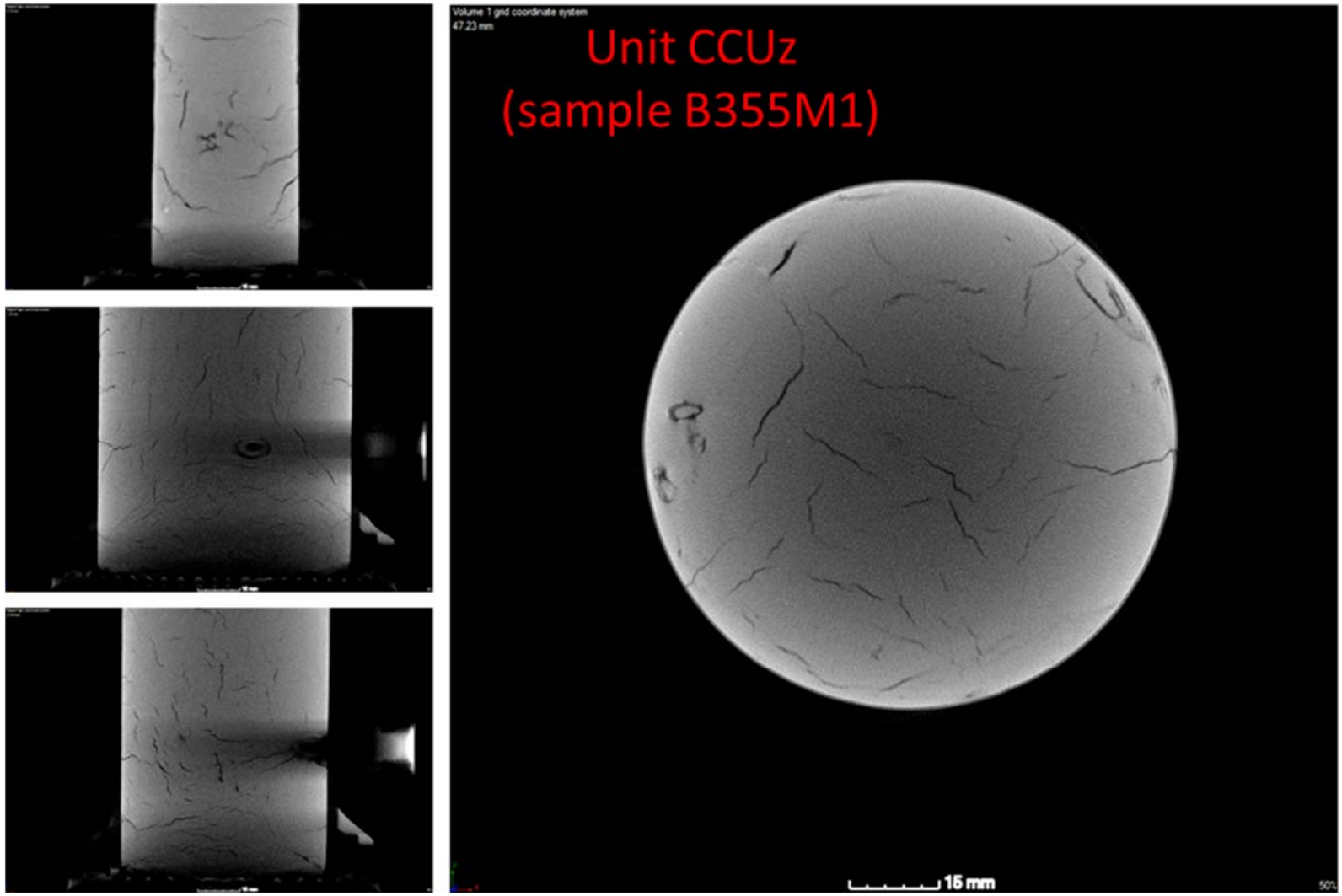

Figure 28. XMT images showing vertical and horizontal slices through a core sample of unit CCUz (sample B355M1).

Photographs of the bottom of core sample B355M0 and the top of core sample B355M1, with end caps removed, following termination of the multistep outflow experiments, are shown in Figure 29 and Figure 30, respectively. No major defects are evident from the photographs, but some of the fractures seen in the XMT for core B355M1 can also be seen in the photograph of this core.

Figure 29. Photograph of the bottom of core B355M0, with end cap removed, after termination of the multistep outflow experiment.

Figure 30. Photograph of the top of core B355M1, with end cap removed, after termination of the multistep outflow experiment.

The failure rate of tensiometers during the multistep outflow experiments was high, with 10 of 16, or ~62%, of tensiometers failing during the experiments. No single cause for failure was identified, but the rocky nature of some of the sediment samples probably led to stress on the porous cups of the tensiometers, and/or on the epoxy used to attach the porous cups to the body of the tensiometers, during installation. More robust stainless steel porous cups are available, but they have a lower bubbling pressure than the ceramic cups, so they were not used. In some cases tensiometer failure may have also been due to loss of hydraulic contact between the porous cup on a tensiometer and the porous media as it desaturated.

In summary, useful water retention data and associated model parameters were obtained for 6 of the 10 intact core samples that were initially selected for characterization in this study. One sample was not analyzed due to its similarity to the other half of the core from which it was cut. One sample was not analyzed due to contamination with MIBK and active corrosion and cracking of the Lexan liner that contained that core. Multistep outflow experiments were unsuccessful on two perched zone silt core samples owing to experimental problems, described in the preceding paragraphs. Water retention data from the successful multistep outflow experiments are tabulated in Appendix A.

3.1.2.2 Parameter Estimation by Inverse Modeling

STOMP-WA (White and Oostrom 2006), was used in conjunction with the parameter estimation software PEST (Doherty 2016) to estimate water retention parameters from transient outflow and pressure data obtained during the multistep outflow experiments. As noted previously, the “WA” in STOMP-WA stands for the –Water-Air operational mode of the code, which solves coupled mass conservation

equations for water and air. Due to the high tensiometer failure rate, and because of the very well-constrained boundary conditions that were applied in the multistep outflow experiments, inverse modeling was performed in some cases using only transient water outflow data as observations. Of the variables that are monitored during a multistep outflow experiment, the cumulative water outflow volume, is the most robust and least error-prone measurement that is collected. Note that all inverse parameter estimation results reported here are For Information Only (FIO) because the version of STOMP-WA that was used has not yet been qualified for use under the quality assurance (QA) program for this project.

Figure 31 shows observed and simulated aqueous pressures and cumulative water outflow volumes for a core sample of unit Rwie (sample B35463). Convergence difficulties were encountered with STOMP-WA when using both the aqueous pressure and outflow data for this sample, so inverse modeling was performed using only the cumulative water outflow data as observations.

Figure 32 shows observed and simulated aqueous pressures and cumulative water outflow volumes for a core sample of unit Rtf (sample B39X68). Aqueous pressure data from the upper and lower tensiometers and cumulative water outflow data were used as observations for inverse parameter estimation.

Figure 33 shows observed and simulated aqueous pressures and cumulative water outflow volumes for a core sample of unit CCUg (sample B39M11). Only the cumulative water outflow data were used as observations for inverse parameter estimation.

It should be noted that when the sediment within a core sample is very heterogeneous, it is difficult to match both the aqueous pressure and water outflow data well at all times. Improvement in the correspondence between measured and modeled results can be obtained sometimes by applying different weights to the data. When both pressure and outflow data were used, the weights applied to the pressure and outflow data points were typically 1 and 100, respectively. Larger weights were applied to the outflow data to compensate for the smaller magnitude of the outflow data values (mL) relative to those of the aqueous pressure data (Pa), so that the observed pressure data would not dominate in the parameter estimation process. When only outflow data were used, all values were given a weight of 1 except for the last value, which was given a weight of 10. A larger weight was given to the last cumulative outflow volume data point in order to achieve closer correspondence between observed and simulated cumulative outflow volumes at the end of the experiment (cf. Figure 33).

Parameter estimates based on the inverse modeling results shown in Figure 31 through Figure 33 are listed in Table 4. Convergence difficulties were encountered with STOMP-WA for the datasets from the other intact core samples, so results for all samples are not shown. Note that parameters were estimated for only the van Genuchten (1980) model since earlier results indicated that the van Genuchten and Brooks-Corey models provide comparable fits to the experimental data.

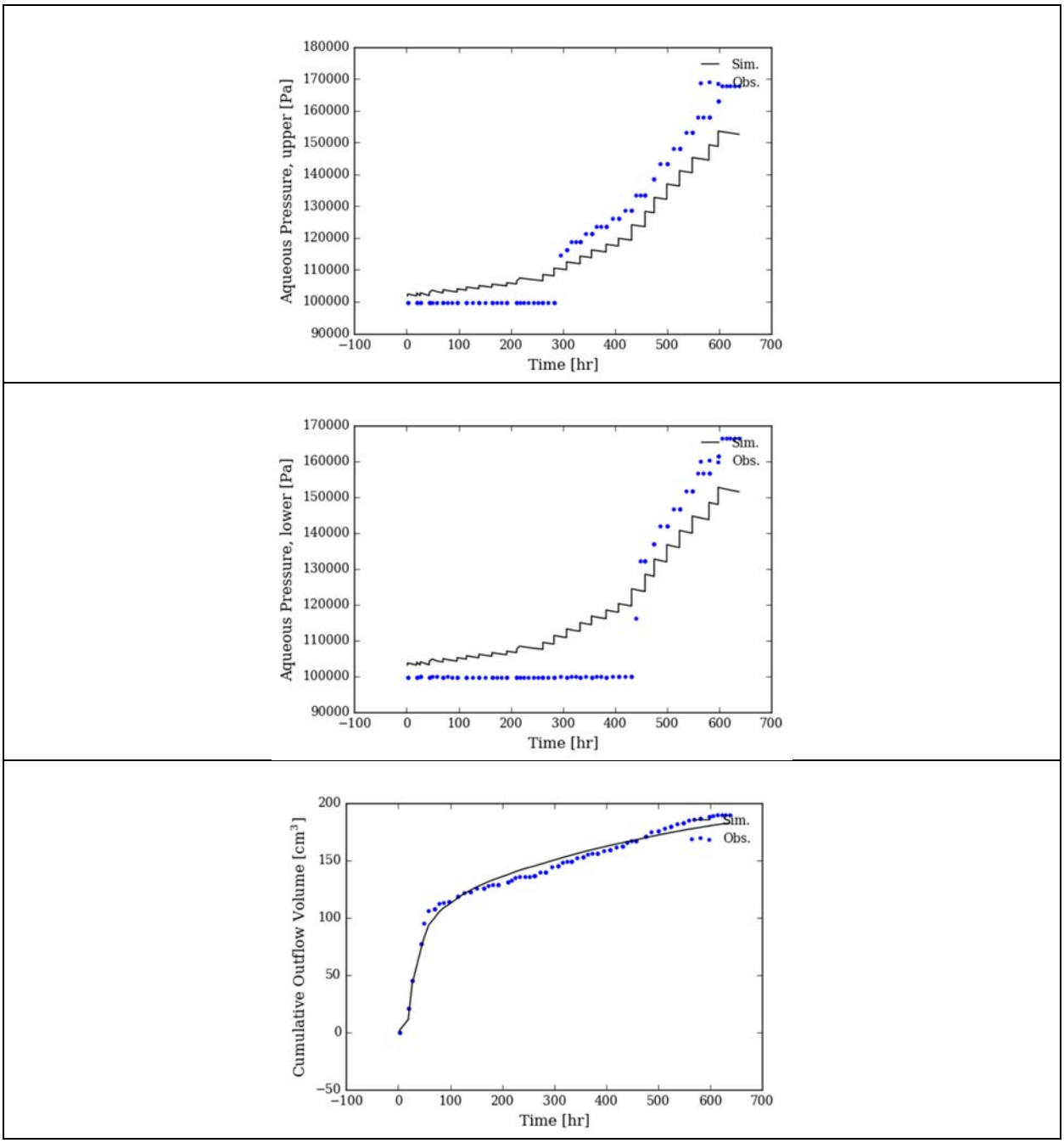

Figure 31. Observed and simulated aqueous pressures (top two plots) and cumulative water outflow volumes (bottom plot) for the multistep experiment performed on an intact core sample from unit Rwie (sample B35463). Only cumulative water outflow data were used as observations for inverse parameter estimation. Data presented in the figure are FIO.

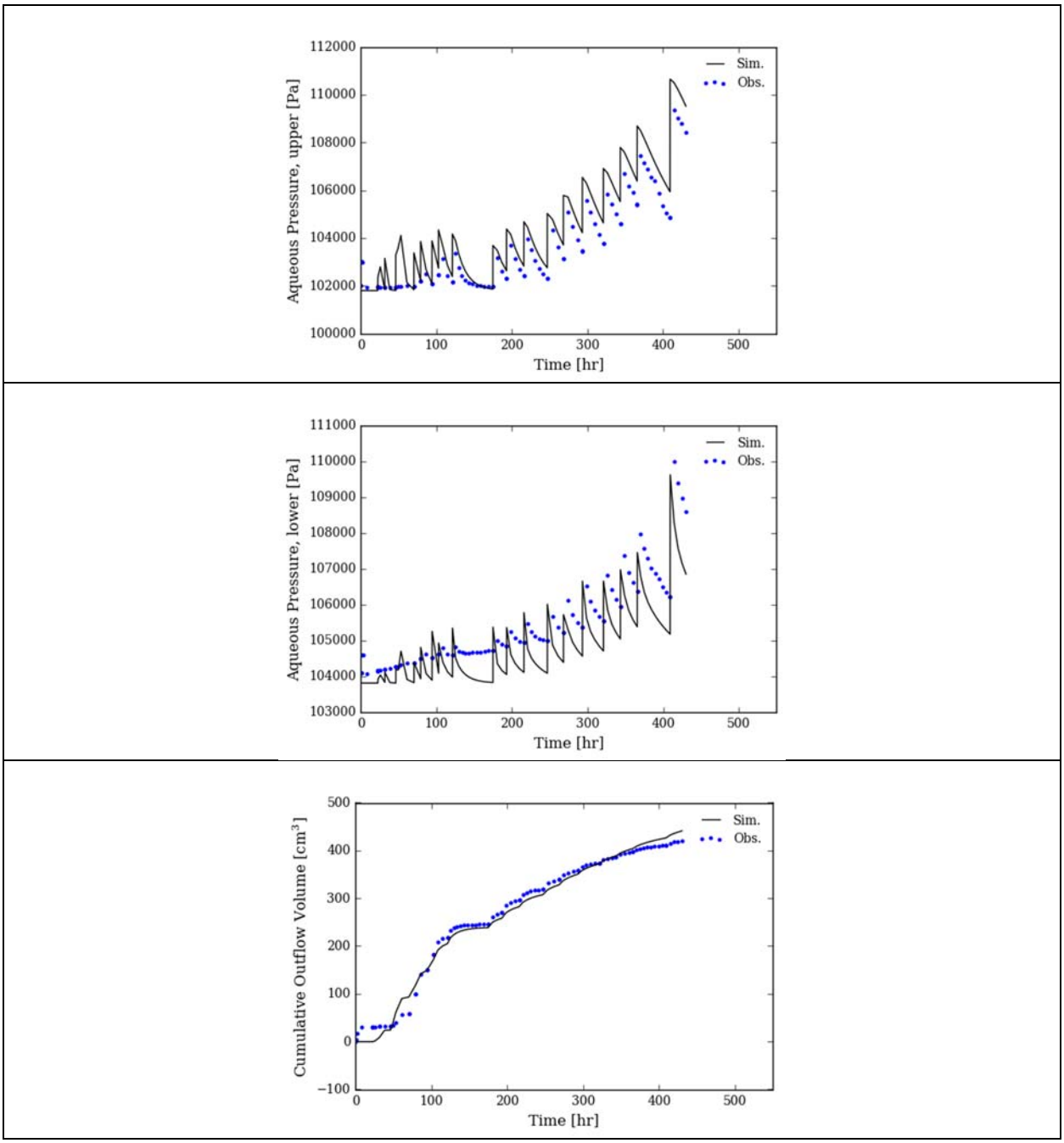

Figure 32. Observed and simulated aqueous pressures (top two plots) and cumulative water outflow volumes (bottom plot) for the multistep experiment performed on an intact core sample from unit Rtf (sample B39X68). Aqueous pressure data from two tensiometers and cumulative water outflow data were used for inverse parameter estimation. Data presented in the figure are FIO.

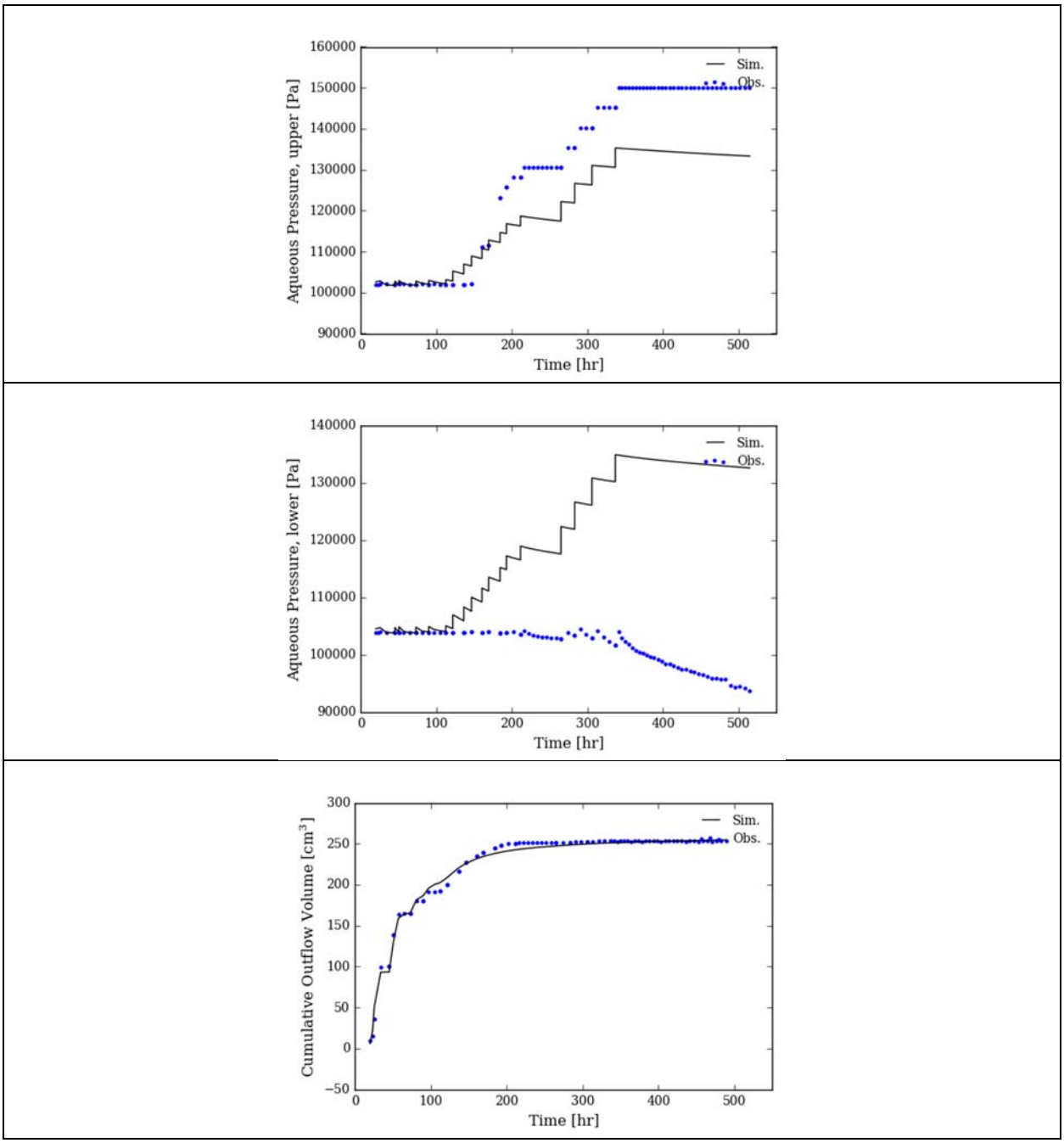

Figure 33. Observed and simulated aqueous pressures (top two plots) and cumulative outflow volumes (bottom plot) for the multistep experiment performed on an intact core samples from unit CCUg (sample B39M11). Only cumulative water outflow data were used as observations for inverse parameter estimation. Data presented in this figure are FIO.

Table 4. van Genuchten (1980) model water retention parameters estimated by inverse modeling of multistep outflow experiments performed on intact core samples from 200-DV-1. Parameters in this table are FIO.

van Genuchten model							
Formation	Sample ID	θ_s[(a)]	θ_r	S_r[(b)]	α [1/cm]	n	R
Rwie	B35463	0.221	4.03e-5	1.37e-4	0.1068	1.2962	0.991
Rtf	B39X68	0.391	9.53e-4	2.44e-3	0.0046	2.2329	0.999
CCUg	B39M11	0.2224	0.0777	0.345	0.0277	2.9321	0.999

(a) θ_s values were fixed.
(b) $S_r = \theta_r / \theta_s$
R = correlation coefficient

Inverse modeling of multistep outflow experiments is generally considered to be the gold standard for estimating hydraulic parameters for variably-saturated porous media. This approach usually works well for relatively uniform porous media with intermediate ranges of textures. Experiments and subsequent analysis can be problematic for porous media that very coarse, very fine, or highly heterogeneous within a core sample. If the sediment is very coarse-textured, or contains significant fractions of gravel or cobble, it can be difficult to install tensiometers without damaging them. For very coarse-textured porous media it may also be difficult to maintain good hydraulic contact between the porous cups on the tensiometers and the porous media as the core desaturates during an experiment. If the sediment is very fine-textured, it may take a long time for the system to equilibrate after a change in air pressure. The multistep outflow experiments for the current study took between approximately 400 hours (16 days) and 1000 hours (41 days) to perform, depending on the sample.

Parameters estimated by inverse modeling utilize dynamic or time-dependent aqueous pressures and/or cumulative water outflow data as observations, and model boundary conditions are specified to match those that are imposed during the experiments. In contrast, the water retention data and fitted functions depicted in Figure 14 through Figure 26 were computed from data representing the end of each pressure step, which are assumed to represent quasi-static equilibrium conditions. These differences may result in different estimates of water retention parameters, as shown in Table 3 and Table 4.

Figure 34 shows the quasi-static water retention data and van Genuchten (1980) model fit for sample B35463 (unit Rwie), together with a curve representing a van Genuchten (1980) model function based on parameters estimated by inverse modeling (cf. Figure 31). For this sample, there is clearly a significant difference between the water retention functions generated by the two approaches. It should be emphasized that the dashed curve, representing parameters generated by inverse modeling, was not fit to the quasi-static water retention data shown in this figure, but instead used the dynamic cumulative water outflow data from the experiment as observations (bottom plot in Figure 31). Parameters estimated by inverse modeling in this case were generated by minimizing the differences between measured (or observed) and simulated cumulative water outflow volumes.

Figure 35 shows the quasi-static water retention data and van Genuchten (1980) model fit for sample B39X68 (unit Rtf), together with a curve representing a van Genuchten (1980) model function based on parameters estimated by inverse modeling (cf. Figure 32). Again, there is a significant difference between the water retention functions generated by the two approaches. In this case, the dashed curve, representing parameters generated by inverse modeling, was generated using dynamic aqueous pressure and cumulative water outflow data from the experiment as observations (Figure 32). Parameters estimated by inverse modeling in this case were generated by minimizing the differences between measured (or observed) and simulated aqueous pressures and cumulative water outflow volumes.

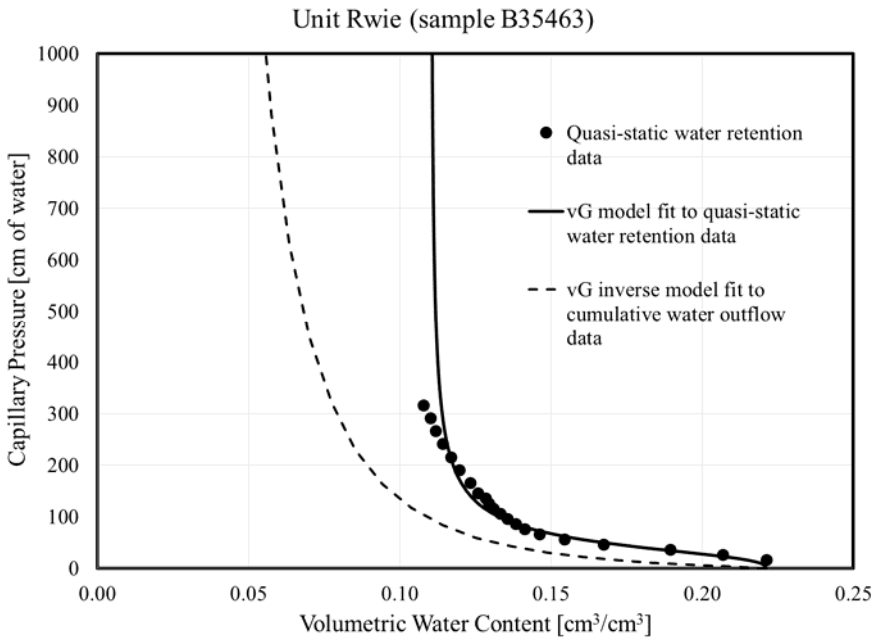

Figure 34. Selected values of quasi-static water retention data fit to the van Genuchten (1980) model, and water retention curve based on inverse modeling using cumulative water outflow data, for a sample of the Rwie unit (sample B35463).

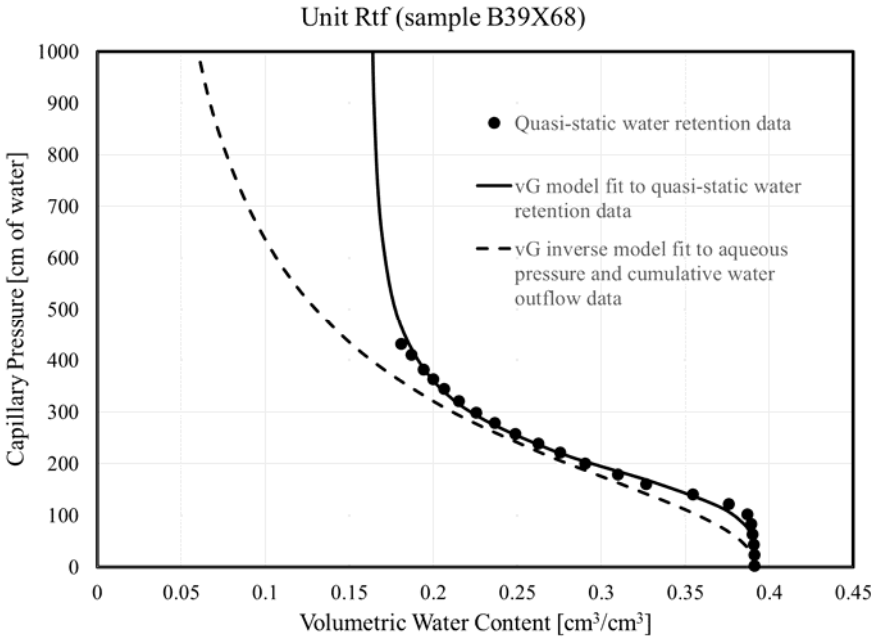

Figure 35. Selected values of quasi-static water retention data fit to the van Genuchten (1980) model, and water retention curve based on inverse modeling using aqueous pressure and cumulative water outflow data for a sample of the Rtf unit (sample B39X68).

Figure 36 shows the quasi-static water retention data and van Genuchten (1980) model fit for sample B39M11 (unit CCUg), together with a curve representing a van Genuchten (1980) model function based on parameters estimated by inverse modeling (cf. Figure 33). There are significant differences between the water retention functions generated by the two approaches, but they are closer than in the previous two cases. In this case, the dashed curve, representing parameters generated by inverse modeling, was generated using dynamic cumulative water outflow data from the experiment as observations (Figure 33). Parameters estimated by inverse modeling in this case were generated by minimizing the differences between measured (or observed) and simulated cumulative water outflow volumes.

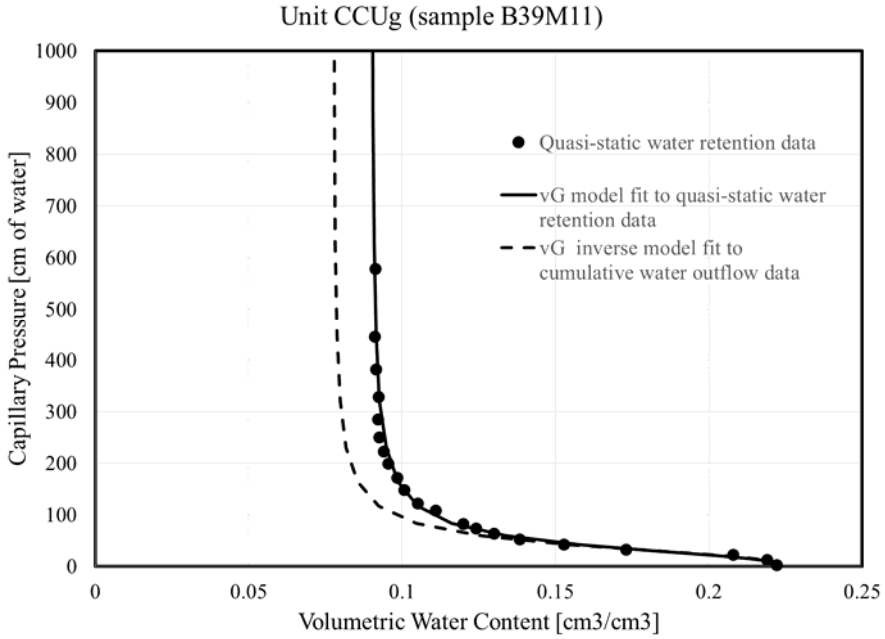

Figure 36. Selected values of quasi-static water retention data fit to the van Genuchten (1980) model, and water retention curve based on inverse modeling using cumulative water outflow data for a sample of the CCUg unit (sample B39M11).

In all three cases (Figure 34, Figure 35, and Figure 36), the values of the S_r and n parameters estimated by inverse modeling are smaller than those that were determined by fitting the quasi-static water retention data. The α parameters estimated by inverse modeling are similar to those estimated by fitting the quasi-static water retention data for 2 of the 3 samples (B39X68 and B39M11), but the inverse parameter estimate of α for one sample (B35463) is larger than that which was generated by fitting the quasi-static water retention data (see Table 3 and Table 4).

When comparing the data and curves shown in Figure 34, Figure 35, and Figure 36, it should be noted that the pressure data used to generate the quasi-static water retention data represent measurements at one to three discrete measurement points within a core. These data were used to determine average values for pairing with the average water content values computed from the water outflow data. If, for example, the lower and middle tensiometers failed during an experiment, such that only the upper tensiometer could be used to estimate the capillary pressure for the core, then the capillary pressures assigned to go with the water content values could be larger than the mean or average capillary pressure for the core (cf. Figure 13). Furthermore, if pressure equilibrium conditions were not achieved prior to increasing the air pressures during the multistep outflow experiments, the water content values ascribed to given pressures

could be larger than the true equilibrium water contents. Issues like these may be responsible, in part, for the differences in the plotted water retention functions shown in Figure 34 through Figure 36.

These comparisons raise the question of which water retention parameters are more accurate or reliable. Parameters estimated from inverse modeling of the multistep outflow experiments (Table 4) should usually be preferred. As noted previously, since a two-phase flow simulator was used to solve the forward flow problem, and since the boundary conditions for the experiments can be well-prescribed for the model, use of only water outflow data as observations for inverse parameter estimation is still expected to yield reasonable results for those cases in which only the outflow data were used. For multistep outflow experiments in which problems were encountered with the inverse modeling for the current study, the parameters generated using the quasi-static water retention data can be used (Table 3). Future work will attempt to identify and mitigate the specific causes for convergence difficulties in STOMP-WA for problematic multistep experimental data sets. Alternative tensiometers will also be tested to develop improved designs that will potentially increase their reliability for future experiments.

3.1.2.3 Relative Permeability

One of the most important properties of vadose zone sediments is the unsaturated hydraulic conductivity. The Mualem (1980) and Burdine (1964) models use different assumptions regarding the connectivity and tortuosity of pores. Given the differences in these models, and the differences in water retention parameters for the van Genuchten model generated using the quasi-static water retention data versus inverse modeling of dynamic data from the multistep outflow experiments, it is of interest to know how predicted relative permeabilities or relative hydraulic conductivities may differ.

All of the samples analyzed in this study are from formations that underlie the Hanford fm, and are therefore closer to the water table. Capillary pressures at the depths of these formations are expected to be less than 1000 cm, and probably less than 400 cm, depending on recharge rates. Figure 37 through Figure 42 show the predicted relative hydraulic conductivities, K/Ks, generated using Eqs. (4) and (6) with the parameters from Table 3 and Table 4. For the most part, the relative hydraulic conductivities generated by the different models and parameter estimation methods differ by less than one-order-of-magnitude for capillary pressures less than 300 cm. Differences increase at larger capillary pressures.

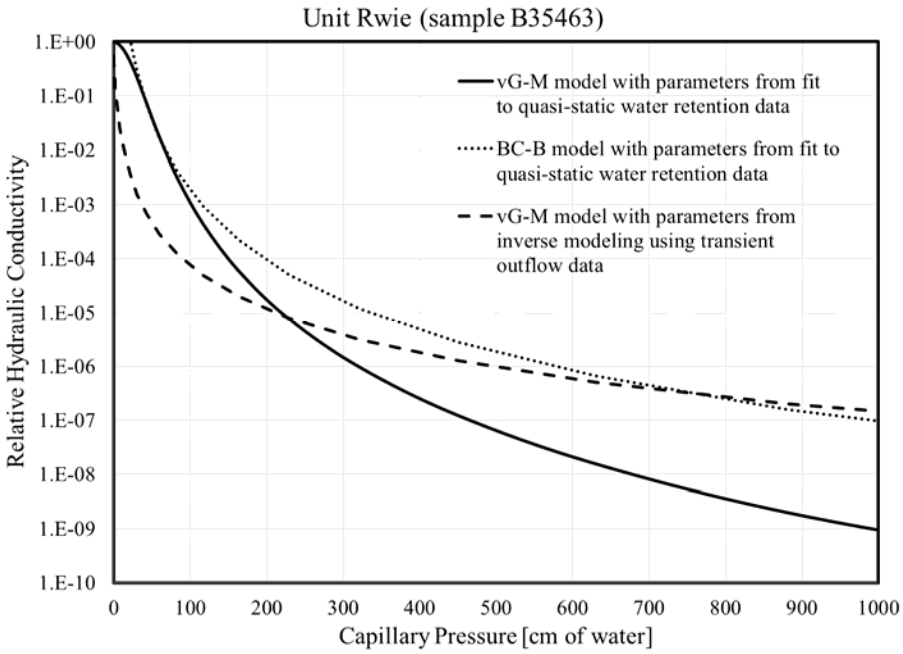

Figure 37. Relative hydraulic conductivity versus capillary pressure predicted by the van Genuchten-Mualem (vG-M) and Brooks-Corey-Burdine (BC-B) models for unit Rwie (sample B35463).

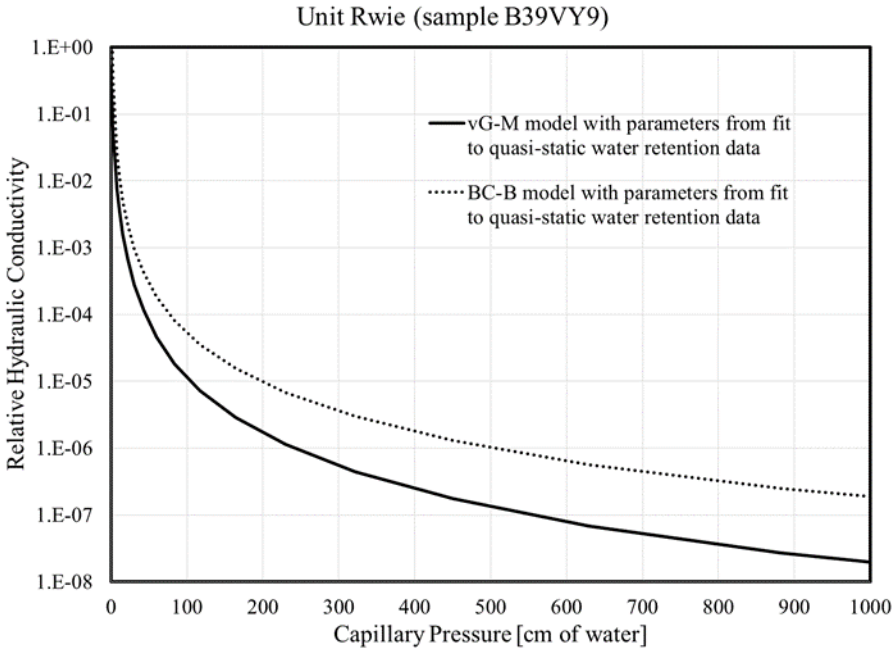

Figure 38. Relative hydraulic conductivity versus capillary pressure predicted by the van Genuchten-Mualem (vG-M) and Brooks-Corey-Burdine (BC-B) models for unit Rwie (sample B39VY9).

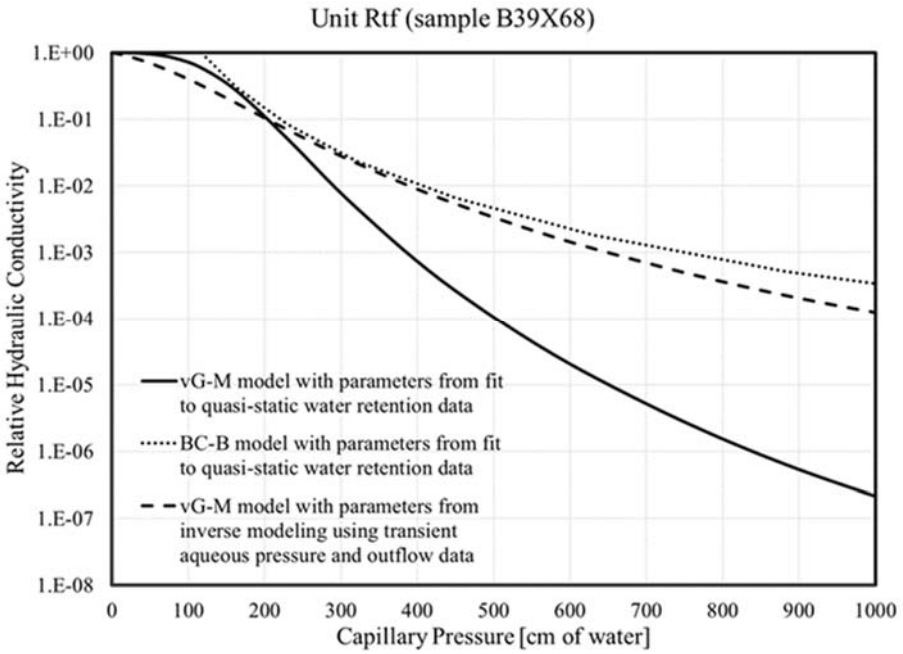

Figure 39. Relative hydraulic conductivity versus capillary pressure predicted by the van Genuchten-Mualem (vG-M) and Brooks-Corey-Burdine (BC-B) models for unit Rtf (sample B39X68).

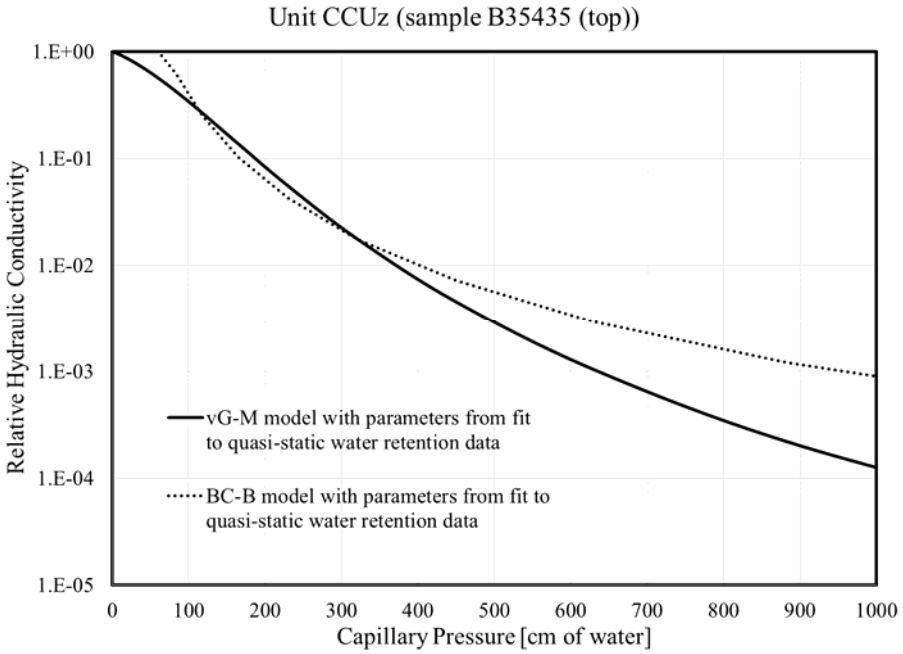

Figure 40. Relative hydraulic conductivity versus capillary pressure predicted by the van Genuchten-Mualem (vG-M) and Brooks-Corey-Burdine (BC-B) models for unit CCUz (sample B35435).

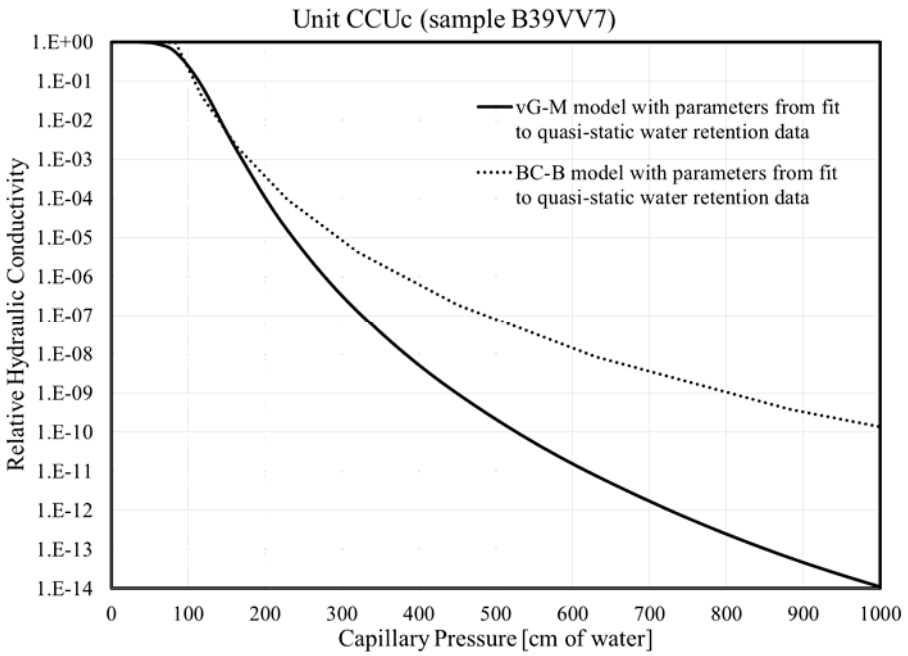

Figure 41. Relative hydraulic conductivity versus capillary pressure predicted by the van Genuchten-Mualem (vG-M) and Brooks-Corey-Burdine (BC-B) models for unit CCUc (sample B39VV7).

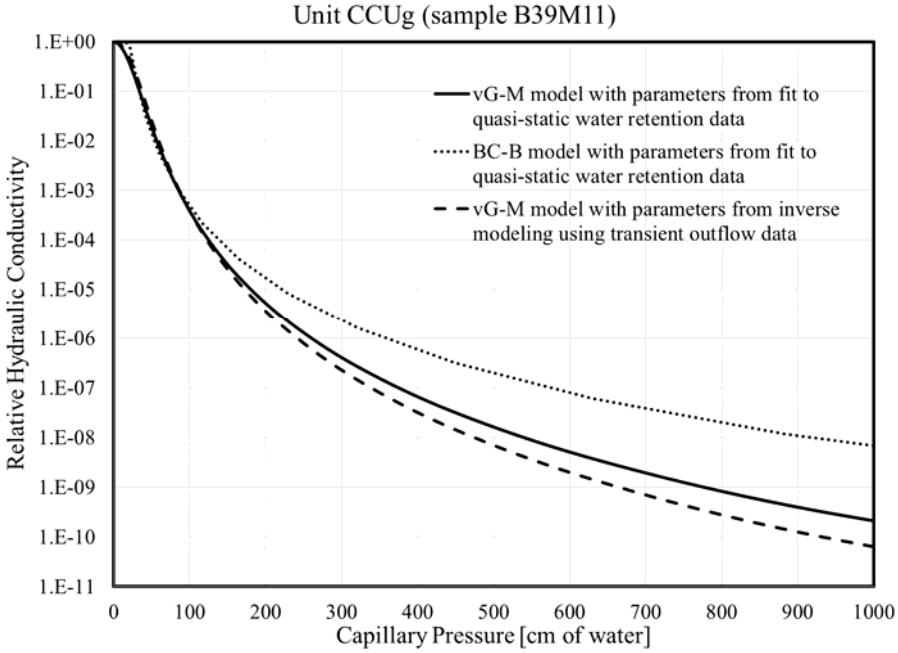

Figure 42. Relative hydraulic conductivity versus capillary pressure predicted by the van Genuchten-Mualem (vG-M) and Brooks-Corey-Burdine (BC-B) models for unit CCUg (sample B39M11).

3.2 Hydraulic Properties – Field Testing

Water extraction is being implemented for the B-Complex perched water as a removal action in the 200-DV-1 OU (DOE 2014, 2015). Results discussed in this section represent a summary of field-derived hydraulic/storage properties for the current PWA in the B-BX Tank Farm area of the B-Complex. These results were obtained from hydraulic tests (i.e., single-well slug tests and single/multi-well pumping tests) that were performed recently at PWA extraction wells 299-E33-344, 299-E33-350 and 299-E33-351. Results from these well tests were previously reported in Newcomer (2014) and DOE (2016a), are discussed in further detail in Appendix B of this report. Note that all results presented here (Section 3.2) are For Information Only (FIO), since they were originally generated on a different project that had different quality assurance requirements. The analytical results from the reported tests provide estimates for hydraulic and storage properties for the current PWA that is of limited areal extent. These results can be used as parameter input for numerical modeling to predict and optimize ongoing PWA dewatering operations.

3.2.1 PWA Hydrogeologic Conditions

General hydrogeologic conditions for the PWA (i.e., associated hydrogeologic units, aquifer formation and lateral extent, etc.) within the central plateau area (B-BX Tank Farm Complex) of the Hanford Site have been previously described in a number of reports (e.g., Serne et al. 2010; Truex et al. 2013). Briefly stated, the primary hydrogeologic units comprising the PWA system include the CCUz-sand (the aquifer unit comprised of silty sand), and overlying and underlying low-permeability CCUz-lower and CCUz-upper units (primarily comprised of silt) (see Figure 43). Underlying the CCUz-lower perching layer is the CCUg, which generally exhibits higher permeability properties than the CCUz-sand and is part of the regional Hanford Site unconfined aquifer system.

As indicated in Figure 43, hydraulic head conditions within the underlying unconfined aquifer are significantly lower (i.e., approximately 9 m) than exhibited for the overlying PWA. Overlying the PWA $CCU_{z\text{-}sand}$ is the low permeability CCU silt, $CCU_{z\text{-}upper}$. Current hydraulic head conditions within existing wells completed in the PWA indicate water-table elevations slightly below the base of the $CCU_{z\text{-}upper}$ (i.e., approximately 1 m), indicating unconfined aquifer conditions for the PWA. This is supported by analysis of monitored PWA well response to observed barometric pressure fluctuations, as reported in DOE (2016a), and as summarized in Appendix B. As indicated in these reports, the barometric pressure response analysis indicates primarily an unconfined aquifer diagnostic pattern near the wells for the PWA, with possible aquifer confinement existing some distance away from these well site locations.

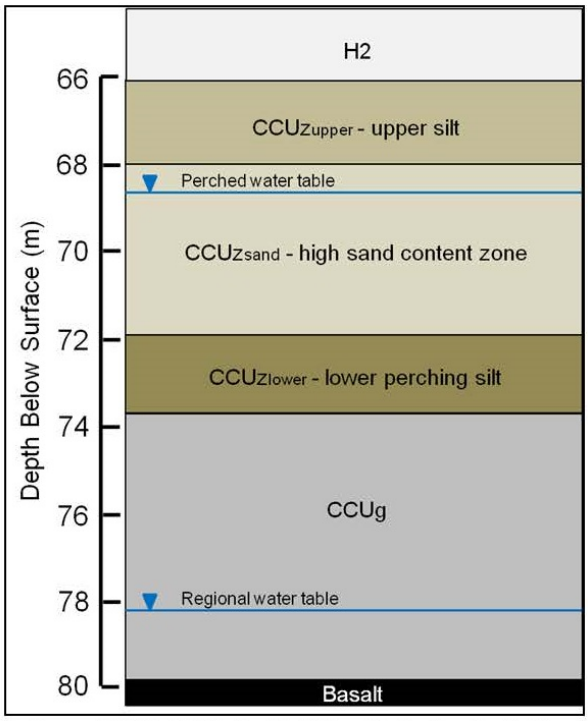

Figure 43. General hydrogeologic relationships in the vicinity of the three PWA test wells (Oostrom et al. 2013; Truex et al. 2013).

3.2.2 PWA Hydraulic Properties

Hydraulic properties reported here for the PWA are representative of the CCUz-sand, and were obtained from hydrologic tests conducted at PWA wells 299-E33-344, 299-E33-350, and 299-E33-351 during FY14, FY16, and FY17. Locations for these test wells and their areal relationship within the PWA and between the PWA well sites are shown in Figure 44 and Figure 45, respectively. Specifically, the hydraulic property values that are reported here for the PWA were obtained from slug tests conducted in 2014 during construction/well completion activities for wells 299-E33-350 and 299-E33-351 (Newcomer 2014); single-well pumping tests performed at these two wells and well 299-E33-344 during 2016 (DOE 2016a); and operational, multi-well pumping test analysis of the interference response observed during 2017 at monitor well 299-E33-344 during long-term, operational pumping activities that were initiated at extraction wells 299-E33-350 and 299-E33-351 (Appendix B). A summary of the hydraulic property estimate values derived from these characterization tests is presented in Table 5.

Table 5. Field-derived hydraulic/storage properties for the PWA, obtained from recently conducted hydraulic characterization tests, B-BX Complex Tank Farm area. This table is FIO.

Single-Well Slug Tests - 2014 (Newcomer 2014)						
Test Well	T (m^2/day)	K_h (m/day)	K_D (K_v/K_h)	S	S_y	Test Scale*
299-E33-350	1.65	0.58	0.012	NA	NA	local
299-E33-351	3.64	1.30	0.059	NA	NA	local
Single-Well Pumping Tests - 2016 (DOE 2016)						
Test Well	T (m^2/day)	K_h (m/day)	K_D (K_v/K_h)	S	S_y	Test Scale*
299-E33-344	0.51	0.13	0.036	1.33e-3	0.151	intermediate
299-E33-350	4.00	1.05	0.021	4.5e-3	0.273	intermediate
299-E33-351	3.49	0.91	0.012	9.0e-4	0.220	intermediate
Multi-Well Pumping/Interference Test - 2017 (qualitative sensitivity analysis)						
Test Well	T (m^2/day)	K_h (m/day)	K_D** (K_v/K_h)	S	S_y	Test Scale*
299-E33-344	0.01 – 1.41	0.03 – 0.37	0.003 – 0.1	2.6e-5 – 4.4e-3	0.102 – 0.372	large
Parameter Best Estimate Values (based on single-well slug and pumping tests; Newcomer 2014 and DOE 2016))						
Description	T (m^2/day)	K_h (m/day)	K_D** (K_v/K_h)	S	S_y	Test Scale*
Range	0.51 – 4.00	0.13 – 1.30	0.012 – 0.059	9.0e-4 – 4.5e-3	0.151 – 0.273	local - intermediate
Geometric Mean	2.12	0.62	0.023	2.38e-3	0.209	local - intermediate
Arithmetic Mean	2.66	0.79	0.028	2.91e-3	0.215	local - intermediate

* approximate test scale length designations: Local = 0.1 to 3 m; Intermediate = 0.1 to 10 m; Large = 0.1 to >30 m

** arbitrarily assigned K_D range for sensitivity analysis

NA not applicable; slug test method is not sensitive for delineating these hydrologic parameters

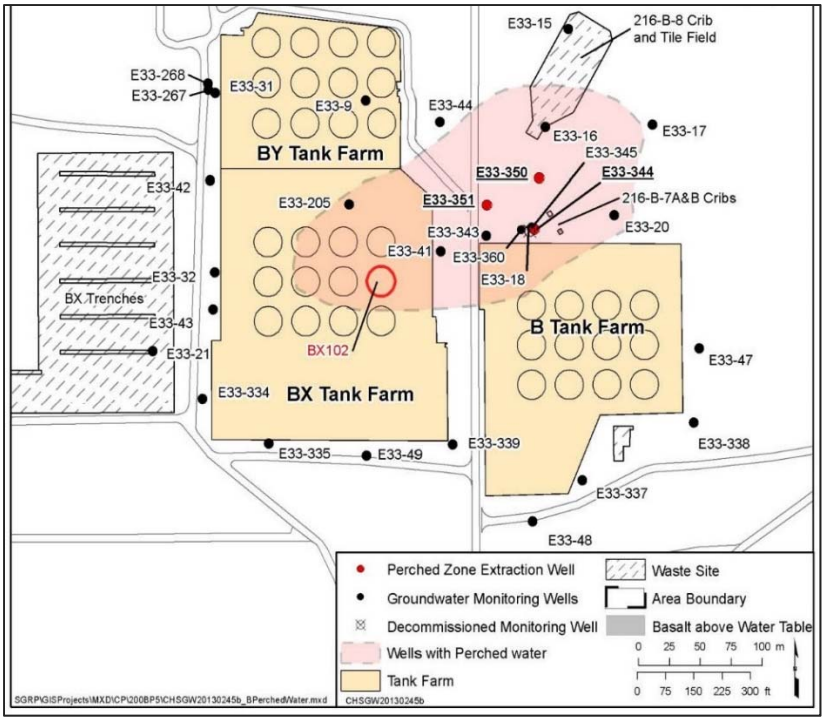

Figure 44. Relationship of PWA test wells 299-E33-344, E33-350, and E33-351 and their location to estimated PWA areal extent (Ref. SGW-59086).

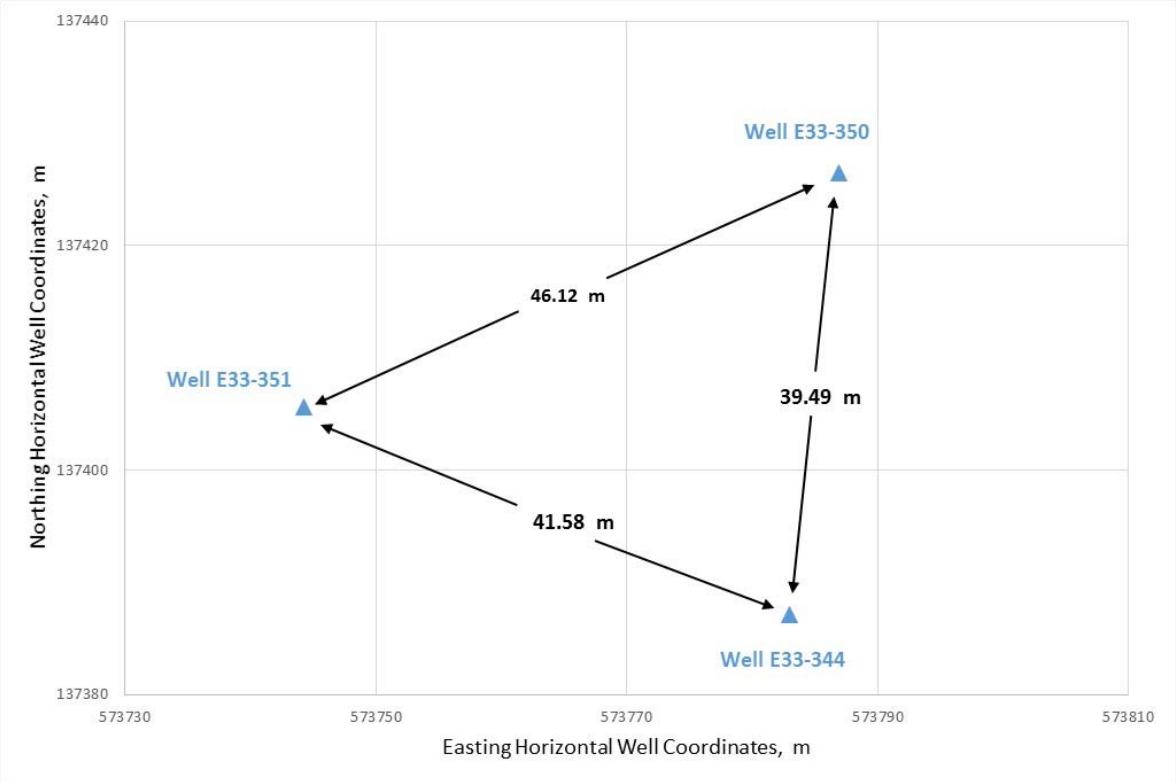

Figure 45. Distance relationship between PWA test wells 299-E33-344, E33-350, and E33-351. This figure is FIO.

As discussed in Appendix B, the hydraulic property estimates from the 2017 multi-well operational pumping test are qualitative in nature due to the number of technical and operationally-based issues identified in the collected monitor well data set. As such, the estimates derived from the 2017 test analysis are qualitative and are provided solely for comparative purposes, and should not be used as input for other quantitative hydrologic applications (e.g., parameter input to numerical model simulations).

3.2.2.1 Transmissivity/Hydraulic Conductivity

As shown in Table 5, similar transmissivity, T, and horizontal hydraulic conductivity, K_h, estimates for the PWA were obtained using single-well slug and pumping test analyses at individual PWA well site locations. The maximum difference exhibited at well 299-E33-350 (i.e., 2.4 factor variance) is approximately within the commonly cited expected variance (i.e., a factor variance of ~2) observed between slug and pumping test results, due to variations in hydraulic properties (with radial distance away from the test well location) and differences in hydrologic scale-of-investigation imposed by these tests (Butler 1996). Similar comparison relationship results between slug and pumping test characterizations for the Hanford Site regional unconfined aquifer have also been observed and reported in Spane et al. (2001a,b, 2002, 2003). As also noted in Butler (1998), a close correspondence between slug and pumping test property estimates (e.g., at well 299-E33-351) suggests a more uniform PWA hydraulic property condition away from the test well location. Given the stress/duration levels imposed by these tests and the hydraulic/storage characteristics of the PWA, the following approximate characterization tests scales are assigned for the respective test methods: slug tests = 0.1 to 3 m (local scale); pumping tests = 0.1 to 10 m (intermediate scale); and pumping interference tests = 0.1 to >30 m (large scale). Note that these approximate test scale designations are based on the relative *radius-of-investigation* of the respective characterization tests over which the estimated aquifer properties are assumed to be representative. These test-scale lengths are significantly less then the *radius-of-influence* imposed by the test methods, which represent the radial test distances over which a detectable test response (e.g., 0.02 m) might be observed.

A comparison of the hydraulic properties listed in Table 5 indicates a significant decrease in T and K_h for the PWA in the vicinity of test well 299-E33-344, in comparison to results obtained at the two other PWA test well locations. This lower hydraulic property condition is also supported by the lower range in hydraulic properties obtained from the sensitivity analysis conducted for the FY17 multi-well interference test that suggests a lower T and K_h condition for the PWA to the south and east of wells 299-E33-350 and 299-E33-351. Results from the single-well slug and pumping tests indicate a range for T and K_h that vary by a factor of 8 from 0.51 to 4.00 m^2/day and 0.13 and 1.05 m/day, respectively. Best estimate values for T and K_h for PWA modeling applications using both slug and pumping test results are 2.12 m^2/day and 0.62 m/day using the geometric mean as a basis, and 2.66 m^2/day and 0.79 m/day when based on the arithmetic mean.

It should be recognized that the cited K_h values listed are an average/uniform (i.e., equivalent hydraulic conductivity) assigned for the entire PWA saturated thickness, and specifically for the $CCU_{z\text{-}sand}$ unit. The slug test-derived K_h values were determined by the actual well, site-specific PWA saturated thickness observed at the well locations during well construction (i.e., ~ 3 m), while the pumping test determined K_h values were calculated based on an assumed, areally-weighted PWA thickness of ~3.8 m. Additionally (as reported in Newcomer 2014), vertical slug test profiling that was conducted at wells 299-E33-350 and 299-E33-351 during construction by systematically testing the lower half of the PWA and then the entire PWA thickness indicated that K_h ranged by a factor of ~7 at test well 299-E33-350 (upper zone = 0.27 m/day, lower zone = 1.92 m/day), and by a factor of ~2 at 299-E33-351 (upper zone = 2.38 m/day, lower zone = 1.26 m/day) This suggests a fair degree of variability in hydraulic properties, due to layering and lithofacies changes (e.g., silt content) that occurs vertically within the $CCU_{z\text{-}sand}$ unit.

3.2.2.2 Vertical Anisotropy

Hydraulic property measurements on vertically-oriented cores in the laboratory provide no information about anisotropy. Estimates of vertical anisotropy, K_D (where $K_D = K_v/K_h$), for the PWA can be obtained directly from field aquifer tests by analysis of well water-level response during pumping, as well as by comparing the results of laboratory core samples (i.e., K_v) with slug testing vertical K_h profile results.

K_D strongly impacts the well test response for constant-rate pumping tests conducted in perched-water aquifers that exhibit unconfined aquifer system conditions. For fully-penetrating wells within unconfined aquifers, well drawdown behavior will exhibit three distinctive test segment patterns during pumping tests (i.e., if testing is performed long enough) : (1) an initial elastic Theissian test response following the elastic storage (storativity), S, property of the aquifer; (2) a subsequent departure and flattening of the drawdown curve (commonly referred to as the "Delayed Yield" portion of the drawdown curve) during intermediate test times; and (3) a later time period when the drawdown curve approaches and becomes coincident with the Theissian test response, but governed by the unconfined aquifer specific yield, S_y. The initial separation in time for the well drawdown departure from the first test response limb/segment pattern to becoming coincident with the third/last test limb/segment is determined by the ratio of the aquifer elastic storativity, S, to the aquifer specific yield, which commonly is assigned as the parameter sigma, σ:

$$\sigma = S/S_y \tag{13}$$

The departure from the initial elastic Theissian S response (i.e., the "Delayed Yield" middle portion of the drawdown response) is dependent on the distance from the pumping well to the point of test observation, r; the thickness of the unconfined aquifer, b; and the aquifer vertical anisotropy, K_D, ($K_D = K_v/K_h$). This composite parameter is generally referred to as Beta, β, (Neuman 1975) where

$$\beta = (r^2/b^2)K_D \tag{14}$$

Figure 46 shows the development of the three drawdown patterns during pumping tests and the influence of σ and β on the departure from the initial early-time, Theissian elastic (S) drawdown response and final coincidence with the late-time Theissian S_y response pattern. For the dimensionless time and drawdown parameters shown in the figure, the following definitions are provided, as reported in Spane (1993) and Spane and Wurstner (1993):

$$t_{DS} = (T\ t)/(r_o^2\ S) \tag{15}$$

and,

$$s_D = (4\pi\ T\ \Delta s)/Q \tag{16}$$

where,

T = aquifer transmissivity; L^2/T
t = pumping test time; T
r_o = radial distance from pumping well to the observation well; L
S = aquifer elastic storage; dimensionless
Δs = drawdown at observation well location; L
Q = pumping rate at stress well location; L^3/T

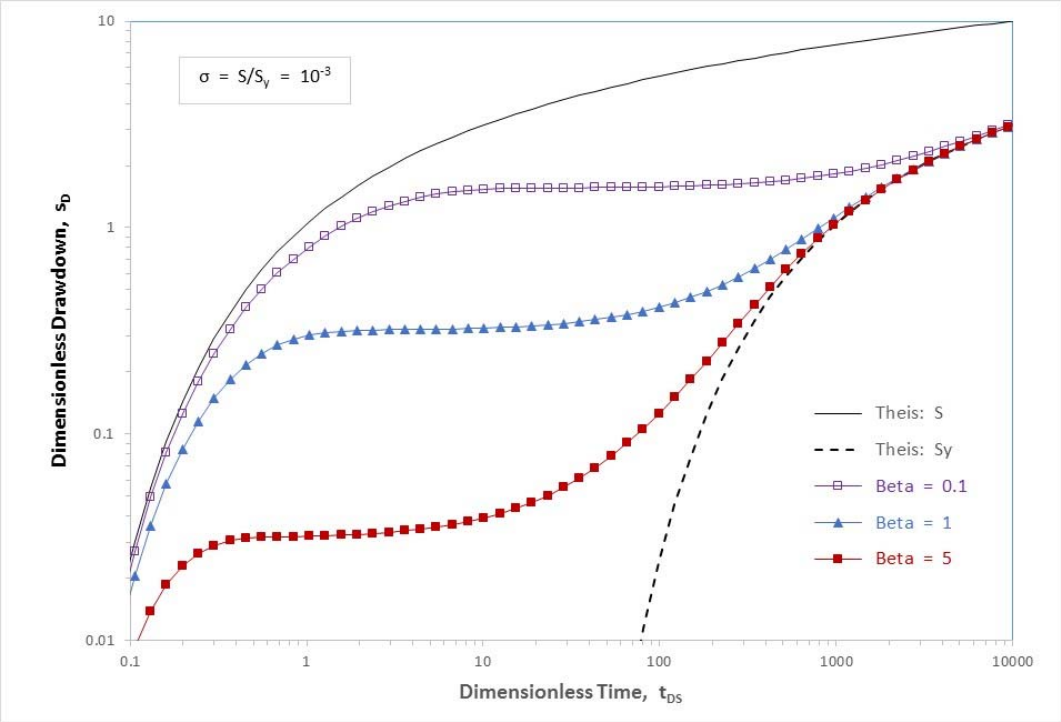

Figure 46. Dimensionless time-drawdown type curves for constant-rate discharge tests in unconfined aquifers for $\sigma = 10^{-3}$ (modified from Spane 1993).

For interference pumping tests, where the test response is being monitored at an observation well at a distance r_o from the pumping well(s), Eq. (14) is modified to

$$\beta_o = (r_o^2/b^2)K_D \quad (17)$$

For single-well pumping tests where the test response is being monitored at the test well location, then the pumping well radius, r_w, is used and Eq. (14) is modified to

$$\beta_w = (r_w^2/b^2)K_D \quad (18)$$

Given that r_w and b are normally well known or constrained, Eq. (18) indicates that analysis of single-well pumping tests then can provide a direct estimate for aquifer vertical anisotropy, K_D, based on the analyzed drawdown pattern response (i.e., β_w).

As discussed in Appendix B, Section B.3, with larger beta, β, values, there is an earlier departure from the initial elastic Theissian S portion of the pumping test drawdown response. As indicated in Eqs. (17) and(18), larger β conditions are produced by (1) larger test observation location distances, r, or well radii, r_w; (2) thinner unconfined aquifer thickness, b; and (3) *higher vertical anisotropy, K_D aquifer conditions*.

The single-well pumping tests results in Table 5 indicate a relatively narrow estimated range for K_D from 0.012 to 0.036 for the PWA. These K_D estimates fall within the lower range for fine-grained, silty-sand materials and are characteristic of a highly layered system (e.g., Freeze and Cherry 1979) and/or indicate the presence of clay layers (e.g., Kruseman and Ridder 2000). For comparative purposes, K_D estimates were also obtained by comparing geometric mean of laboratory-derived vertical permeability (K_v) measurements of intact core sample results, and associated K_h slug test-derived estimates obtained for the upper $CCU_{z\text{-}sand}$ section that the cores were obtained. Newcomer (2014) reports K_D values of 0.012 and

0.059 for the upper $CCU_{z\text{-}sand}$ section of the PWA at wells 299-E33-350 and 299-E33-351, respectively, which closely brackets the K_D estimate range obtained from single-well pumping test results. A best estimate K_D value for PWA modeling applications using both slug and pumping test results is 0.023 using the geometric mean as a basis, and 0.028 when based on the characterization results arithmetic mean.

The previous discussion pertains specifically to drawdown (and recovery) well water-level responses observed during constant-rate pumping tests. However because of the relative thinness of the PWA and characteristics of the pumping equipment system deployed at the various PWA extraction wells, the previous hydraulic tests and operational pumping activities at the PWA well sites were/are conducted in cyclical pumping fashion (i.e., repetitive pumping/on followed by pumping/off recovery periods). As discussed in Appendix B, the same diagnostic unconfined aquifer test response patterns would be exhibited at PWA pumped wells during extended recovery periods following termination of cyclical pumping activities, or for drawdown responses monitored at distant PWA observation well locations during extended cyclical pumping sequences.

3.2.2.3 PWA Storage Parameters

As noted previously by a number of investigators (Spane and Wurstner 1993; Spane 1996) elastic storage (storativity), S, and specific yield, S_y, cannot be determined using the slug test method because this method is not sensitive for delineating these parameters. However, as noted in Appendix B, S and S_y exhibit discernable impacts on well water-level responses during specific phases of pumping tests (i.e., S → early-time well response; S_y → late-time well response).

The single-well pumping test results in Table 5 indicate a relatively narrow estimated range for S from 9.0e-4 to 4.5e-3 (specific storage, S_s from 2.4e-4 to 1.2e-3 m^{-1}; given b = 3.81 m) for the PWA based on single-well pumping test results. These S estimates fall within the range for fine-grained, clayey aquifer formations as reported in Shestakov (2002). Table 5 also lists a narrow range for S_y as determined from the pumping test analysis ranging between 0.151 and 0.273. This range falls within values reported for very fine to medium sand, as identified in Johnson (1967). Best estimate values for S and S_y for PWA modeling applications based on the pumping test results are 2.38e-3 (S_s = 6.3e-4 m^{-1}) and 0.209 using the geometric mean as a basis, and 2.91e-3 (S_s = 7.6e-4 m^{-1}) and 0.215 when based on the characterization results arithmetic mean.

3.2.3 PWA Boundaries/Lateral Extent

Theoretically, it may be possible to assess the presence of hydrologic boundaries, possible dimensional relationships for the PWA, and impact of operational pumping activities in dewatering of the PWA. To facilitate this type of an assessment, two methods can be used:

1. Extended recovery monitoring (at extraction and observation well locations) following cessation of long-term, operational cyclical pumping sequences, and/or
2. Drawdown monitoring at an observation well (e.g. well 299-E33-344), during extended long-term operational cyclical pumping periods at the PWA extraction wells.

Figure 47 and Figure 48 show conceptually how the presence of hydrologic boundaries and possible dewatering assessment of PWA might be exhibited during extended recovery or extended drawdown periods using these two respective analysis methods. From a perspective of operational practicality, the first method (i.e., extended recovery monitoring periods) is not a feasible option due the significantly long periods of recovery that would be required following extended pumping periods. Using general hydrologic *rules-of-thumb* that recommend that recovery periods be equal to or up to 1.5 times the

preceding pumping period, this would suggest that for this option to be practical, recovery times in excess of 1.5 years would be required, given the FY17 and ongoing PWA operational pumping sequence that is being implemented.

For detection of PWA hydrologic boundaries within the drawdown response monitored at an observation well (e.g., 299-E33-344 as was used in the 2017 testing) during long-term pumping periods, this option requires that the drawdown at the observation well location has reached late-time, unconfined aquifer response behavior (i.e., coincident with the Theissian test response, governed by the unconfined aquifer specific yield, S_y).

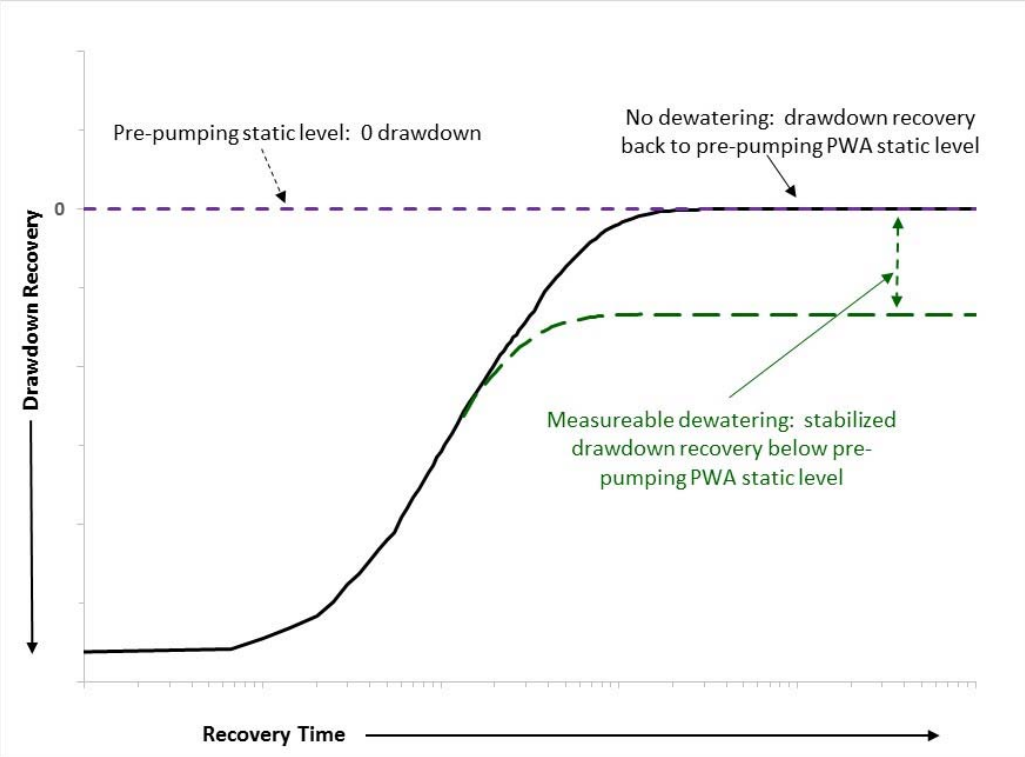

Figure 47. Conceptual long-term recovery response after cessation of extended pumping to measure a dewatering response (DOE 2016a).

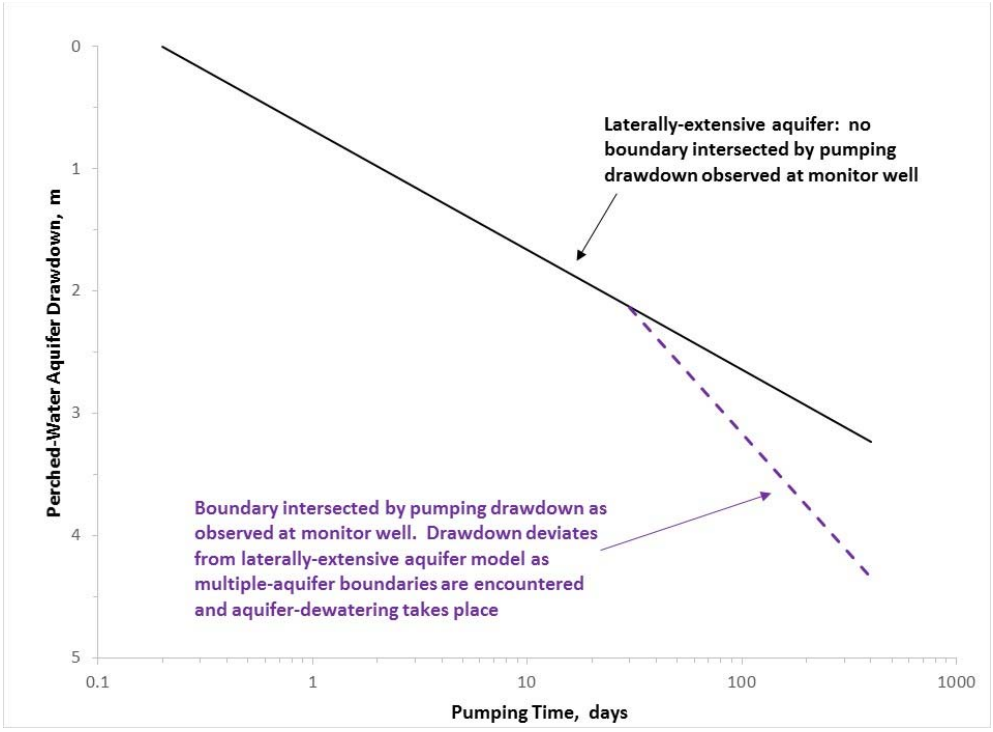

Figure 48. Conceptual drawdown response at a monitoring well (e.g., 299-E33-344) during pumping with and without contacting PWA hydrologic boundaries (DOE 2016a).

As an example, to assess the length of time that might be required to first reach late-time pattern coincidence requires a PWA beta curve, β_o, estimate and its coincidence with the Theis-S_y curve, as indicated in Figure 46. Using the previously reported PWA best estimate value for K_D of 0.023, an average PWA thickness b of 3.81 m, and an observation well distance from the pumping well(s), r_o, of 40 m, Eq. (17) indicates a β_o value of 2.5 for the monitor well 299-E33-344 location. Examination of Figure 46 indicates that an unconfined aquifer beta curve of 2.5 becomes coincident with the Theis curve based on S_y starting at a t_{DS} of ~1000 (i.e., t_{DSy} of ~1; given $\sigma = 10^{-3}$). Note: Eq. (15) can also be re-written with respect of S_y and dimensionless time with respect to S_y, and T_{DSy} defined as

$$t_{DSy} = (T\ t)/(r_o^2\ S_y) \quad (19)$$

Using this example point of coincidence with the Theis-S_y curve at a $t_{DSy} = 1$, and previously reported best estimate values for T of 2.12 m^2/day and $S_y = 0.209$, Eq. (19) can then be used to calculate a starting coincidence time on the Theis-S_y curve of ~158 days (~0.43 year). This represents the minimum time required at this monitor well location for hydrologic boundary detection using this drawdown analysis method. Assuming that an additional 1/4 to 1/3 of a time log cycle may be required for fully resolving detection of a hydrologic boundary at the monitor well location, a total monitored drawdown period of 365 to 548 days (1 to 1.5 years) may be necessary to fully implement this method using this monitor well location.

To qualitatively assess the possibility of detecting PWA lateral extent boundaries using observation well drawdown response (i.e., 299-E33-344), operational average pumping rates during FY17 at PWA extraction wells 299-E33-350 (Q_{avg} = 1.953 L/min) and 299-E33-351 (Q_{avg} = 1.166 L/min) were utilized using the Moench unconfined aquifer model option within AQTESOLV software (Duffield 2007) to simulate when hydrologic impact of the PWA boundaries might be observed in the drawdown response. Figure 49 shows the predicted drawdown response at observation well 299-E33-344, using these

continuous, constant pumping rates, the best estimate PWA hydrologic properties, with and without hydrologic boundaries. For the hydrologic boundary simulation, an assumed PWA areal extent of ~33,525 m^2 (360,920 ft^2) was used (as estimated from aquifer areal relationships presented in Figure 44). Note: The PWA areal extent boundaries in this qualitative assessment were partitioned as a square with width-lengths of 183 m, centrally situated around the observation well location.

As indicated in Figure 49, it takes ~1000 days before predicted well drawdown starts to deviate from the simulated no-boundary condition (i.e., infinite extent aquifer). The predicted observation time to intersect a PWA hydrologic boundary on the drawdown response can be reduced if the average/best estimate PWA T values are actually higher [and/or S_y is lower as indicated in Eq.(19)], and/or the PWA is more restrictive in areal extent. While this hydrologic boundary assessment is qualitative in nature, it does suggest that it will take significantly long periods of time to be able to meaningfully assess current PWA dewatering activities, given existing operational pumping scheme deployments. Incorporation of additional PWA extraction well centers and monitor wells would enhance the ability to detect a hydrologic boundary and accelerate PWA dewatering activities.

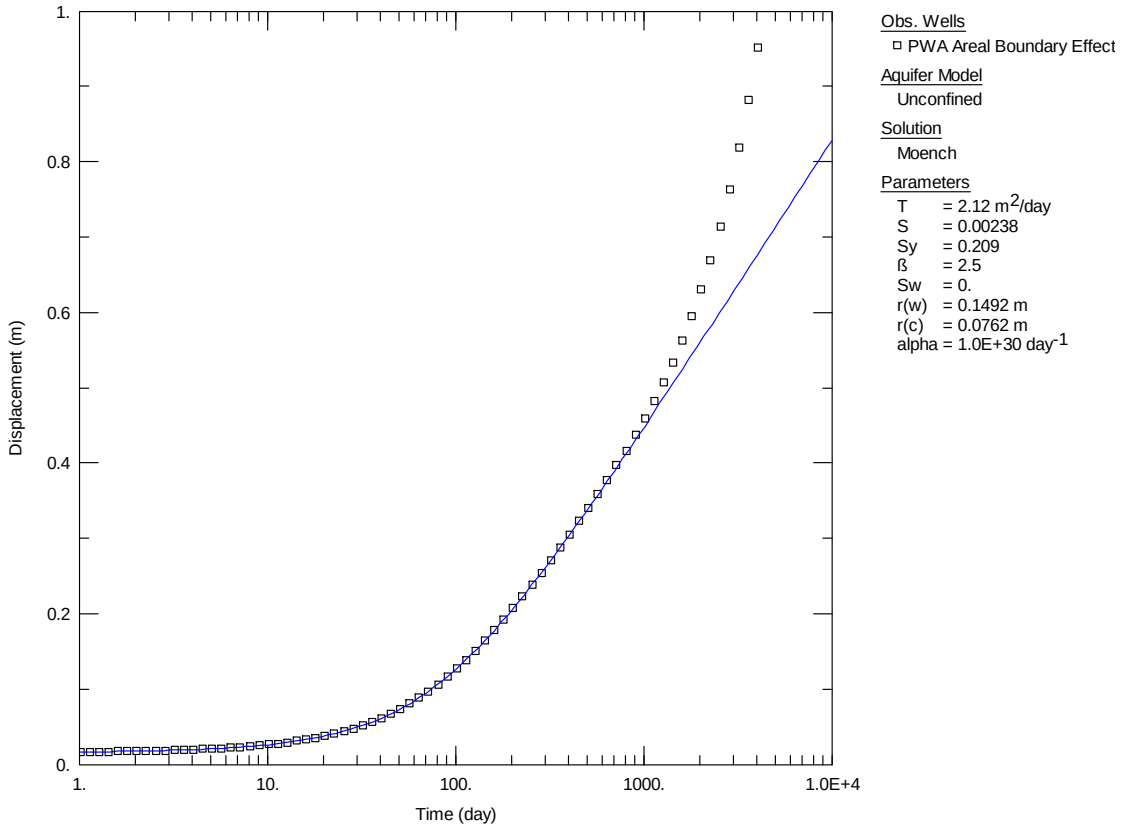

Figure 49. Qualitative predicted drawdown response at a monitoring well (e.g., 299-E33-344) during pumping with and without contacting a PWA hydrologic boundaries. (Note: Solid line indicates infinite-aquifer response.) This figure is FIO.

3.3 Physical Properties

Measured or calculated physical properties for core materials included bulk and particle densities, total porosity (Table 6), and particle-size distributions. As noted in the methods section, total porosity was calculated in two ways: (1) from the volume of water contained in the core sample when fully saturated, divided by the volume of the Lexan liner, and (2) from bulk and particle densities using Eq. (9). Both values represent apparent total porosity, owing to potential disturbance of the structure of the sediments within the cores during drilling and sampling. Differences in the values of the apparent total porosities are due, in part, to differences in average particle density of the bulk core material versus the subsamples taken for direct measurement of particle density. Note that the calculated apparent total porosity values in Table 6 are generally greater than the θ_s values determined from the average water content values at near-zero capillary pressure reported in Table 3.

Table 6. Physical property data for sediment samples from the 200-DV-1.

Formation	Sample ID	Dry Bulk Density, ρ_b [g/cm^3]	Particle Density[(a)], ρ_s [g/cm^3]	Total Porosity, volume basis [cm^3/cm^3]	Total Porosity[(b)], density basis [cm^3/cm^3]
Rwie	B35463	2.119	2.864 ± 0.005 (3)	0.2212	0.2723
	B39VY9	2.205	2.729 ± 0.046 (3)	0.1578	0.1920
Rtf	B39X68	1.653	2.723 ± 0.004 (3)	0.4073	0.3929
CCUz	B35435 (top)	1.632	2.785 ± 0.039 (3)	0.4322	0.4251
	B35435 (bot)	NA	NA	NA	NA
CCUz (perching silt)	B355M1 (top)	1.64	2.697 ± 0.021 (3)	0.4467	0.3919
	B355M0 (bot)	1.557	2.716 ± 0.034 (3)	0.4686	0.4267
CCUc	B39X53	1.891	2.567 ± 0.037 (2)	NA	0.2633
	B39VV7	1.604	2.709 ± 0.011 (3)	0.4271	0.4079
CCUg	B39M11	1.952	2.706 ± 0.019 (3)	0.251	0.2786

(a) Numbers represent the average ± one standard deviation, and with the number of measurements listed in parentheses.
(b) Calculated using Eq. (9).
NA Not available; measurements were not performed due to similarity of top and bottom subsamples.

Of the hydrogeologic formations that were sampled and characterized, samples from the CCUz unit generally have smaller bulk densities and larger total porosities, while samples of the CCUg and Rwie units have larger bulk densities and smaller total porosities, owing to larger mass fractions of coarser particles (gravel and cobble) in the samples of the latter units.

Table 7 provides gravel, sand, and mud (silt+clay) percentages for the characterized sediments. Plots of the particle-size distributions of the sampled materials are presented in Figure 51 through Figure 58. As shown in these figures, most of the particle-size distributions exhibit very skewed and/or multi-modal character. One notable exception is the particle-size distribution for sample B355M1, from the CCUz perching silt unit underlying the B-Complex, which has a uni-modal and very symmetric particle-size distribution (on a log scale).

The measured physical properties for these sediments are consistent with the hydraulic properties that were determined for these sediments on the intact core samples. For example, the finer-textured materials have larger values of the Brooks-Corey model h_b parameter (air-entry pressure), and smaller values of the

van Genuchten model α parameter relative to the coarser-textured materials. The coarser-textured materials also generally have lower porosities than the finer-textured materials.

Table 7. Summary of gravel, sand, and mud (silt + clay) percentages for 200-DV-1 samples.

Formation	Sample ID	% Gravel (> 2mm)	% Sand (0.0625 – 2 mm)	% Mud (< 0.0625 mm)
Rwie	B35463	66	21	13
	B39VY9	57	31	12
Rtf	B39X68	0	42	58
CCUz	B35435 (top)	0	2	98
	B35435 (bot)	NA	NA	NA
CCUz (perching silt)	B355M1 (top)	0	13	87
	B355M0 (bot)	0	17	83
CCUc	B39X53	33	48	19
	B39VV7	2	59	39
CCUg	B39M11	17	73	10

NA Not available; measurements were not performed due to similarity of top and bottom subsamples.

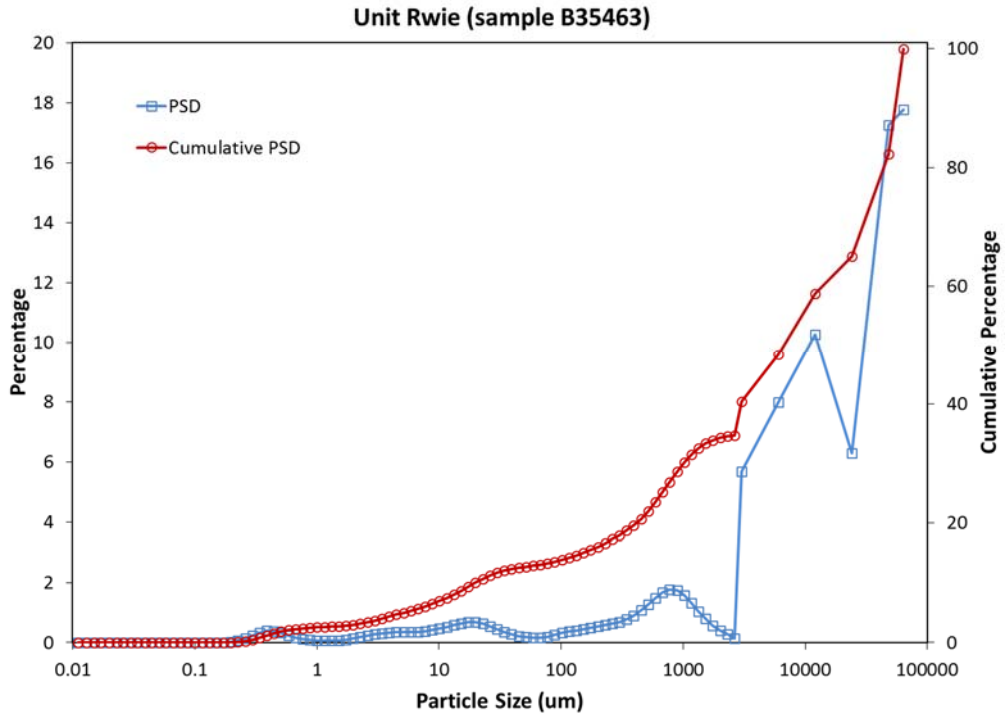

Figure 50. Particle size distribution and cumulative distribution for sediment from unit Rwie (sample B35463).

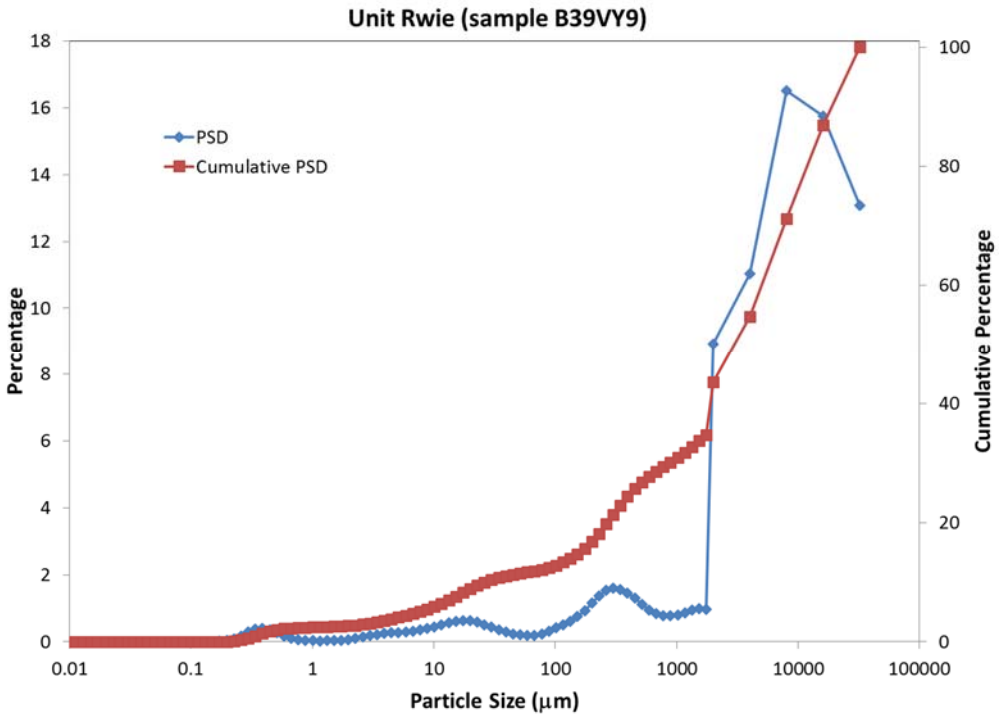

Figure 51. Particle Size Distribution and Cumulative Distribution for Sediment from Unit Rwie (sample B35463).

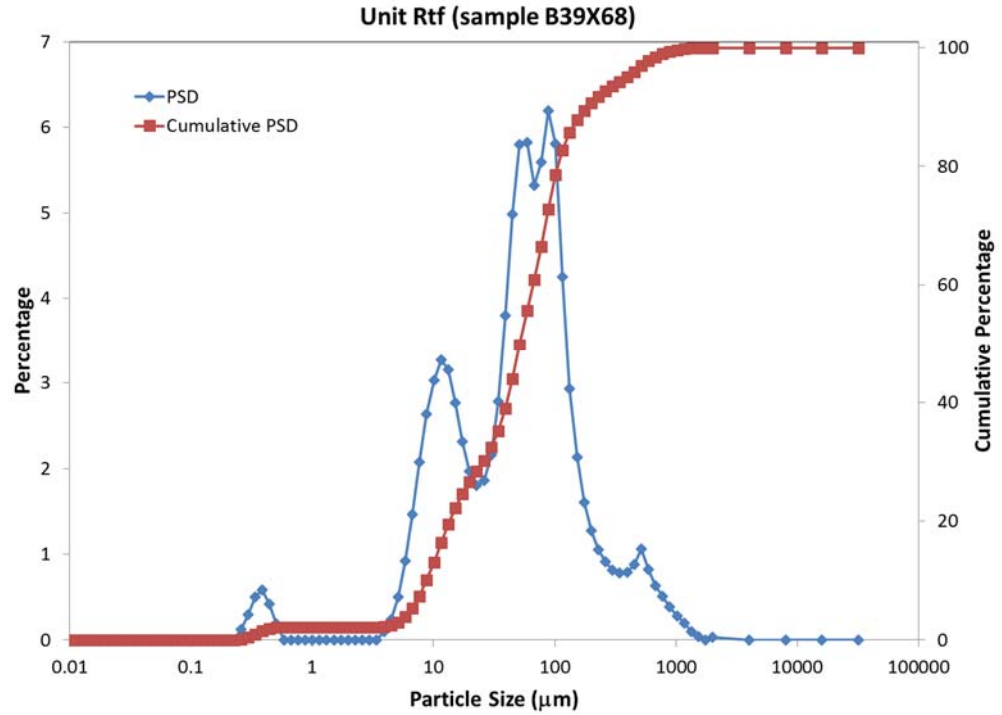

Figure 52. Particle size distribution and cumulative distribution for sediment from unit Rtf (sample B39X68).

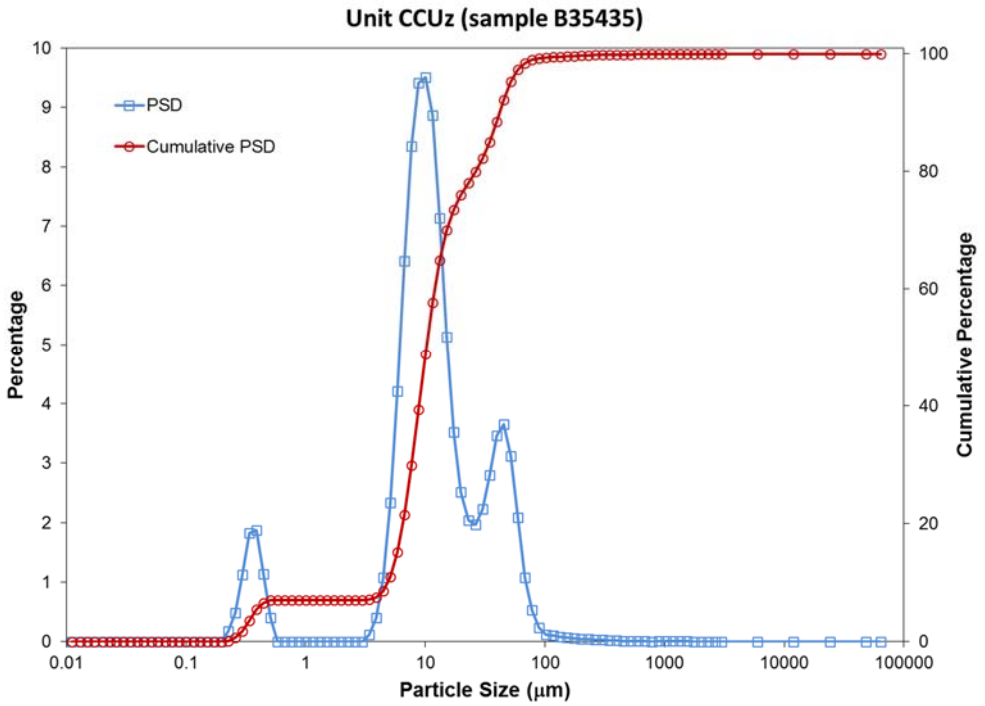

Figure 53. Particle size distribution and cumulative distribution for sediment from unit CCUz (sample B35435).

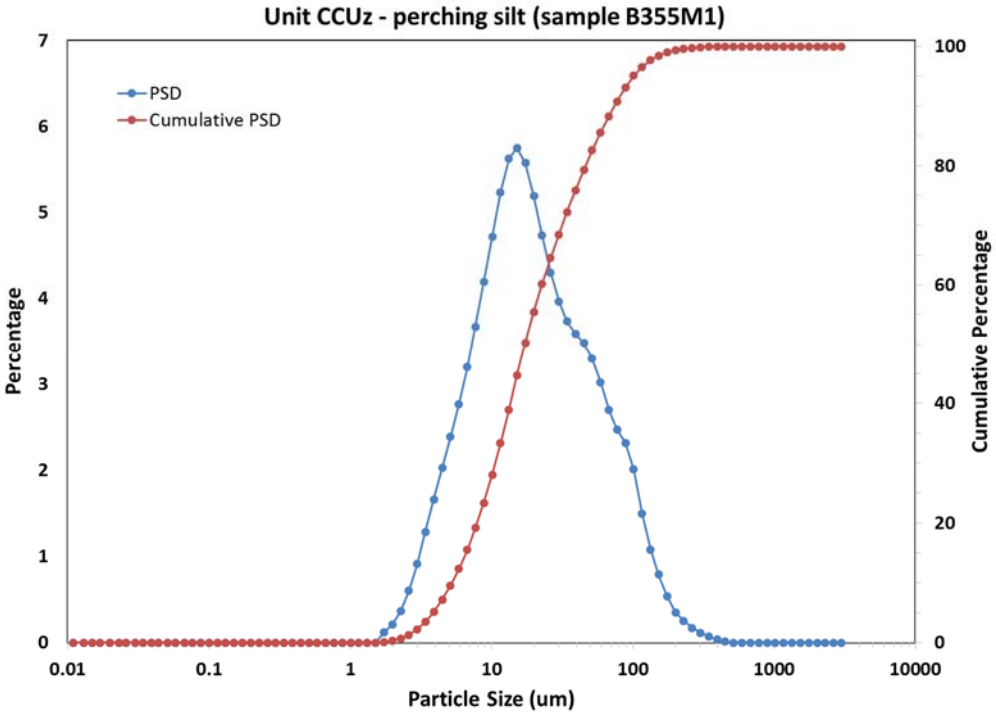

Figure 54. Particle size distribution and cumulative distribution for sediment from unit CCUz (sample B355M1).

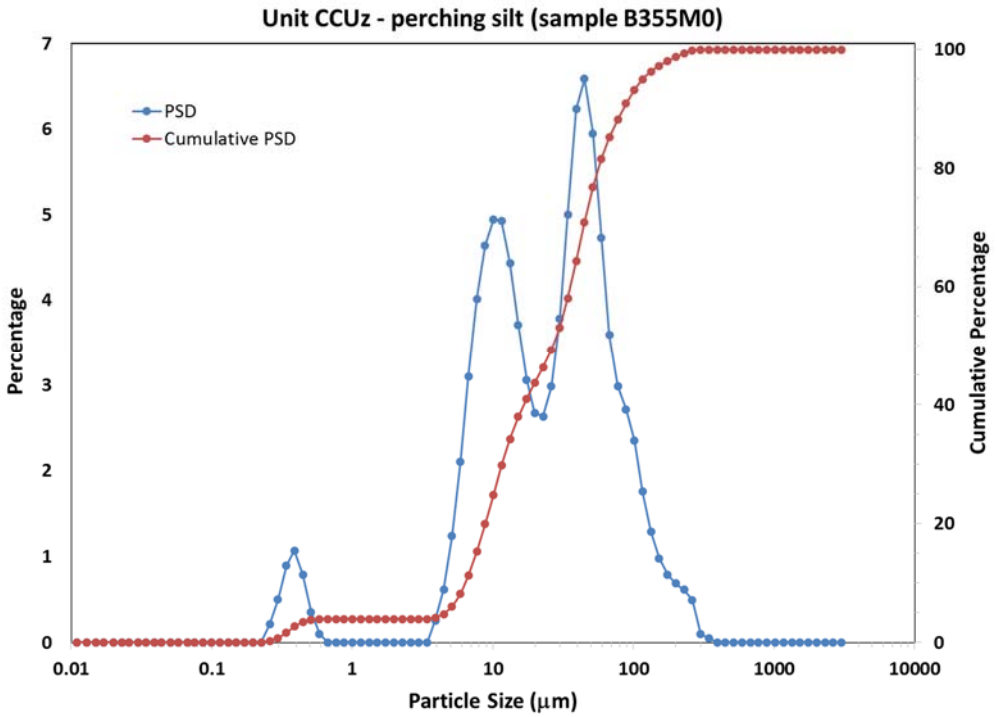

Figure 55. Particle size distribution and cumulative distribution for sediment from unit CCUz (sample B355M1).

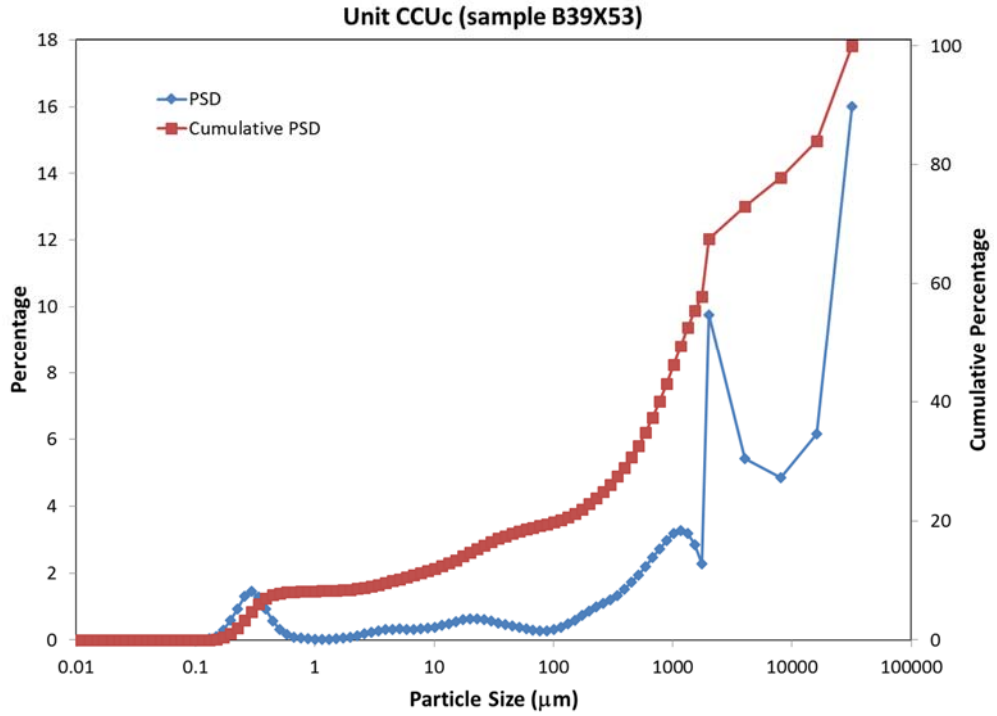

Figure 56. Particle size distribution and cumulative distribution for sediment from unit CCUz (sample B39X53).

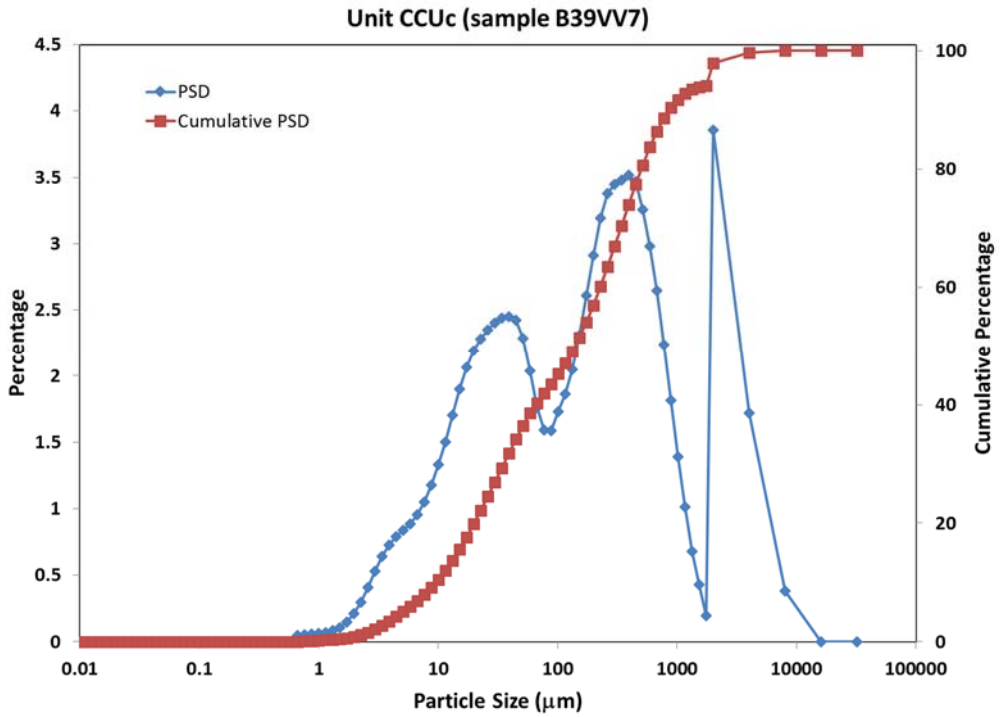

Figure 57. Particle size distribution and cumulative distribution for sediment from unit CCUz (sample B39VV7).

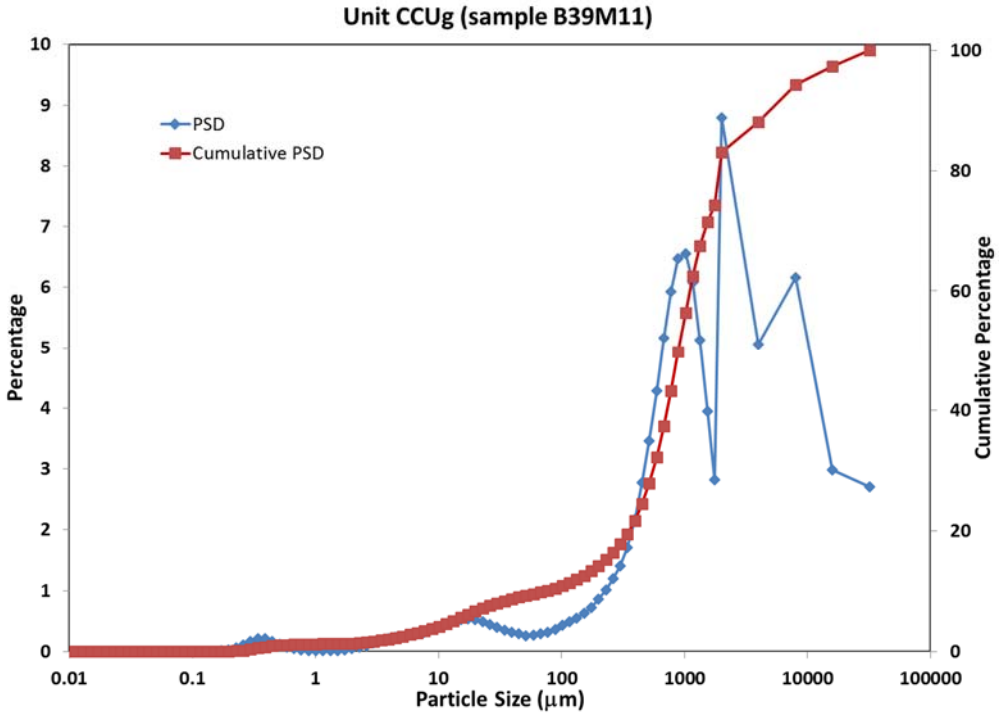

Figure 58. Particle size distribution and cumulative distribution for sediment from unit CCUg (sample B39M11).

4.0 Conclusions

The data collected in this study addressed the objectives listed in the first and third bullets below as part of the overall characterization of attenuation and transport processes jointly described herein and in other attenuation and transport process characterization reports for the 200-DV-1 OU (Truex et al. 2017; Szecsody et al. 2017; Demirkanli et al. 2018):

- Define the contaminant distribution and the hydrologic and biogeochemical setting
- Identify attenuation processes and describe the associated attenuation mechanisms
- Quantify attenuation and transport parameters for use in evaluating remedies.

The collective objectives of this work used in conjunction with results reported by Truex et al. (2017), Szecsody et al. (2017), and Demirkanli et al (2018), are elements of the framework identified in EPA guidance (EPA 2015) for evaluating monitored natural attenuation of inorganic contaminants. The generated data directly support updating the CSM for these waste sites (and generally for the Hanford Central Plateau). More specifically, the information contained herein supports efforts to define hydraulic parameter values needed to evaluate transport of contaminants through the vadose zone and to the groundwater. This type of transport assessment supports a coupled analysis of groundwater and vadose zone contamination.

Physical and hydraulic property characterization was performed on CCU and Ringold Formation sediments from 200-DV-1 OU. For the core samples that were characterized, samples from the Ringold Formation, Rwie unit, and the CCU gravel, CCUg, had larger bulk densities, smaller porosities, and larger hydraulic conductivities relative to the Ringold Formation Taylor Flats unit, Rtf, and the CCU silts (CCUz). Laboratory-measured saturated hydraulic conductivity values for these samples vary by three orders-of-magnitude, ranging from high values of 4.48e-03 and 2.5e-03 cm/s for samples of the Rwie and CCUg units, respectively, to low values of 3.03e-06 and 3.36e-6 cm/s for samples of the CCUz unit. The lowest hydraulic conductivity values measured were on two CCUz samples of the “perching silt” unit that creates a flux-limiting layer underlying the B-Complex. Water retention parameters were also estimated using data from multistep outflow experiments on intact core samples of these sediments. Samples of finer-textured CCU units have higher air-entry pressures relative to the coarser Rwie unit, while the entry pressure of the Rtf unit is similar to that of the CCU units.

Hydraulic and storage properties were also characterized for a sandy subunit of the CCU silts that lies above the CCU gravel (CCUg), and that forms a perched water aquifer above the CCUz perching silt in the B-Complex. Pump test results described herein provide information of storage capacity, saturated hydraulic conductivity and anisotropy. The hydraulic boundary assessment described herein is qualitative in nature, but suggests that it will take ~1000 days before predicted well drawdown starts to deviate from the simulated no-boundary condition (i.e., infinite extend aquifer). This suggests that it will take significantly long periods of time to be able to meaningfully assess the current perched water aquifer dewatering activities given the existing operational scheme used for the current pumping system. As such, the extent of the boundary cannot fully be determined without incorporation of additional PWA extraction well centers and monitor wells that could enhance the ability to detect a hydrologic boundary and accelerate PWA dewatering activities.

The 200-DV-1 OU RI/FS effort, associated conceptual site model, and fate and transport models need this information about subsurface hydraulic properties as a technical basis to describe the contaminant conditions and estimate future transport. This study provides both direct measurements and quantitative estimates of hydraulic and physical properties to support parameterization of fate and transport models

used for site assessments. This type of site-specific information enhances the technical defensibility of this assessment and its use to support remedy evaluation. Quantifying transport of contaminants in the vadose zone in terms of a source to groundwater under existing and future conditions without additional intervention is a basic element of remedy evaluation for the vadose zone. For cases where future contaminant discharge from the vadose zone will create or continue plumes of concern in the groundwater, the transport behavior and magnitude of the source discharge are used to define the target for vadose remediation (i.e., the extent of an engineered remedy needed in addition to natural attenuation) and assess potential remedy options. Thus, the information in this laboratory study was included in the 200-DV-1 OU characterization efforts to support the upcoming remedy evaluation in the 200-DV-1 OU feasibility study.

5.0 Quality Assurance

The results presented in this report originate from work governed by the *DVZ-AFRI Quality Assurance Plan* (DVZ-QAP). The DVZ-QAP implements the requirements of the United States Department of Energy Order 414.1D, *Quality Assurance* and 10 CFR 830 Subpart A*, Quality Assurance Requirements*. The DVZ-QAP uses ASME NQA-1-2000, *Quality Assurance Requirements for Nuclear Facility Applications* as its consensus standard and NQA-1-2000 Subpart 4.2 as the basis for its graded approach to quality.

The technology level defined for this effort is Development, because its information may be used directly by the Hanford Site to support remediation decisions. The bulk of the work reported herein was conducted under the Development level to ensure the reproducibility and defensibility of the experimental results. Exceptions are flagged by "For Information Only" (FIO) identifiers. FIO exceptions include inverse modeling results, because the mode of the STOMP simulator that was used for this work has not been qualified under the NQA-1 testing and documentation procedures, and perched water aquifer testing results, which were generated primarily under an earlier project that had different QA requirements.

QA reviews of data and analyses were conducted for this work in accordance with the DVZ-QAP. There were no reportable issues with the data included in this report.

6.0 References

ASTM D4464-15. 2015. *Standard Test Method for Particle Size Distribution of Catalytic Materials by Laser Light Scattering*. American Society for Testing and Materials, West Conshohocken, Pennsylvania.

Brooks RH and AT Corey. 1964. *Hydraulic Properties of Porous Media. Hydrology*. Paper No. 3, Colorado State University, Fort Collins, Colorado.

Burdine NT. 1953. "Relative permeability calculations from pore-size distribution data." *Petr. Trans. Am. Inst. Mining Metall. Eng.* 198:71-78.

Butler JJ, Jr. 1996. "Slug Tests in Site Characterization: Some Practical Considerations." *Environmental Geosciences* 3(3):154-163.

Butler JJ, Jr. 1998. *The Design, Performance, and Analysis of Slug Tests*. Lewis Publishers, CRC Press, Boca Raton, Florida.

CHPRC. 2015a. *Conceptual Site Models for the 200-DV-1 Operable Unit Waste Sites in the T Complex Area, Central Plateau, Hanford, Washington*. SGW-49924, Rev. 0, CH2M Hill Plateau Remediation Company, Richland, Washington.

CHPRC. 2015b. *Conceptual Site Models for the 200-DV-1 Operable Unit Waste Sites in the S Complex Area, Central Plateau, Hanford, Washington*. SGW-50280, Rev. 1, CH2M Hill Plateau Remediation Company, Richland, Washington.

Dane JH and JW Hopmans. 2002a. "Hanging Water Column." In *Methods of Soil Analysis Part 4 Physical Methods*, JH Dane and CT Topp (eds.), pp. 680-683. Soil Science Society of America, Inc., Madison, Wisconsin.

Dane JH and JW Hopmans. 2002b. "Pressure Plate Extractor." In *Methods of Soil Analysis Part 4 Physical Methods*, JH Dane and CT Topp (eds.), pp. 688-690. Soil Science Society of America, Inc., Madison, Wisconsin.

DOE. 2012. *Characterization Sampling and Analysis Plan for the 200-DV-1 Operable Unit*. DOE/RL-2011-104, U.S. Department of Energy, Richland Operations Office, Richland, Washington.

DOE. 2014. *Action Memorandum for 200-DV-1 Operable Unit Perched Water Pumping / Pore Water Extraction*. DOE/RL-2014-34, Rev. 0, U.S. Department of Energy Richland Operations Office, Richland, Washington.

DOE. 2015. *Removal Action Work Plan for 200-DV-1 Operable Unit Perched Water Pumping / Pore Water Extraction*. DOE/RL-2014-37, Rev. 0, U.S. Department of Energy Richland Operations Office, Richland, Washington.

DOE. 2016a. *Calendar Year 2016 Annual Summary Report for the 200-ZP-1 and 200-UP-1 Operable Unit Pump-and-Treat Operations*. DOE/RL-2016-69, Rev. 0, Prepared for U.S. Department of Energy by CH2M Hill, Richland, Washington.

DOE. 2016b. *Remedial Investigation/Feasibility Study and RCRA Facility Investigation/Corrective Measures Study Work Plan for the 200-DV-1 Operable Unit*. DOE/RL-2011-102, Rev. 0, U.S. Department of Energy Richland Operations Office, Richland, Washington.

DOE. 2017. *Characterization Sampling and Analysis Plan for the 200-DV-1 Operable Unit Addendum 1: Attenuation Process Characterization*. DOE/RL-2011-104-ADD1, Rev. 0, U.S. Department of Energy, Richland Operations Office, Richland, Washington.

Demirkanli DI, MJ Truex, JE Szecsody, MM Snyder, JJ Moran, MK Nims, AR Lawter, CT Resch, DL Saunders, NP Qafoku, SR Baum, and BD Williams. 2018. *Contaminant Attenuation and Transport Characterization of 200-DV-1 Operable Unit Sediment Samples from Boreholes C9497, C9498, C9603, C9488, and C9513.* PNNL-27524, Pacific Northwest National Laboratory, Richland, Washington.

Doherty J. 2016. *PEST – Model-Independent Parameter Estimation, User Manual Part 1: PEST, SENSAN, and Global Optimizers*. Sixth Edition, Watermark Numerical Computing, Australia.

Duffield GM. 2007. *AQTESOLV for Windows Version 4.5 User's Guide*. HydroSOLVE, Inc., Reston, Virginia (http://www.aqtesolv.com).

Durner W. 1992. “Predicting the unsaturated hydraulic conductivity using multiporosity water retention curves.” p. 185-202. In M Th Van Genuchten et al. (ed.). Proceedings of the International Workshop on Indirect Methods for Estimating the Hydraulic Properties of Unsaturated Soils. University of California, Riverside.

Durner W. 1994. “Hydraulic conductivity estimation for soils with heterogeneous pore structure.” *Water Resour. Res*. 30:211-223.

Eching SO and JW Hopmans. 1993a. “Optimization of hydraulic functions from transient outflow and soil water pressure data.” *Soil Sci. Soc. Am. J.* 57:1167-1175.

Eching SO and JW Hopmans. 1993b. *Inverse solution of unsaturated soil hydraulic functions from transient outflow and soil water pressure data*. Land, Air and Water Resources Report No. 100021, Univ. of California, Davis.

Eching SO, JW Hopmans, and O Wendroth. 1994. “Unsaturated hydraulic conductivity from transient multi-step outflow and soil water pressure data.” *Soil Sci. Soc. Am. J.* 58:687-695.

EPA. 2015. *Use of Monitored Natural Attenuation for Inorganic Contaminants in Groundwater at Superfund Sites*. OSWER Directive 9283.1-36, U.S. Environmental Protection Agency, Office of Solid Waste and Emergency Response, Washington, D.C.

Flint AL and LE Flint. 2002. “Particle density.” pp. 229-240, In *Methods of Soil Analysis, Part 4 – Physical Methods,* JH Dane and G Clarke Topp (eds.). Soil Science Society of America, Inc., Madison, Wisconsin.

Freeze RA and JA Cherry. 1979. *Groundwater.* Prentice-Hall, Inc., Englewood Cliffs, New Jersey, 604 p.

Gee GW and D Or. 2002. “Particle-size analysis.” Section 2.4, pp. 255-293, In *Methods of Soil Analysis, Part 4 – Physical Methods*, JH Dane and G Clarke Topp (eds.). Soil Science Society of America, Inc., Madison, Wisconsin.

Hopmans JW, J Simunek, N Romano, and W Durner. 2002. “Inverse Methods.” In *Methods of Soil Analysis Part 4 Physical Methods*, JH Dane and CT Topp (eds.), pp. 963-1008. Soil Science Society of America, Inc., Madison, Wisconsin USA.

Johnson AI. 1967. “Specific Yield – Compilation of Specific Yields for Various Materials.” *Water-Supply Paper WSP 1662-D.* U.S. Geological Survey, Washington, D.C.

Kool JB and JC Parker. 1988. “Analysis of the inverse problem for transient unsaturated flow.” *Water Resour. Res.* 24:817-830.

Kruseman GP and NA de Ridder. 2000. *Analysis and Evaluation of Pumping Test Data.* Publication 47 - Second Edition, International Institute for Land Reclamation and Improvement, Wageningen, The Netherlands, 377 p.

Levenberg K. 1944. “A method for the solution of certain non-linear problems in least squares.” *Quart. Appl. Math*. 2(2):164-168.

Marquardt DW. 1963. “An algorithm for least-squares estimation of nonlinear parameters.” *J. Soc. Indust. Appl. Math.* 11(2):431-441.

Mualem Y. 1976. “A new model for predicting the hydraulic conductivity of unsaturated porous media.” *Water Resour. Res.* 12(3):513-522.

Neuman SP. 1975. “Analysis of pumping test data from anisotropic unconfined aquifers considering delayed gravity response.” *Water Resour. Res.* 11(2):329-342.

Newcomer DR. 2014. *Field-Derived Hydraulic Properties for Perched-Water Aquifer Wells 299-E33-350 and 299-E33-351, Hanford Site B-Complex Area*. PNNL-23380, Pacific Northwest National Laboratory, Richland, Washington.

Oostrom M, MJ Truex, KC Carroll, and GB Chronister. 2013. “Perched-water Analysis Related to Deep Vadose Zone Contaminant Transport and Impact to Groundwater.” *J. Hydrology.* 505: 228-239. doi:/10.1016/j.jhydrol.2013.10.001

Priesack E and W Durner. 2006. “Closed-form expression for multi-modal unsaturated hydraulic conductivity function.” *Vadose Zone J.* 5:121-124.

Reynolds WD and DE Elrick. 2002. “Constant Head Soil Core (Tank) Method.” Section 3.4.2.2, pp. 804-808, In *Methods of Soil Analysis, Part 4 – Physical Methods*, JH Dane and G Clarke Topp (eds.). Soil Science Society of America, Inc., Madison, Wisconsin.

Richards LA. 1931. “Capillary conduction of liquids through porous mediums.” *Physics*. 1:318-333.

Serne R, B Bjornstad, J Keller, P Thorne, D Lanigan, J Christensen, and G Thomas. 2010. *Conceptual Models for Migration of Key Groundwater Contaminants Through the Vadose Zone and Into the Upper Unconfined Aquifer Below the B-Complex*. PNNL-19277, Pacific Northwest National Laboratory, Richland, Washington.

SGW-59086, Rev. 0. 2015. *Annual Performance Report for the 200-DV-1 Operable Unit Perched Water Extraction, Fiscal Year 2015*. Prepared for U.S. Department of Energy by CH2M Hill, Richland, Washington.

Shestakov VM. 2002. “Development of Relationship between Specific Storage and Depth of Sandy and Clay Formations.” *Environmental Geology*, 42:127-129. doi:/10.1007/s00254-001-0481-z

Spane FA, Jr. 1993. *Selected Hydraulic Test Analysis Techniques for Constant-Rate Discharge Tests*. PNL-8539, Pacific Northwest Laboratory, Richland, Washington.

Spane FA, Jr. 1996. “Applicability of Slug Interference Tests for Hydraulic Characterization of Unconfined Aquifers: (1) Analytical assessment.” *Ground Water* 34(1):66-74.

Spane FA, Jr., and SK Wurstner. 1993. “DERIV: A Program for Calculating Pressure Derivatives for use in Hydraulic Test Analysis.” *Ground Water* 31(5):814-822.

Spane FA, Jr., PD Thorne, and DR Newcomer. 2001a. *Results of Detailed Hydrologic Characterization Tests – Fiscal Year 1999*. PNNL-13378, Pacific Northwest National Laboratory, Richland, Washington.

Spane FA, Jr., PD Thorne, and DR Newcomer. 2001b. *Results of Detailed Hydrologic Characterization Tests – Fiscal Year 2000*. PNNL-13514, Pacific Northwest National Laboratory, Richland, Washington.

Spane FA, Jr., PD Thorne, and DR Newcomer. 2002. *Results of Detailed Hydrologic Characterization Tests – Fiscal Year 2001*. PNNL-14113, Pacific Northwest National Laboratory, Richland, Washington.

Spane FA, Jr., PD Thorne, and DR Newcomer. 2003. *Results of Detailed Hydrologic Characterization Tests – Fiscal Year 2002*. PNNL-14186, Pacific Northwest National Laboratory, Richland, Washington.

Szecsody JE, BD Lee, MJ Truex, CE Strickland, JJ Moran, MMV Snyder, CT Resch, AR Lawter, L Zhong, BN Gartman, DL Saunders, SR Baum, II Leavy, JA Horner, B Williams, BB Christiansen, EM McElroy, MK Nims, RE Clayton, and D Appriou. 2017. *Geochemical, Microbial, and Physical Characterization of 200-DV-1 Operable Unit Cores from Boreholes C9552, C9487, and C9488, Hanford Site Central Plateau*. PNNL-26266, Pacific Northwest National Laboratory, Richland, Washington.

Tadepalli R, H Rahardjo, and DG Fredlund. 1992. "Measurements of matric suction and volume changes during inundation of collapsible soils." *Geotech. Test. J.* 15:115-122.

Truex MJ and KC Carroll. 2013. *Remedy Evaluation Framework for Inorganic, Non-Volatile Contaminants in the Deep Vadose Zone*. PNNL-21815, Pacific Northwest National Laboratory, Richland, Washington.

Truex MJ, M Oostrom, KC Carroll, and GB Chronister. 2013. *Perched-Water Evaluation for the Deep Vadose Zone beneath the B, BX and BY Tank Farms Area of the Hanford Site*. PNNL-22499, Pacific Northwest National Laboratory, Richland, Washington.

Truex MJ, M Oostrom, and GD Tartakovsky. 2015. *Evaluating Transport and Attenuation of Inorganic Contaminants in the Vadose Zone for Aqueous Waste Disposal Sites*. PNNL-24731, Pacific Northwest National Laboratory, Richland, Washington.

Truex MJ, JE Szecsody, NP Qafoku, CE Strickland, et al. 2017. *Contaminant attenuation and transport characterization of 200-DV-1 operable unit sediment*. PNNL-26208, Pacific Northwest National Laboratory, Richland, Washington.

Tuli A, MA Denton, JW Hopmans, T Harter, and JL MacIntyre. 2001. *Multi-Step Outflow Experiment: From Soil Preparation to Parameter Estimation*. Land, Air and Water Resources Report No. 100037, University of California, Davis.

van Genuchten M Th. 1980. "A closed-form equation for predicting the unsaturated hydraulic conductivity of unsaturated soils." *Soil Sci. Soc. Am. J* 44:892-898.

White MD and M Oostrom. 2006. *STOMP – Subsurface Transport Over Multiple Phases, Version 4.0 User's Guide*. PNNL-15782, Pacific Northwest National Laboratory, Richland, Washington.

Wildenschild D and AP Sheppard. 2013. "X-ray imaging and analysis techniques for quantifying pore-scale structure and processes in subsurface porous medium systems." *Adv. Water Resour.* 51:217-246.

Wietsma TW, M Oostrom, MA Covert, TE Queen, and MJ Fayer. 2009. "An automated tool for three types of saturated hydraulic conductivity laboratory measurements." *Soil Sci Soc Am J* 73(2):466-470.

Appendix A

Quasi-Static Water Retention Data from Multistep Outflow Experiments

Appendix A

Quasi-Static Water Retention Data from Multistep Outflow Experiments

Table A.1. Water Retention Data from Multistep Outflow Experiments Performed on Intact 200-DV-1 Core Samples.

Sample B35463		Sample B39VY9		Sample B39X68		Sample B35435 (top)		Sample B39VV7		Sample B39M11	
θ	h [cm]	θ	h [cm]	θ	h [cm]	θ	h [cm]	θ	h [cm]	θ	h [cm]
0.2212	16.4	0.1578	2.6	0.3909	3.8	0.4075	1.8	0.3890	2.4	0.2220	3.2
0.2068	26.3	0.1370	3.2	0.3908	24.0	0.4070	2.9	0.3885	22.4	0.2189	13.2
0.1895	36.6	0.1370	5.2	0.3904	43.9	0.4068	12.8	0.3884	42.3	0.2078	22.7
0.1673	46.8	0.1248	6.1	0.3896	63.7	0.4065	22.8	0.3879	62.2	0.1730	33.4
0.1545	56.3	0.1175	16.5	0.3890	83.6	0.4055	32.8	0.3818	81.4	0.1526	42.8
0.1461	66.5	0.1173	26.3	0.3865	103.2	0.4055	43.0	0.3306	101.9	0.1383	53.5
0.1414	76.6	0.1165	36.3	0.3756	123.1	0.4042	52.8	0.3074	124.9	0.1300	63.7
0.1383	86.6	0.1160	46.4	0.3542	141.3	0.4014	62.8	0.2907	136.2	0.1240	73.9
0.1355	96.6	0.1146	71.4	0.3265	161.6	0.4007	72.6	0.2789	149.5	0.1199	83.2
0.1333	106.6	0.1135	96.2	0.3096	179.4	0.3803	83.0	0.2726	157.6	0.1109	108.5
0.1309	116.6	0.1131	121.0	0.2902	201.3	0.3782	92.9	0.2668	167.6	0.1051	122.9
0.1294	126.6	0.0847	157.0	0.2753	221.6	0.3754	102.3	0.2624	190.5	0.1007	148.7
0.1283	136.4	0.0840	182.0	0.2625	239.3	0.3718	111.9	0.2592	208.1	0.0983	172.5
0.1259	146.6	0.0834	206.9	0.2484	258.7	0.3646	122.4	0.2568	229.0	0.0954	199.3
0.1232	166.6	0.0834	231.8	0.2363	279.0	0.3608	132.6	0.2538	280.1	0.0939	223.1
0.1198	191.5	0.0833	256.5	0.2254	299.3	0.3576	142.1	0.2523	313.0	0.0924	251.1
0.1168	216.5	0.0833	281.2	0.2152	322.1	0.3527	151.7			0.0921	285.1
0.1142	241.6	0.0833	306.2	0.2063	344.9	0.3460	162.4			0.0923	328.7
0.1118	266.7	0.0818	355.9	0.1998	363.9	0.3421	172.1			0.0913	382.6
0.1101	291.5	0.0818	405.8	0.1939	383.0	0.3362	177.9			0.0910	445.8
0.1079	316.5	0.0818	455.7	0.1866	411.4	0.3320	187.3			0.0913	579.4
		0.0819	504.8	0.1807	432.5	0.3250	198.0				
						0.3149	217.6				
						0.3039	237.8				
						0.2906	262.7				

Appendix B

Recent Perched-Water Aquifer Hydraulic Test Characterization Results

Appendix B

Recent Perched-Water Aquifer Hydraulic Test Characterization Results

The general hydraulic test characterization discussion presented in this appendix represents a summary of field-derived hydraulic/storage properties for the current perched-water aquifer (PWA) in the B-BX Complex Tank Farm area of the Hanford Site. These results were obtained from recently performed hydraulic tests (i.e., single-well slug tests and single/multi-well pumping tests) conducted at PWA extraction/monitor wells 299-E33-344, 299-E33-350, and 299-E33-351. Results from these well tests were previously presented in Newcomer (2014) and DOE (2016). The analytical results from these tests provide estimates for hydraulic and storage properties for the current limited PWA areal extent, which can be used as parameter input for numerical modeling simulations used to predict and optimize ongoing PWA dewatering operations. All results reported in this appendix are For Information Only (FIO) because this work was originally performed on a different project with different quality assurance requirements.

B.1 FY14 Slug Test Analysis Results

Results of the FY14 PWA slug test analysis were previously reported in Newcomer (2014). These slug tests were performed during construction and immediately prior to completion of PWA wells 299-E33-350 and 299-E33-351. Pertinent findings and technical discussion of the slug test characterization results are taken from Newcomer (2014) and are summarized below.

Slug-test analysis results were obtained for four PWA test/depth intervals within the B-Complex Area during the construction process at test wells 299-E33-350 and 299-E33-351, after reaching their respective total drill depths (Table B.1). The PWA was characterized after the final well-screen/casing was installed and partially completed with a sand filter pack. The lower PWA section was tested by back-pulling the temporary drill casing, exposing the well screen to the formation. Following testing of the lower PWA section, the temporary drill casing was pulled up to/above the PWA water table, allowing testing of the entire composite PWA section. The purpose of the slug-test characterization was to provide estimates of transmissivity and hydraulic conductivity for the PWA at these selected well locations. The unconfined PWA lies within the silty-sand subunit of the Cold Creek (i.e., the $CCU_{z\text{-}sand}$). These slug-test analysis results represent the first known in situ, field-scale, hydraulic property estimates for the Cold Creek fine-grained sand unit ($CCU_{z\text{-}sand}$) at the Hanford Site.

The analysis of the PWA test well slug test responses follows the procedure previously described in Spane and Newcomer (2009) and Newcomer (2014), which relies on the use of slug test type curve and derivative plot matching, using the slug test KGS (Kansas Geological Survey) model described in Liu and Butler (1995) and Butler (1998). As a corroborative check, the slug test analysis method by Bouwer and Rice (1976) and Bouwer (1989) was also used for comparative purposes. As noted previously in Spane et al. (2001a,b, 2002, 2003), the type-curve and derivative plot matching analysis procedure is attributed to providing more quantitative results (i.e., in comparison to the Bouwer and Rice method), due to the use of the entire slug test response in the analysis process, and the diagnostic use of the test response and its derivative plot for formation-type response characteristics.

All PWA test/depth intervals within the $CCU_{z\text{-}sand}$ exhibit exponential-decay (over-damped) slug-test response behavior. This type of slug-test response pattern is indicative of test intervals with low-to-

medium permeability. For test/depth intervals within the lower half of the perched $CCU_{z\ sand}$, analyses indicated a best estimate average range for transmissivity of 1.26 to 1.92 m^2/day for the four slug tests (two injection and two withdrawal slug tests) conducted within this zone (i.e., Zone 1). This average transmissivity range yields a best estimate average range for hydraulic conductivity of 0.72 to 1.36 m/day for the lower half of the perched $CCU_{z\text{-}sand}$ at these two well locations (Table B.2). Figure B.1 shows an example of a slug-test type-curve and derivative plot analysis for a selected test within the lower half of the $CCU_{z\text{-}sand}$ (Zone 1) at test well 299-E33-351.

For test/depth intervals that represented the ~ PWA full saturated thickness (i.e., $CCU_{z\text{-}sand}$), analyses indicated a best estimate average range for transmissivity of 1.65 to 3.64 m^2/day for the three slug tests (one injection and two withdrawal tests) conducted for the composite PWA thickness (i.e., Zone 2). This average transmissivity range yields a best estimate average range for hydraulic conductivity of 0.58 to 1.30 m/day for the full composite $CCU_{z\text{-}sand}$ saturated thickness at these two well locations (Table B.2). Figure B.2 illustrates an example of a slug-test type-curve and derivative plot analysis for a selected test of the full/composite PWA thickness at test well 299-E33-350 (Zone 2).

A best estimate for average transmissivity for the upper PWA zone was inferred using the principle of superposition (Reilly et al. 1987), by subtracting the best estimate transmissivity values for the lower PWA test section from the composite/full PWA thickness test rest result. Based on this application, the upper PWA test-section transmissivity was inferred to range from 0.27 to 2.38 m^2/day and hydraulic conductivity was inferred to range from 0.18 to 2.27 m/day for the upper $CCU_{z\text{-}sand}$ (Figure B.3 and Figure B.4). These estimates, which assume uniform hydraulic conductivity across each individual test/depth interval, are representative of the silty-sand subunit, $CCU_{z\text{-}sand}$, conditions at these PWA test well locations.

Table B.1. PWA slug-test characteristics for selected test/depth intervals at test wells 299-E33-350 and 299-E33-351 (from Newcomer 2014). This table is FIO.

PWA Test Well	Test Zone	Test Parameters				Diagnostic Slug-Test Response Model	Hydrogeologic Unit Tested
		Test Date	Number of Slug Tests	Depth to Water (m bgs)[(a)]	Depth/Test Interval (m bgs)		
299-E33-350	Zone 1	3/5/14	2	68.21	69.68–71.09	Nonelastic, Homogeneous Formation/ Exponential-Decay (over-damped)	Cold Creek fine-grained unit ($CCU_{z\text{-}sand}$)
	Zone 2	3/5/14 to 3/6/14	2	68.24	68.24–71.09	Nonelastic, Heterogeneous, Composite-Formation/ Exponential-Decay (over-damped)	Cold Creek fine-grained unit ($CCU_{z\text{-}sand}$)
299-E33-351	Zone 1	2/26/14	2	68.24	69.22–70.97	Nonelastic, Homogeneous Formation/ Exponential-Decay (over-damped)	Cold Creek fine-grained unit ($CCU_{z\text{-}sand}$)
	Zone 2	3/5/14	2	68.17	68.17–70.97	Elastic, Homogeneous Formation/ Exponential-Decay (over-damped)	Cold Creek fine-grained unit ($CCU_{z\text{-}sand}$)

(a) bgs = below ground surface

Table B.2. PWA slug-test-analysis results for wells 299-E33-350 and E33-351 (from Newcomer 2014). This table is FIO.

PWA Test Well	Test Zone	Type-Curve Analysis Method		Bouwer and Rice Method
		Hydraulic Conductivity, $K_{h,}$[(a)] (m/day)	Specific Storage, S_s (m^{-1})	Hydraulic Conductivity, $K_{h,}$[(a)] (m/day)
299-E33-350	Zone 1	1.20 – 1.51 (1.36)	2.0E-3 – 3.0E-3	1.12 – 1.43 (1.28)
	Zone 2 (Inner Zone)	2.88	1.0E-5	2.55
	Zone 2 (Outer Zone)	0.58	1.0E-5	0.40
299-E33-351	Zone 1	0.62 – 0.82 (0.72)	1.0E-5 – 9.0E-4	0.57 – 0.67 (0.62)
	Zone 2	1.15 – 1.44 (1.30)	8.0E-4 – 1.0E-3	1.15 – 1.47 (1.31)

Note: Number in parentheses is the average value for all tests.
(a) Assumed to be uniform within the well-screen test section.

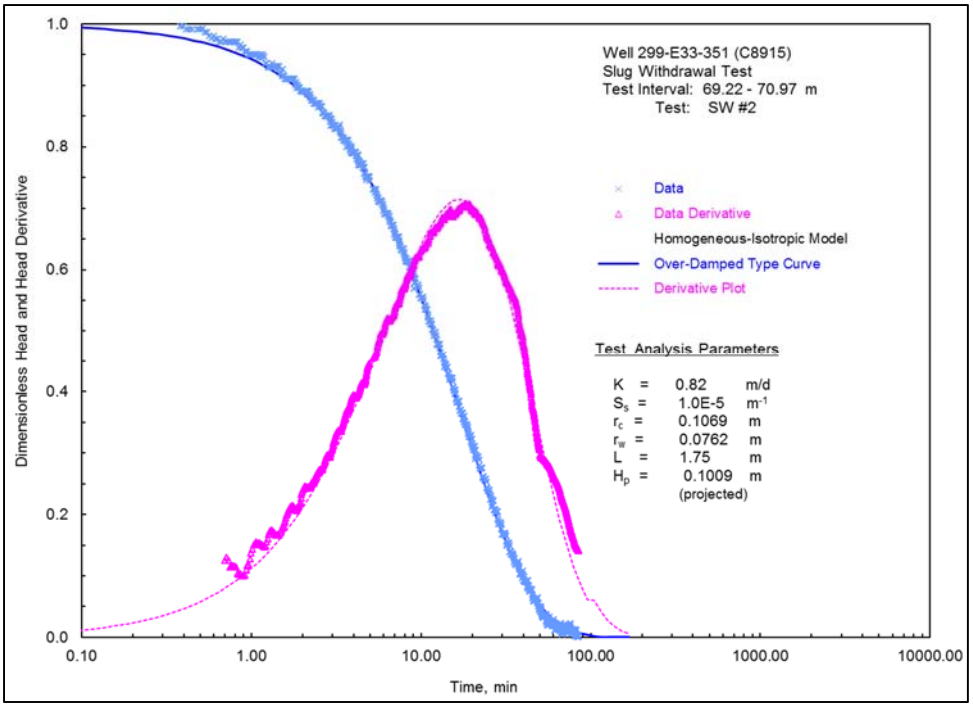

Figure B.1. Selected type-curve analysis plot for lower PWA section (Zone 1), Well 299-E33-351 (from Newcomer 2014). This figure is FIO.

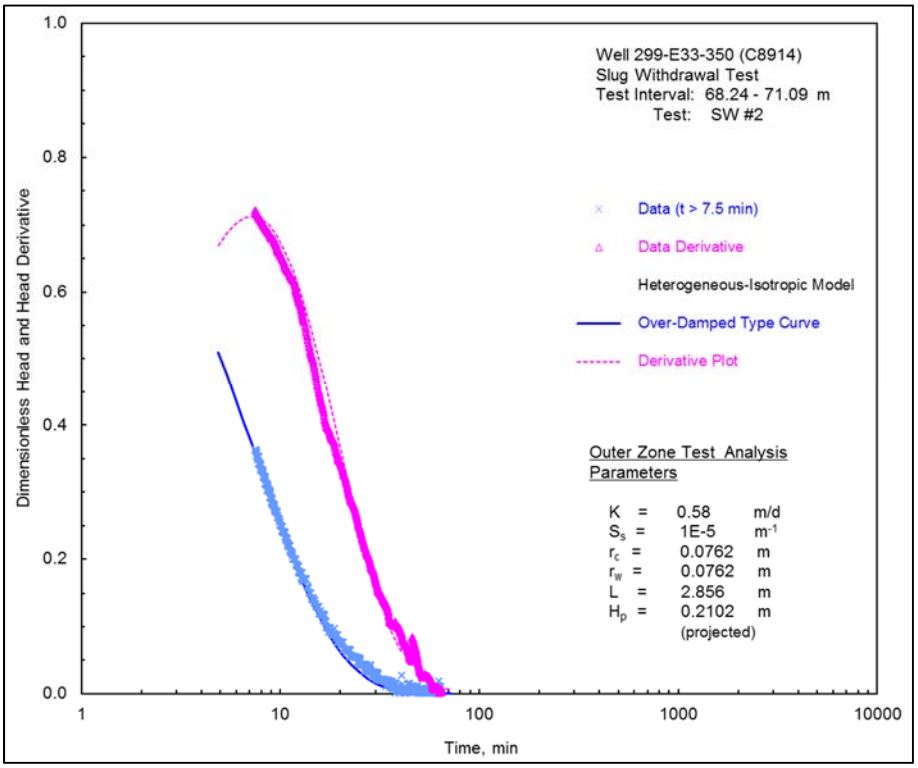

Figure B.2. Selected type-curve analysis plot for composite PWA thickness (Zone 2), Well 299-E33-350, for the lower permeability outer-zone formation (from Newcomer 2014). This figure is FIO.

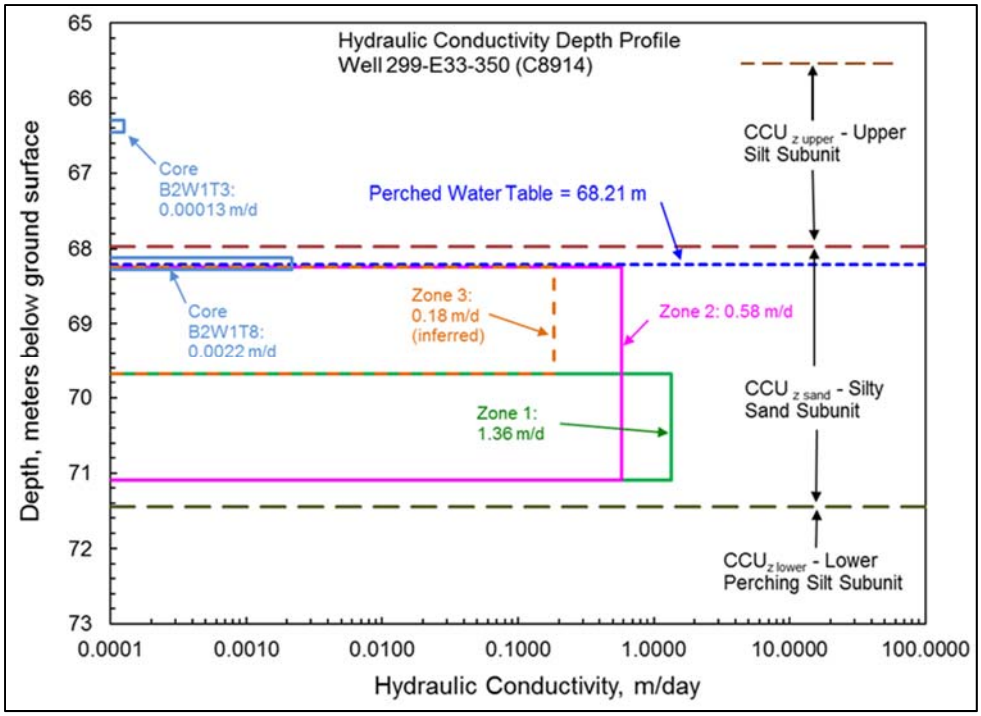

Figure B.3. Hydraulic-conductivity depth profile for well 299-E33-350 (from Newcomer 2014). This figure is FIO.

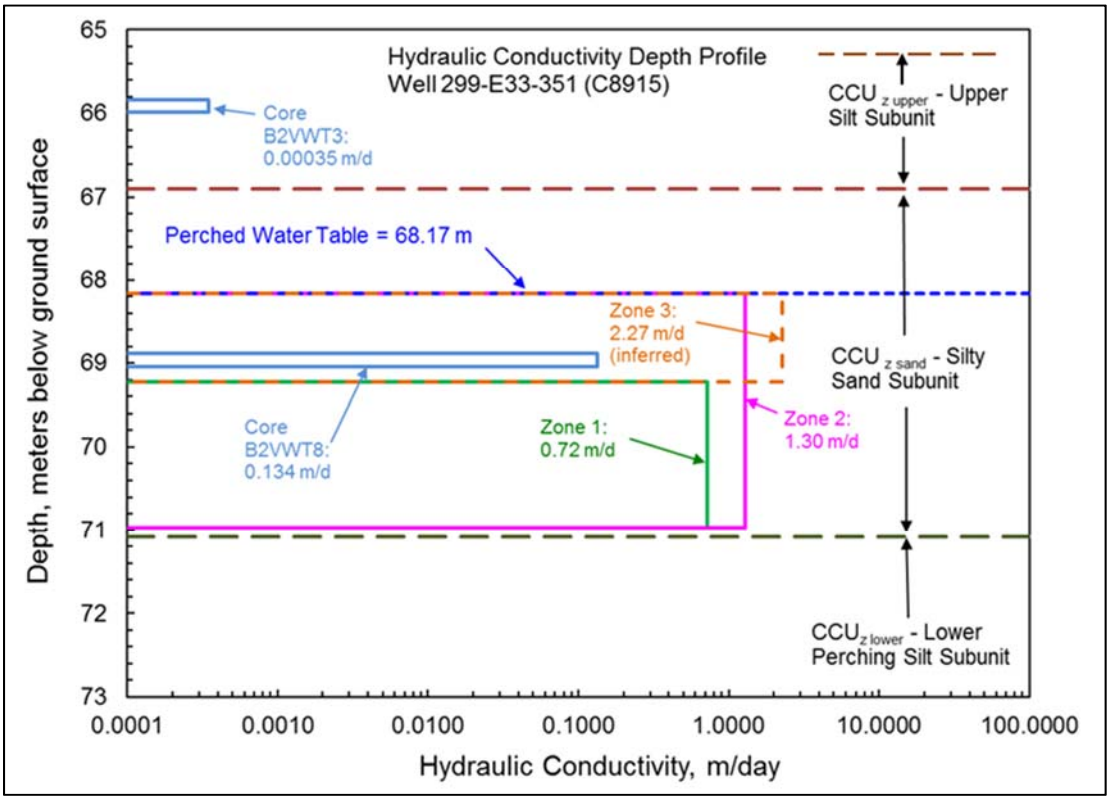

Figure B.4. Hydraulic-conductivity depth profile for well 299-E33-351 (from Newcomer 2014). This figure is FIO.

B.2 FY16 Barometric Response Function Analysis

Because of the significant impact that surface barometric pressure fluctuations have on the temporal water-level response at PWA wells (see Figure B.5), barometric response analysis was conducted prior to performing detailed hydraulic characterization tests at each of the three PWA test well locations. The objective of the analysis was to establish the time-dependent relationships for each well site for the observed barometric signal to facilitate removal of barometric effects from the monitored well water-level response. Results of the FY16 barometric response analysis were previously reported in DOE (2016). Salient findings and discussion pertaining to the FY16 barometric response function analysis of PWA wells 299-E33-344, 299-E33-350, and 299-E33-351 are taken from these reporting sources and summarized below.

Baseline monitoring of well water-level response and site barometric pressures were observed for an extended, non-stressed period of ~30 days, between February 20 and March 21, 2016, at the three PWA well-site locations. Based on this baseline period, barometric response functions (BRFs) were developed for each of the PWA test wells, using the BRF procedures described in Rasmussen and Crawford (1997), and Spane (1999, 2002). The BRF analysis plots were obtained using the MRCX software program described in Mackley et al. (2010) and Spane and Mackley (2011). The BRF well relationships were used to remove barometric pressure effects from the well water-level records observed at the three PWA test wells during subsequent hydraulic test characterizations and during operational pump-and-treat activities that occurred during FY16 and FY17.

As shown in Figure B.5 the collected barometric and water-level data fluctuate inversely over a range of about 0.37 m (1.2 ft). The fluctuation is due to the imbalance in pressure measured within the well (with a vented pressure probe) and the pressure within the surrounding PWA. Each of the three PWA wells exhibited a similar response pattern, indicating a general similarity in vadose zone barometric transmission characteristics for the area investigated by each of these wells. Spectral analysis of the data (not shown here) indicates that the water-level response was highly associated with the barometric pressure signal over the entire frequency spectrum.

The barometric response functions developed for each test well exhibited complex time-lag patterns (i.e., in excess of 14-days), likely caused by multiple barometric transmission pathways/conditions from the surface to the PWA well screened interval. For wells 299-E33-350 and 299-E33-351, the early-time (0 to 80 hours of time lag) shows a vertical (vadose zone) pressure transmission pattern. The subsequent prolonged constant barometric response function pattern suggests the presence of surrounding confined aquifer conditions for the PWA (Figure B.6). In contrast, well 299-E33-344 shows a delayed pattern in the first 8 hours, indicative of wellbore storage effects (Figure B.7), which is attributed to lower transmissivity conditions surrounding this well location, as indicated also by results from hydraulic characterization tests. This initial response is followed by multiple barometric response pattern segments. While the developed barometric response functions enabled adequate barometric pressure response removal from the well water-level record (see Figure B.8), more extended baseline (quiescent) monitoring (e.g., 30- to 60-day baseline) may be required to improve the barometric response function analysis process. A more detailed discussion of barometric response function analysis and possible applications as it relates to characterization and optimization of pump-and-treat activities is provided in DOE (2016).

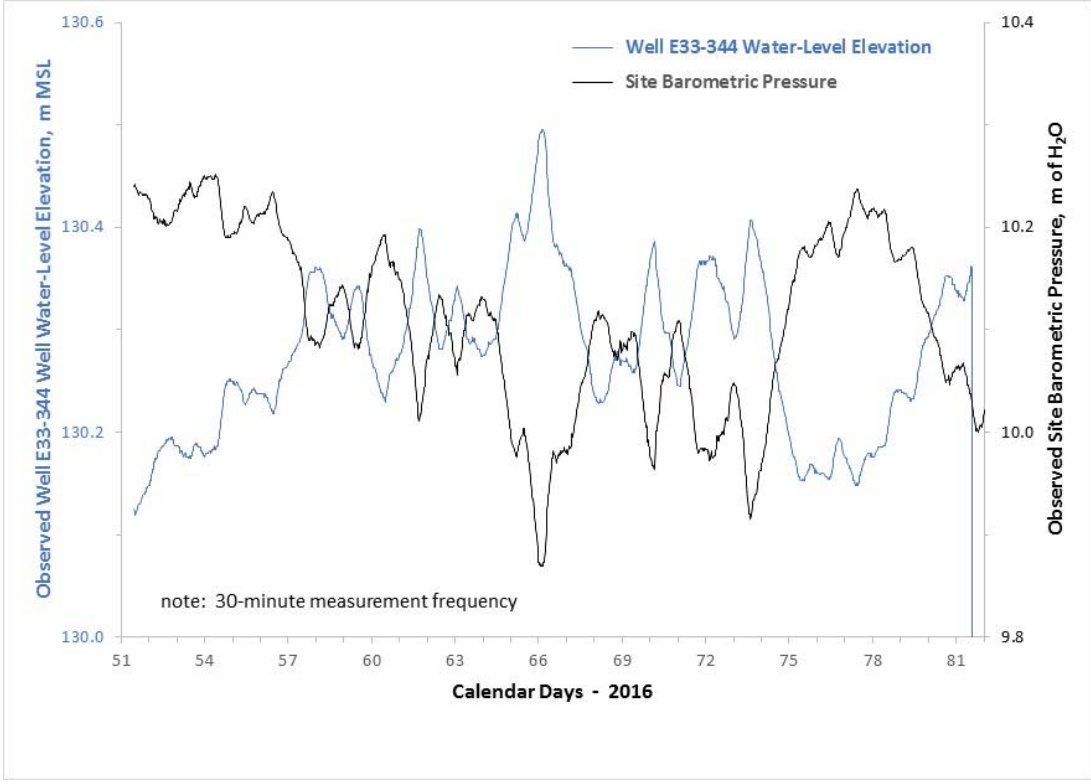

Figure B.5. Baseline water-level and barometric data for well 299-E33-344 (modified from DOE 2016). This figure is FIO.

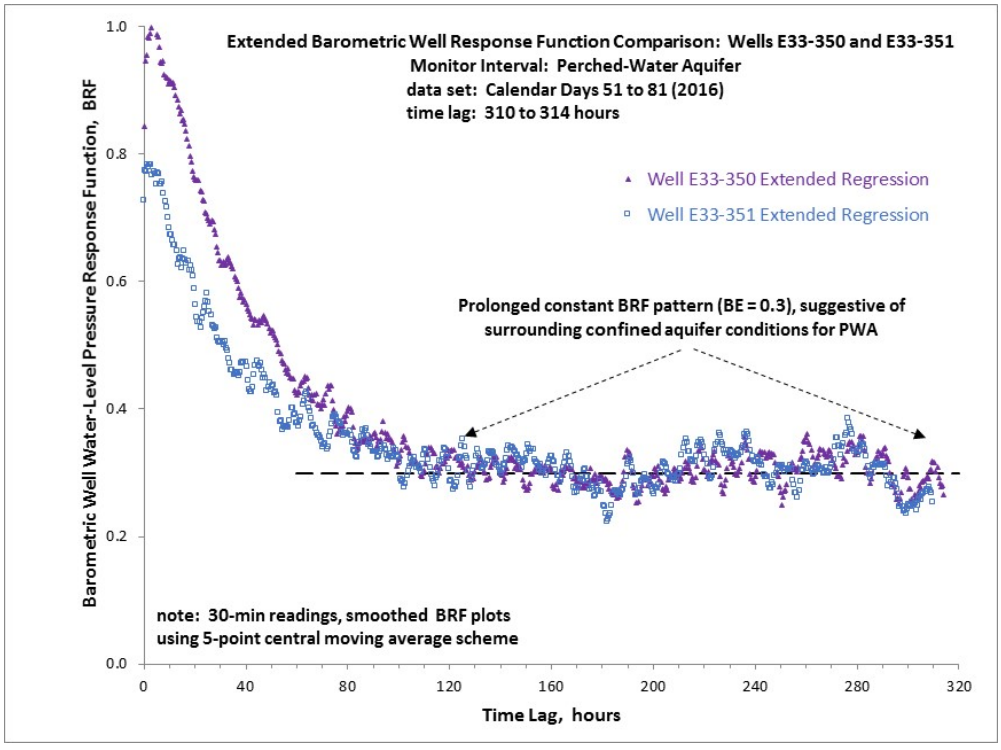

Figure B.6. Barometric response function analysis for PWA wells 299-E33-350 and 299-E33-351 (from DOE 2016). This figure is FIO.

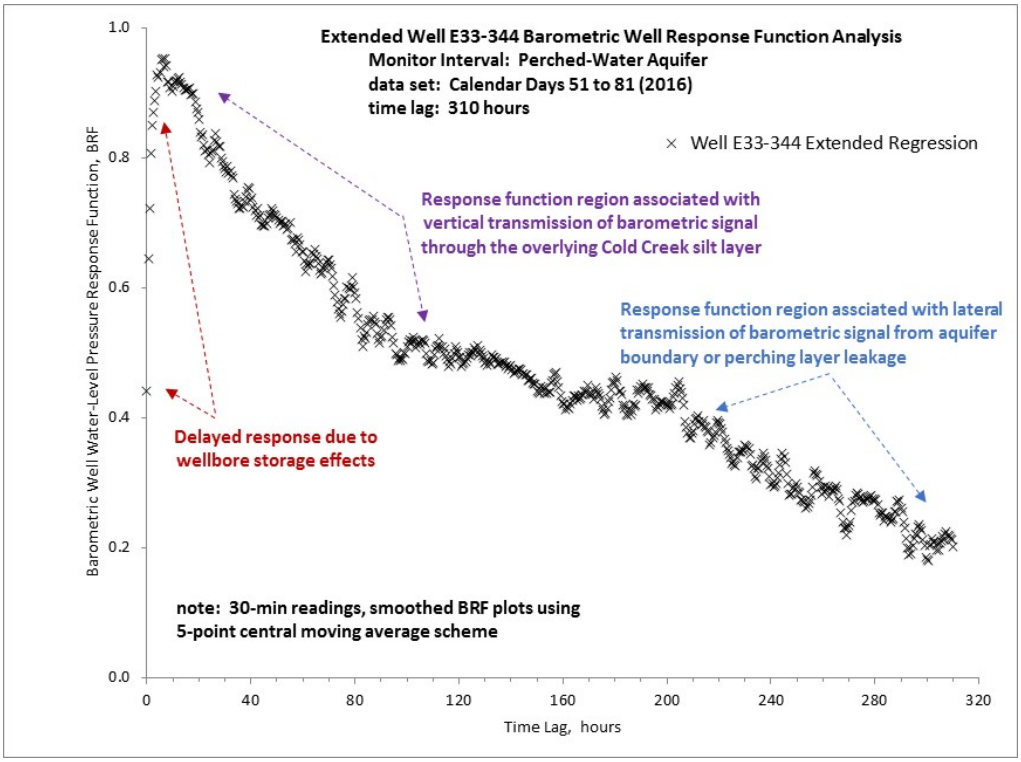

Figure B.7. Barometric response function analysis for well 299-E33-344 (from DOE 2016). This figure is FIO.

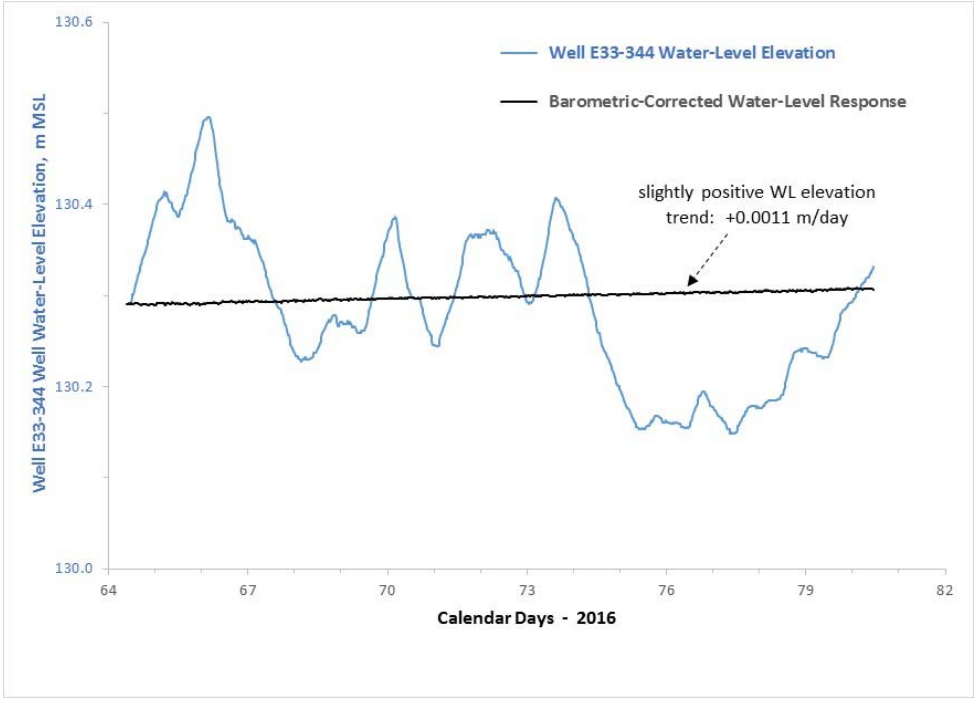

Figure B.8. Comparison of observed vs. corrected barometric well 299-E33-344 water-level response during FY16 baseline monitoring period (modified from DOE 2016). This figure is FIO.

B.3 FY16 Single-Well Cyclical Pumping Test Results

Because of the varying, transient impact that aquifer hydrologic/storage properties have on pumping test drawdown response, this hydrologic test method can be applied to provide representative, intermediate-scale estimates for these characterization properties. In this section, the test response characteristics of unconfined aquifer pumping tests are first discussed, followed by reporting the results of single-well pumping tests conducted in FY16 at three PWA test well locations. Results of these tests have been previously reported in varying degrees of detail in DOE (2016).

B.3.1 Test Response Characteristics for Unconfined Aquifer Pumping Tests

For constant-rate pumping tests conducted in PWAs (exhibiting unconfined aquifer system conditions), test drawdown behavior should exhibit three distinctive test segment patterns during testing (if testing is performed long enough). As originally presented in a series of papers by Neuman (1972, 1973, 1974, 1975, 1979), these three distinctive test response patterns include (1) an initial elastic Theissian test response following the elastic storage (storativity), S, property of the aquifer; (2) a subsequent departure and flattening of the drawdown curve (commonly referred to as the "Delayed Yield" portion of the drawdown curve); and (3) a later time period when the drawdown curve approaches and becomes coincident with the Theissian test response, but governed by the unconfined aquifer specific yield, S_y. The separation in time when drawdown departed from the first test limb/segment pattern to becoming coincident with the third/last test limb/segment is determined by the ratio of the aquifer elastic storativity, S, to the aquifer specific yield, which Neuman assigned the parameter sigma, σ:

$$\sigma = S/S_y \tag{B.1}$$

For example, an unconfined aquifer with a S of 0.00015 and a S_y of 0.15, the point of drawdown coincidence with the Theissian S_y in late-test time would be three orders of magnitude in time (a factor of 1000) from whence the drawdown departed from early-time Theissian S response pattern. In this case, if the Theissian S response departure occurred 10 minutes into the test, then the drawdown response would become coincident with the Theissian S_y curve at 10,000 minutes.

Controlling when the departure from the initial elastic Theissian S response occurs (i.e., the "Delayed Yield" middle portion of the drawdown response) is dependent on the distance from the pumping well to the point of test observation, r; the thickness of the unconfined aquifer, b; and the aquifer vertical anisotropy, K_D, ($K_D = K_v/K_h$). This composite parameter is generally referred to as Beta, β, (Neuman 1975) where

$$\beta = (r^2/b^2)K_D \tag{B.2}$$

Figure B.9 shows the development of the three drawdown patterns during pumping tests and the influence of σ and β on the departure from the initial early-time, Theissian elastic (S) drawdown response and final coincidence with the late-time Theissian S_y response pattern. For the dimensionless time and drawdown parameters shown in the figure the following definitions are provided, as reported in Spane (1993) and Spane and Wurstner (1993):

$$t_{DS} = (T\ t)/(r_o^2\ S) \tag{B.3}$$

and,

$$s_D = (4\pi\ T\ \Delta s)/Q \quad (B.4)$$

where,

T = aquifer transmissivity; L^2/T

t = pumping test time; T

r_o = radial distance from pumping well to the observation well; L

S = aquifer elastic storage; dimensionless

Δs = drawdown at observation well location; L

Q = pumping rate at stress well location; L^3/T

For interference pumping tests, where the test response is being monitored at an observation well at a distance r_o from the pumping well(s), Eq. (B.2) is modified to

$$\beta_o = (r_o^2/b^2)K_D \quad (B.5)$$

For single-well pumping tests where the test response is being monitored at the test well location, then the pumping well radius, r_w, is used and Eq. (B.2) is modified to

$$\beta_w = (r_w^2/b^2)K_D \quad (B.6)$$

Given that r_o, r_w and b are normally well known or constrained, Eqs. (B.5) and (B.6) indicate that analysis of pumping tests then can provide a direct estimate for aquifer vertical anisotropy, K_D, based on the analyzed drawdown pattern response (i.e., β). With larger beta, β, values, the earlier the departure from the initial elastic Theissian S portion of the pumping test drawdown response. As indicated in Eqs. (B.5) and (B.6), larger β conditions are produced (1) at larger test observation location distances, r_o, or well radii, r_w; (2) thinner unconfined aquifer thickness, b; and (3) for higher vertical anisotropy, K_D aquifer conditions.

The previous discussion pertains specifically to drawdown (and recovery) well water-level responses observed during constant-rate pumping tests. However because of the relative thinness of the PWA and characteristics of the pumping equipment deployed at the various PWA extraction wells, the previous hydraulic tests and operational pumping activities at the PWA well sites were/are conducted in cyclical pumping fashion (i.e., repetitive pumping on followed by pumping off periods). The same diagnostic unconfined aquifer test response patterns, however, would be exhibited at PWA pumped wells during extended recovery periods following termination of cyclical pumping activities, or for drawdown responses monitored at distant PWA observation well locations during extended cyclical pumping sequences.

B.3.2 Results of Single-Well Pumping Tests

A brief description of the performance and analytical results for performing the individual FY16 single-well, cyclical pumping tests is described in this section. Summary aspects of this test characterization element have previously been presented in DOE (2016). Cyclical pumping test durations ranging between 3.5 to 7 days were utilized at the individual PWA extraction well location, followed by an extended ~10- to 14-day recovery period after termination of pumping activities was implemented at the three PWA extraction well locations. Table B.3 lists the timing/durations implemented during the FY16 cyclical pumping characterization tests.

The cyclical pumping drawdown and subsequent recovery following termination of the pumping phase were analyzed as a combined test history match (i.e., both cyclical drawdown and recovery) for determining aquifer hydraulic/storage parameters surrounding each of the PWA test wells. The observed cyclical drawdown and recovery were matched using the Moench model contained within the analytical AQTESOLV software program, as described in Duffield (2007). Aquifer property estimates obtained from the test history analyses of the individual cyclical pumping well tests are listed in Table B.4. A brief description of the individual well tests and test analyses is provided in the following section.

B.3.2.1 Well 299-E33-344

A ~7-day cyclical pumping test was conducted at well 299-E33-344 between March 21 and 28, 2016. In total, 299 continuous pumping cycles were performed over the ~7 days of testing, with an average pumping cycle time of 1.3 minutes pumping/on and 32.6 minutes pumping/off describing an individual pumping cycle. An average pumping rate of 16.28 L/min (4.3 gpm) was observed during the actual pumping/on phase of the cycle. A total of 6,190 L (1635 gal) were extracted during the cyclical pumping test conducted at PWA well 299-E33-344.

Figure B.10 shows the observed well 299-E33-344 water-level response during cyclical pumping and during the extended recovery period following termination of pumping. As indicated in the figure, the cyclical pumping appears to be relatively uniform during the entire pumping phase of the test. Figure B.11 shows the test history analysis match of the barometric-corrected drawdown response during pumping and recovery periods, utilizing the developed barometric response function developed for this test well, as previously described in Section B.2. It should be noted that a log-log plot format was utilized for the test history match to accentuate the sensitivity of the drawdown and recovery analysis process. As shown, a very good history match was obtained using the PWA parameters indicated.

B.3.2.2 Well 299-E33-350

A ~3.5-day cyclical pumping test was conducted at well 299-E33-350 between April 11 and 14, 2016. In total, 113 continuous pumping cycles were performed over the ~3.5 days of testing, with an average pumping cycle time of 5.7 minutes pumping/on and 39.3 minutes pumping/off describing an individual pumping cycle. An average pumping rate of 9.09 L/min (2.4 gpm) was observed during the actual pumping/on phase of the cycle. A total of 5,770 L (1524 gal) were extracted during the cyclical pumping test conducted at PWA well 299-E33-350.

Figure B.12 shows the observed well 299-E33-350 water-level response during cyclical pumping and during the extended recovery period following termination of pumping. As noted in Table B.3, the abbreviated cyclical pumping period of ~3.5 days was a result of operational pump/well pressure setting constraints that were utilized at the test well. However as indicated in the figure, the cyclical pumping appears to be relatively uniform during the entire (abbreviated) pumping phase of the test. Figure B.13 shows the test history analysis match of the barometric-corrected drawdown response during pumping and recovery periods, utilizing the developed barometric response function developed for this test well, as previously described in Section B.2. As previously noted, a log-log plot format was utilized for the test history match to accentuate the sensitivity of the drawdown and recovery analysis process. As shown, a very good history match was obtained using the PWA parameters indicated.

B.3.2.3 Well 299-E33-351

A ~7-day cyclical pumping test was conducted at well 299-E33-351 between April 25 and May 2, 2016. In total, 496 continuous pumping cycles were performed over the ~7 days of testing, with an average

pumping cycle time of 2.5 minutes pumping/on and 17.8 minutes pumping/off describing an individual pumping cycle. An average pumping rate of 9.84 L/min (2.6 gpm) was observed during the actual pumping/on phase of the cycle. A total of 9763 L (2579 gal) were extracted during the cyclical pumping test conducted at PWA well 299-E33-351.

Figure B.14 shows the observed well 299-E33-351 water-level response during cyclical pumping and during the extended recovery period following termination of pumping. As indicated in the figure, the cyclical pumping shows a distinct change in drawdown characteristics during the pumping phase of the test. This is due to an operational change in the pumping on/off well depth set points during the test. Figure B.15 shows the test history analysis match of the barometric-corrected drawdown response during pumping and recovery periods, utilizing the developed barometric response function developed for this test well, as previously described in Section B.2. As previously noted, a log-log plot format was utilized for the test history match to accentuate the sensitivity of the drawdown and recovery analysis process. As shown, a reasonable history match was obtained using the PWA parameters indicated.

Table B.3. FY16 single-well pumping test activity description. This table is FIO.

Test Period	Test Element Activity Description
3/21/16 – 3/28/16	Continuous pumping cycles at well 299-E33-344 with monitoring
3/28/2016 – 4/11/16	Monitored water table recovery under quiescent (non-pumping) conditions
4/11/16 – 4/14/16	Continuous pumping cycles at well 299-E33-350 with monitoring. Abbreviated cyclical pumping period due to operational pump/well pressure setting constraints
4/14/16 – 4/25/16	Monitored water table recovery under quiescent (non-pumping) conditions
4/25/16 – 5/2/16	Continuous pumping cycles at well 299-E33-351 with monitoring
5/2/16 – 5/17/16	Monitored water table recovery under quiescent (non-pumping) conditions

Table B.4. Estimated PWA hydraulic/storage properties determined from FY16 single-well pumping test results (modified from DOE 2016). This table is FIO.

Single-Well Pumping Tests - 2016
(DOE 2016)

Test Well	T (m^2/day)	K_h (m/day)	K_D (K_v/K_h)	S	S_y	Test Scale*
299-E33-344	0.51	0.13	0.036	1.33e-3	0.151	intermediate
299-E33-350	4.00	1.05	0.021	4.5e-3	0.273	intermediate
299-E33-351	3.49	0.91	0.012	9.0e-4	0.220	intermediate

• approximate test scale length designation: Intermediate = 0.1 to 10 m
Note: K_h estimates based on an assumed PWA average areal thickness of 3.81 m

Nomenclature:
T = transmissivity
K_h = horizontal hydraulic conductivity
K_v = vertical hydraulic conductivity
K_D = vertical anisotropy
S = storativity
S_y = specific yield

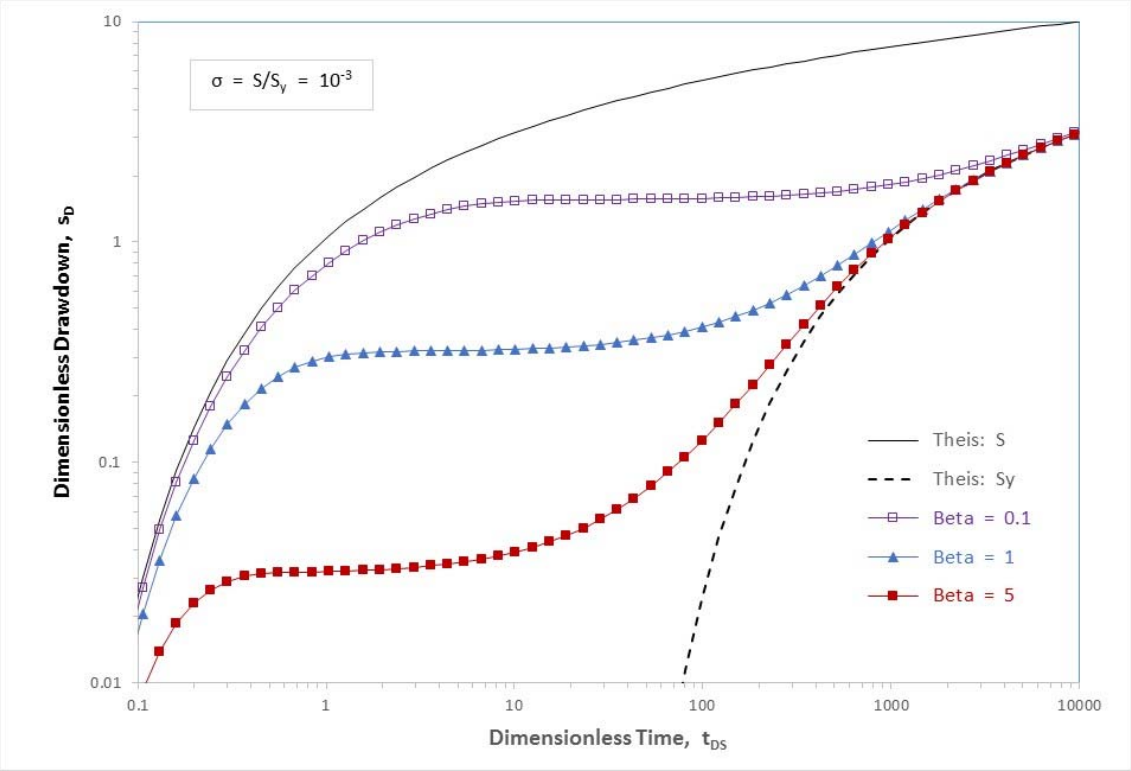

Figure B.9. Dimensionless time-drawdown type curves for constant-rate discharge tests in unconfined aquifers for $\sigma = 10^{-3}$ (modified from Spane 1993).This figure is FIO.

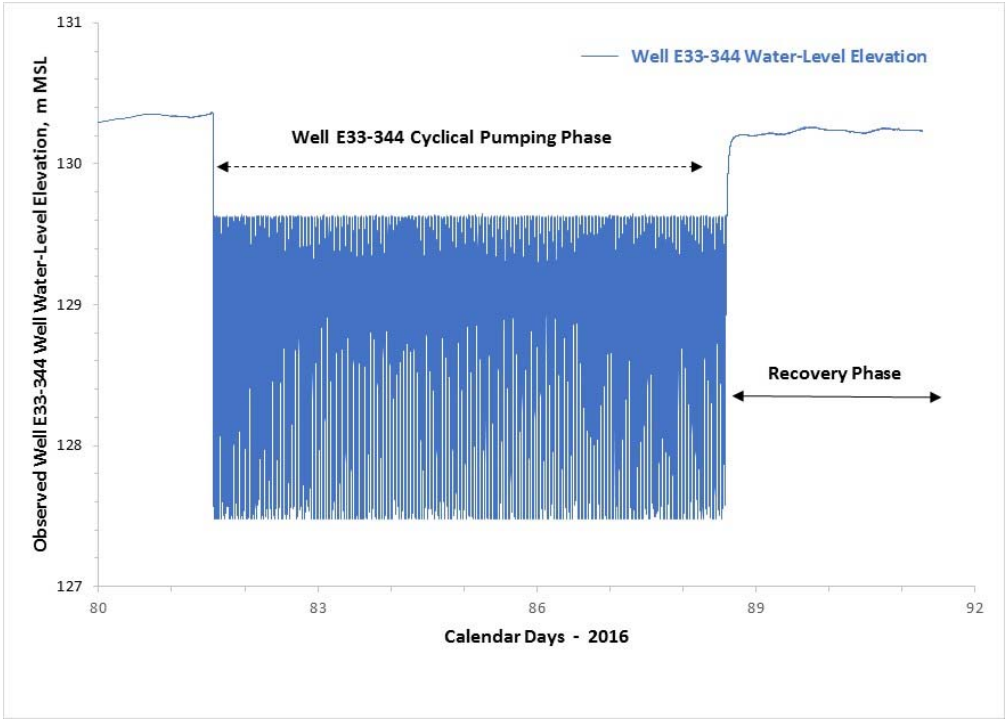

Figure B.10. Observed well 299-E33-344 water-level response during cyclical pumping test and recovery. This figure is FIO.

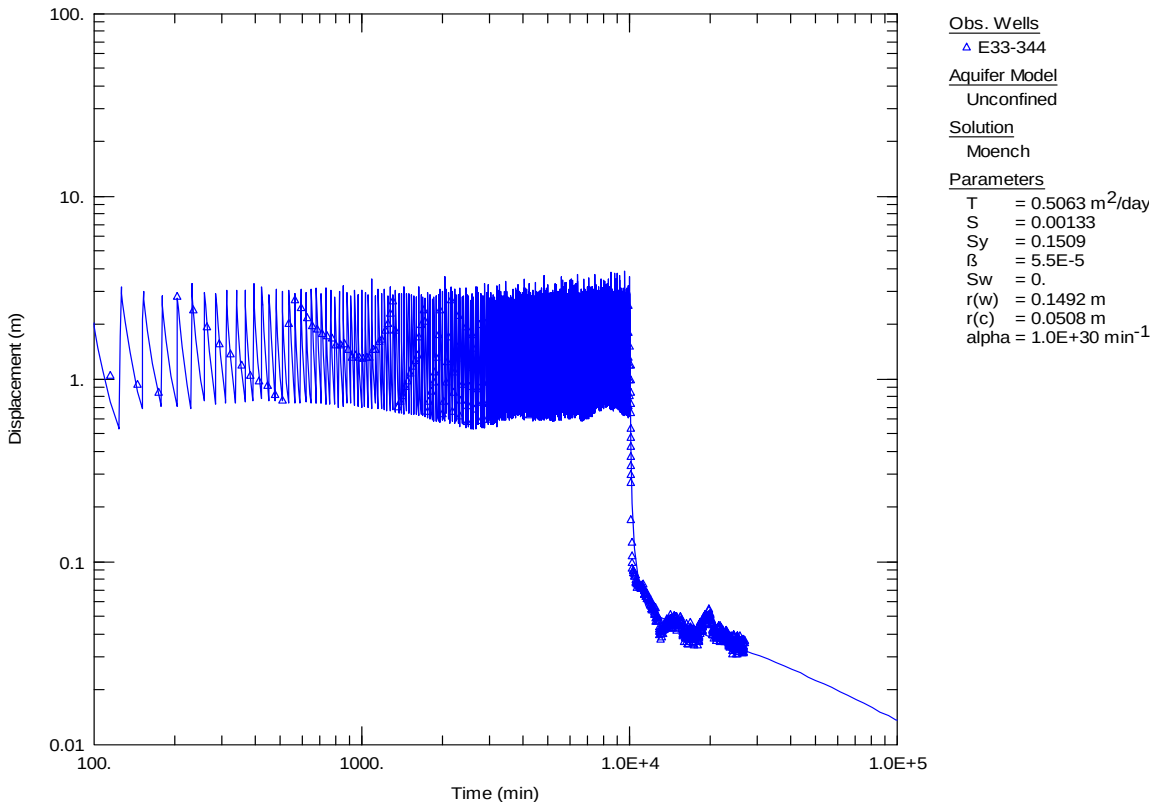

Figure B.11. Test history match of barometric-corrected drawdown response for well 299-E33-344 water-level response during cyclical pumping test and recovery. This figure is FIO.

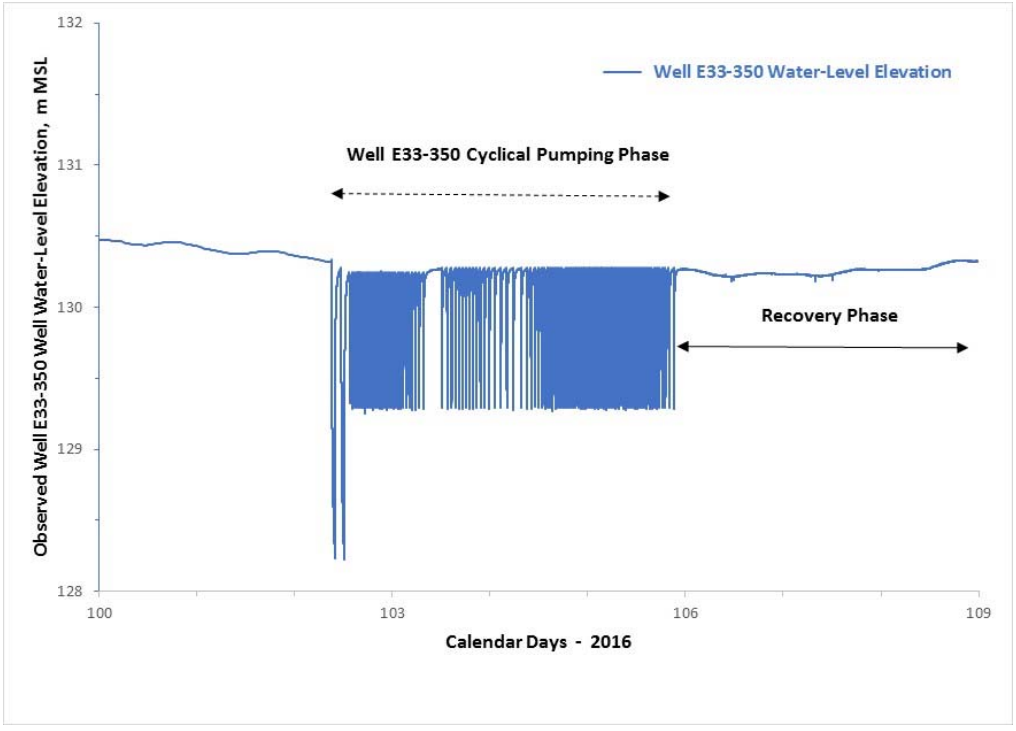

Figure B.12. Observed well 299-E33-350 water-level response during cyclical pumping test and recovery. This figure is FIO.

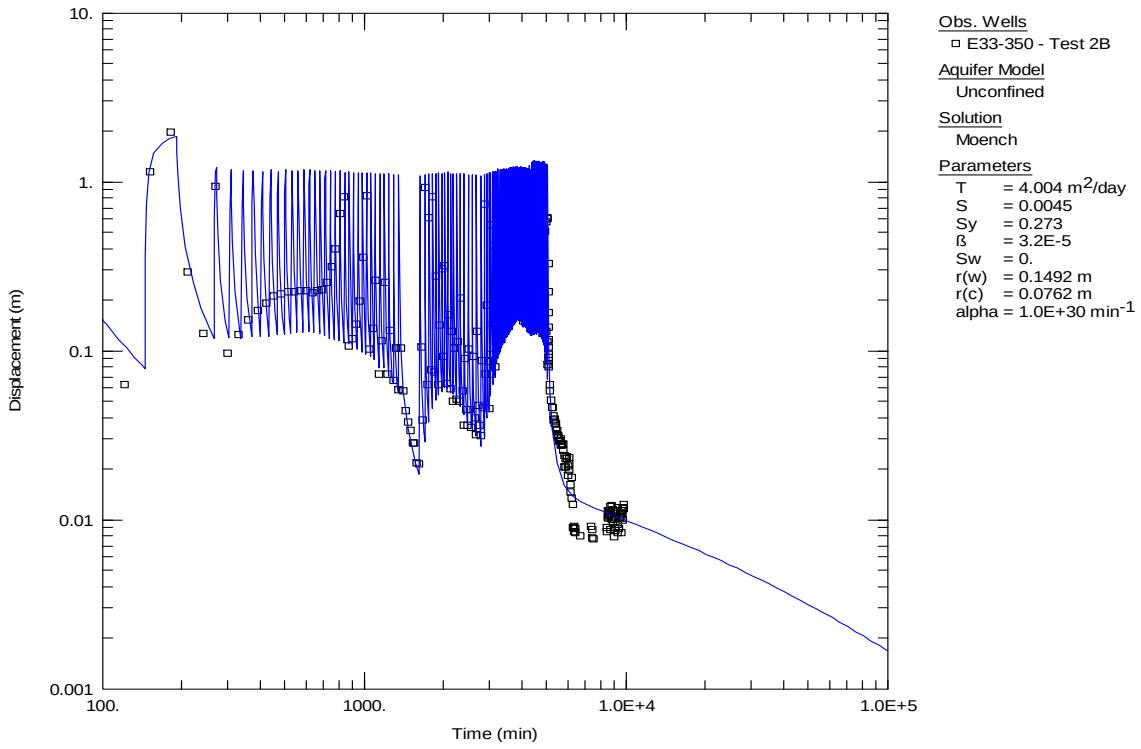

Figure B.13. Test history match of barometric-corrected drawdown response for well 299-E33-350 water-level response during cyclical pumping test and recovery. This figure is FIO.

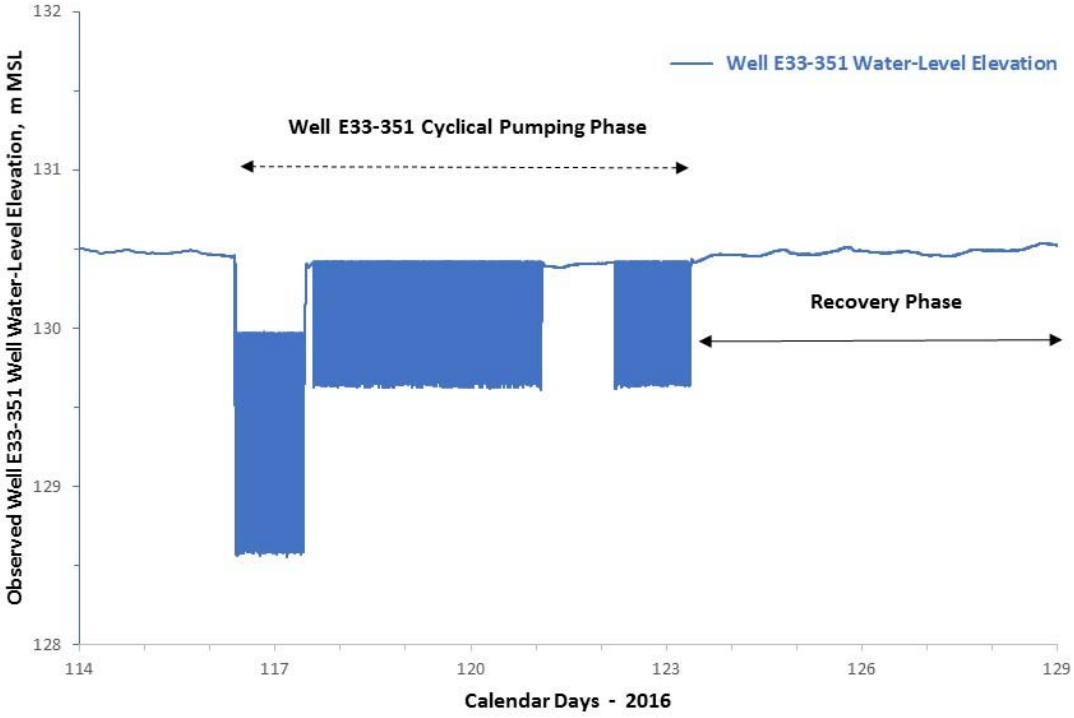

Figure B.14. Observed well 299-E33-351 water-level response during cyclical pumping test and recovery. This figure is FIO.

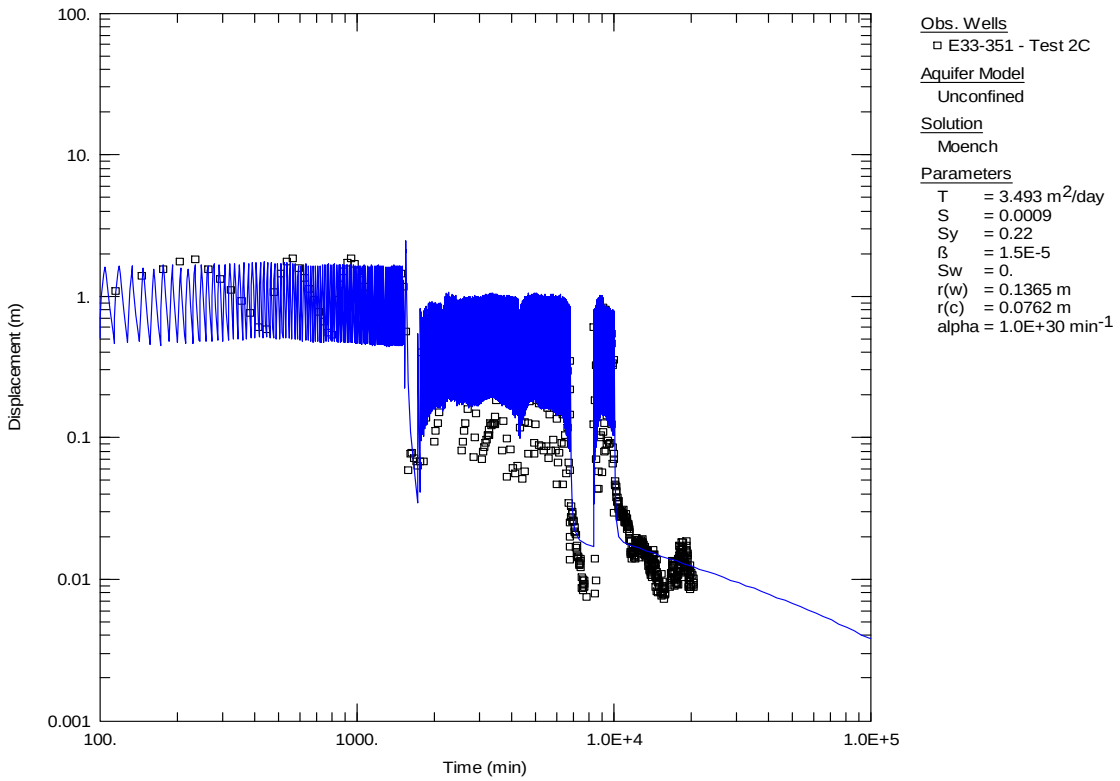

Figure B.15. Test history match of barometric-corrected drawdown response for well 299-E33-351 water-level response during cyclical pumping test and recovery. This figure is FIO.

B.4 FY17 PWA Operational Pumping Test

Results from multi-well pumping tests conducted in FY16 were the basis for conducting the longer-duration multi-well pumping test in FY17. DOE (2016) previously identified the advantages of using PWA well 299-E33-344 as an observation well to monitor the imposed drawdown during planned, long-term, operational multi-well pumping at PWA extraction wells 299-E33-350 and 299-E33-351. These identified advantages include the determination of large-scale PWA hydraulic/storage properties and the possibility of detecting PWA lateral extent boundaries, assessing aquifer dewatering progress, and optimization of operational pumping design. Realization of these possible characterization and operational objectives, however, is dependent on the accurate collection and recording of a detailed drawdown response data set from PWA observation well 299-E33-344 during prolonged, continuous pumping at PWA extraction wells 299-E33-350 and E33-351. A number of factors occurred during the FY17 operational pumping period that significantly impacted the ability to acquire a continuous and detailed drawdown data set at PWA observation well 299-E33-344. These factors eliminated the possibility to quantitatively analyze the FY17 test drawdown data. In spite of these identified testing deficiencies, a qualitative sensitivity analysis was performed for the discontinuous drawdown record obtained for PWA observation well 299-E33-344 as corroborative means to examine whether the range of aquifer hydraulic/storage properties obtained during the FY17 fall within the range of property estimates obtained from previous quantitative PWA test characterizations (i.e., as reported in Newcomer 2014, DOE 2016, and in this report). These identified test data deficiencies and results from the qualitative FY17 operational pumping test analysis is discussed in the following sections.

B.4.1 FY17 PWA Operational Pumping Activities

Long-term operational, cyclical pumping was initiated at PWA extraction wells 299-E33-350 and 299-E33-351 at ~0930 hours on February 27, 2017. Cyclical pumping continued for the remainder of FY17 at well 299-E33-350, except between: 6/7 - 8/17, and 6/12 - 13/17, when no pumping cycles were recorded. Cyclical pumping was less continuous for well 299-E33-351 for the remainder of FY17, with many intermittent pumping outages recorded in particular during the months of August and September. A total combined 979,138 L (258,661 gal) of pumped groundwater (Q_{avg} = 3.12 L/min; 0.824 gpm) was extracted from both wells during FY17, with the following breakdown by extraction well location:

- Well 299-E33-350 = 612,847 L (161,897 gal); (Q_{avg} = 1.95 L/min; 0.516 gpm)
- Well 299-E33-351 = 366,291 L (96,764 gal); (Q_{avg} = 1.17 L/min; 0.308 gpm)

The accumulated pumped volume and average pumping rate observed at each of the PWA extraction wells during FY17 are shown in Figure B.16 and Figure B.17, respectively. As indicated in the figures, the accumulated pumped volume and average pumping rates were fairly constant throughout the fiscal year.

B.4.2 Technical Issues with FY17 PWA Well 299-E33-344 Data Set

As previously noted, a number of technical issues were identified that adversely impacted the collection of a continuous and detailed data set for PWA observation well 299-E33-344 during operational pumping activities during FY17. These identified technical issues specifically identified for PWA well 299-E33-344 include:

- Numerous, extended non-recording periods
- Replacement of the well water-level sensor with a low-resolution pressure probe
- Numerous occasions during the monitoring period, when observation well 299-E33-344 was cyclically pumped

Figure B.18 shows the monitored well water-level response and occurrences where technical issues adversely impacted the data collection record at PWA observation well 299-E33-344. Of particular importance is the significant loss of in-well pressure probe resolution that occurred beginning on December 8, 2016 (Figure B.19). It is not known whether the lower pressure resolution of the replacement probe is attributable to instrument sensitivity or data acquisition settings. As shown in the figure, the replacement pressure probe resolution is ~0.03 m (0.1 ft).

The 2-month loss of observation well drawdown data between April 3 and June 3, 2017, that occurred shortly after initiation of FY17 operational pumping is also significant, since it occurs rather early in the operational pumping drawdown phase, when areal drawdown response would be expected to be more significant (i.e., drawdown over time would be greater) for analysis applications. The loss of drawdown data and lack of sensitivity of the in-well pressure probe response greatly diminishes the level of barometric pressure correction possible for observed PWA well 299-E33-344 test response. Figure B.20 shows the observed and barometric-corrected well water-level response at well 299-E33-344. The corrected response utilizes the barometric response functions developed previously in FY16 and described in Section B.2. To compensate for some of the inherent noise added by the replacement probe resolution issue, a 2-hour, central moving-average scheme was also applied to the barometric-corrected response. This corrected, moving-average response was used as the drawdown data set that was subjected for additional hydrologic test analysis.

B.4.3 Test Analysis Results of the FY17 PWA Well 299-E33-344 Corrected Data Set

The previously discussed, technical issues significantly diminished the ability to perform a robust, quantitative hydrologic test analysis of the FY17 drawdown response recorded at PWA observation well 299-E33-344. Initially, it was recommended in DOE (2016) to analyze the observed monitor well 299-E33-344 drawdown response during pumping of PWA extraction wells 299-E33-350 and 299-E33-351 during the FY17 pumping campaign for the purpose of determining large-scale PWA hydraulic/storage properties, detecting boundary conditions, and possibly assessing the progress of PWA dewatering actions. However, the numerous "issues" that occurred during FY17 for the PWA data set, as described in this section, precluded the ability to quantatively address these particular characterization objectives. Based on these limitations, a more ***qualitative assessment*** of large-scale PWA aquifer properties was attempted to see if the analysis results were consistent with local-scale hydrologic test results reported in Newcomer (2014), and for local to intermediate-scale hydrologic test results presented previously in DOE (2016).

As a result, only a qualitative, sensitivity analysis was performed using a range of β_o values (0.32 to 10.8) that are reflective of a K_D range of 0.003 to 0.1, r_o distances to the respective PWA extraction wells as indicated in Figure B.21, and an assumed, uniform PWA thickness, b of 3.81 m. The drawdown analysis was performed on barometric-corrected WLE responses observed at PWA monitor well 299-E33-344, during cyclical pumping at PWA extraction wells 299-E33-350 and 299-E33-351, using the Moench (1997) solution for unconfined aquifer test response, as presented in the AQTESOLV analytical software program (Duffield 2007). The Moench (1997) analysis is essentially identical to the Neuman solution, but includes the capability of addressing the relatively minor additional effects of wellbore storage/skin at the observation and extraction well locations. The AQTESOLV program allows "fixing" and constraining (setting limits) for various analytical parameters for the Moench solution during manual or automated drawdown curve matching procedures. This includes aquifer parameter values: T, S, S_y, β_o, and alpha (α = time release of groundwater from the transient/declining water-table boundary), for the known/given well diameter/distance relationships. The AQTESOLV software was used to compute observation well drawdown at well 299-E33-344, from pumping at the two neighboring PWA extraction wells (i.e., 299-E33-350 and 299-E33-351) through the rule of superposition (Reilly et al. 197), and accounts for aquifer dewatering using the Jacobian correction. As shown previously in DOE (2016), an average pumping rate (rather than actually superimposing the multitude of cyclical pumping cycles) can be used to provide satisfactory drawdown/recovery analysis at the PWA well sites under some limited conditions (e.g., for observation well locations, particularly for intermediate and late-time well drawdown test response analysis).

A sensitivity analysis series was performed over the K_D value range of 0.003 to 0.1 (where $K_D = K_v/K_h$). Efforts were made for this analysis series to consistently fit the Moench type-curve solution uniformly from early through the late-time drawdown response (with an emphasis placed on fitting the middle and late-time corrected response), for each assigned K_D value. Individual type-curve matching results for each of the K_D values examined are provided in Figure B.22 to Figure B.30. Table B.5 provides a summary of the sensitivity analysis results with respect to K_D variation, as it relates to PWA aquifer property estimates for T, β_o, S, and S_y.

Given the qualitative nature of analysis (and limitations imposed by the test data collected), it is difficult to place any quantitative characterization relevance for the PWA based on the FY17 analysis results. However, the sensitivity analysis results provided in Table B.5 do suggest that with increasing K_D (and subsequently increasing associated β_o values), consistently lower values for aquifer T and S are required to match the corrected drawdown response. The generally lower sensitivity analysis estimates for T are also somewhat consistent in indicating a more pervasively lower aquifer T condition in the vicinity of

monitor well 299-E33-344, which was also identified previously from single-well pumping tests for the PWA wells as reported in DOE (2016). No consistent, definitive pattern for S_y was indicated, although the estimates for this parameter fall between an acceptable range for unconsolidated sedimentary materials as reported in Johnson (1967).

Table B.5. FY17 PWA observation well 299-E33-344 sensitivity drawdown analysis. This table is FIO.

FY-2017 Observation Well 299-E33-344 Drawdown Analysis Results
Sensitivity Analysis: K_D Range = 0.003 to 0.1

K_D (K_v/K_h)	β_o	T (m^2/day)	K_h (m/day)	K_v (m/day)	S	S_y
0.003	0.322	1.408	0.370	1.08e-3	4.44e-3	0.177
0.005	0.537	0.953	0.250	1.22e-3	3.89e-3	0.259
0.007	0.752	0.706	0.185	1.26e-3	3.07e-3	0.316
0.01	1.075	0.492	0.129	1.26e-3	2.37e-3	0.372
0.02	2.149	0.224	0.059	1.15e-3	1.26e-3	0.341
0.03	3.224	0.120	0.032	9.4e-4	7.39e-4	0.321
0.05	5.373	0.047	0.012	5.8e-4	3.17e-4	0.245
0.07	7.522	0.021	0.006	3.8e-4	1.29e-4	0.186
0.10	10.75	0.009	0.002	2.3e-4	2.60e-5	0.102

Notes: Assumes 1) an average perched-water aquifer thickness of 3.81 m; 2) constant pumping rates of 1.953 L/min (0.516 gpm) for PWA extraction well E299-E33-350, and 1.166 L/min (0.308 gpm) for E33-351 during FY-2017 operational pump-and-treat activities

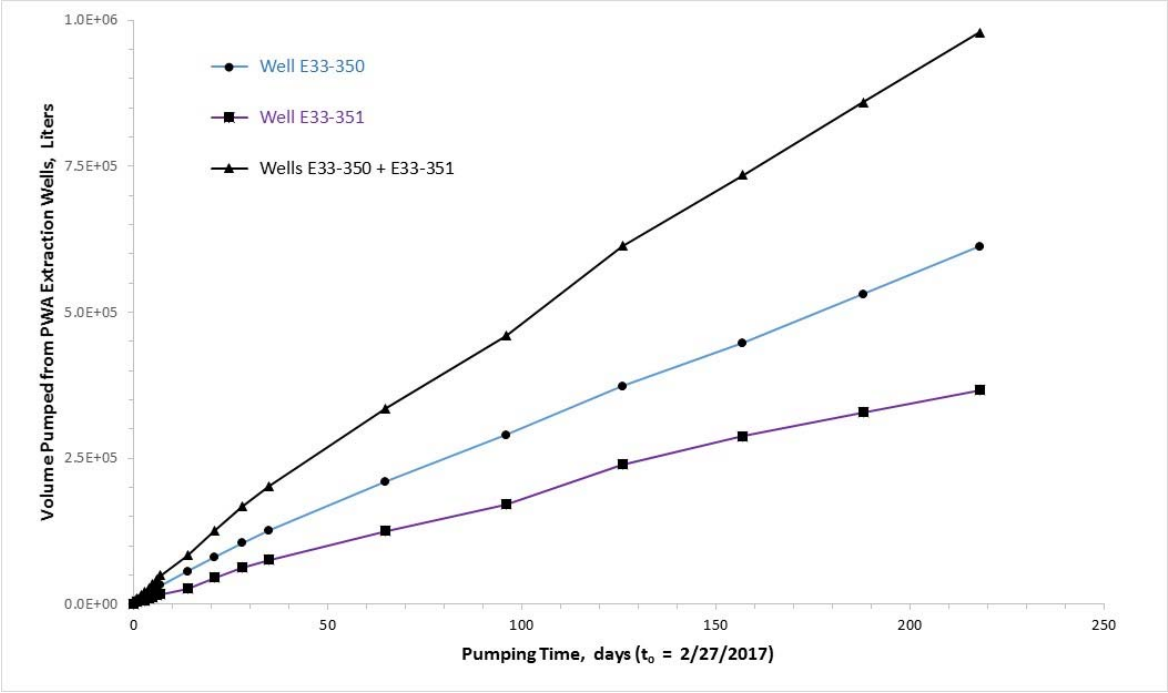

Figure B.16. FY17 pumped volume from PWA extraction wells 299-E33-350 and 299-E33-351. This figure is FIO.

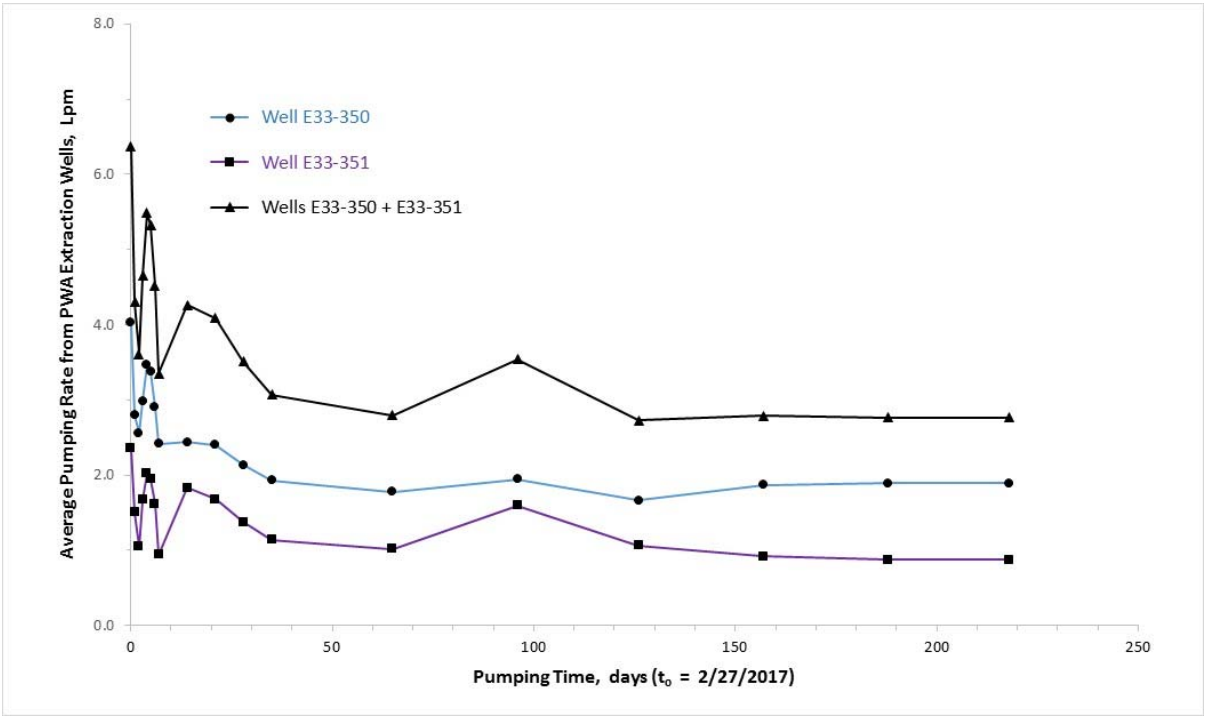

Figure B.17. FY17 average pumping rate from PWA extraction wells 299-E33-350 and 299-E33-351. This figure is FIO.

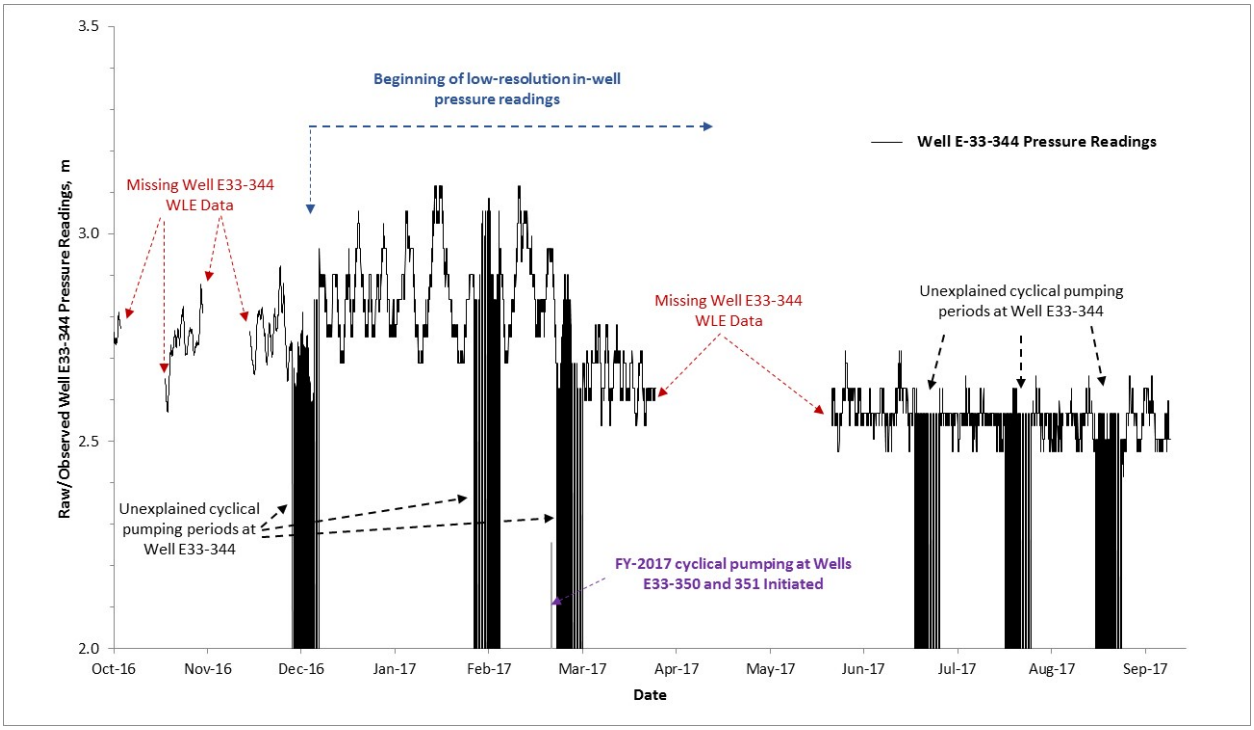

Figure B.18. Technical issues impacting observation well 299-E33-344 during FY17. This figure is FIO.

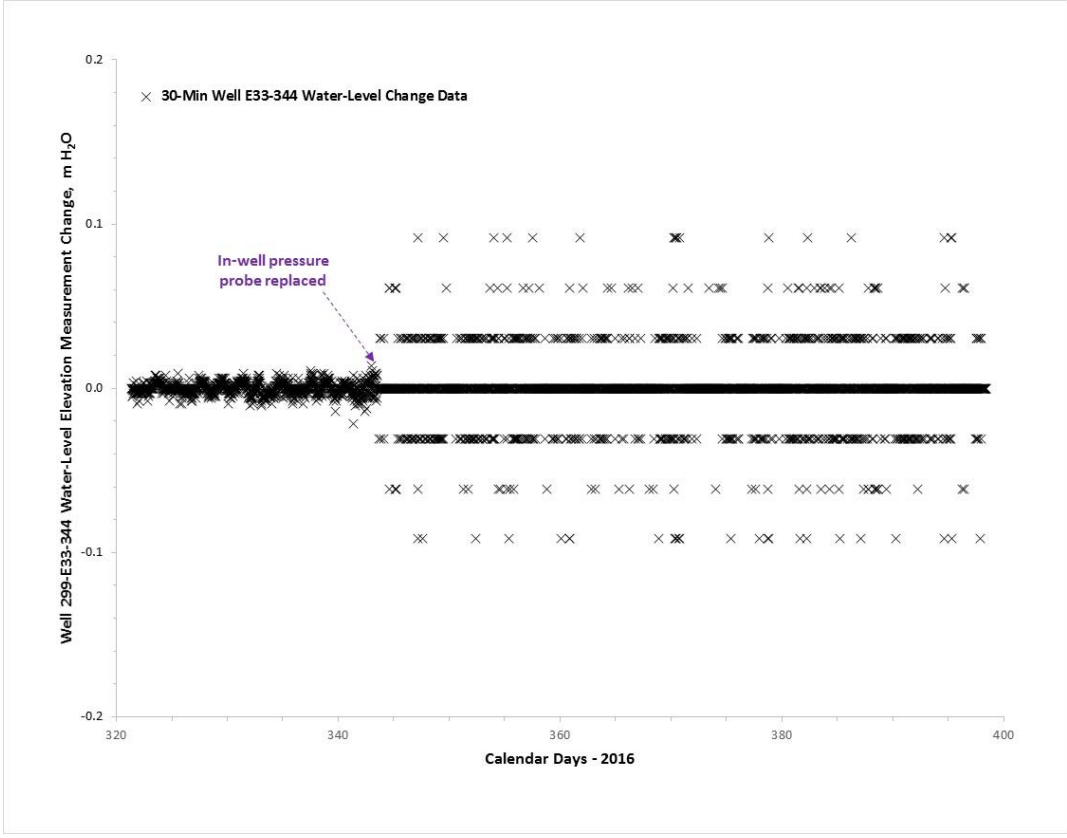

Figure B.19. Change in well 299-E33-344 replacement probe pressure resolution. This figure is FIO.

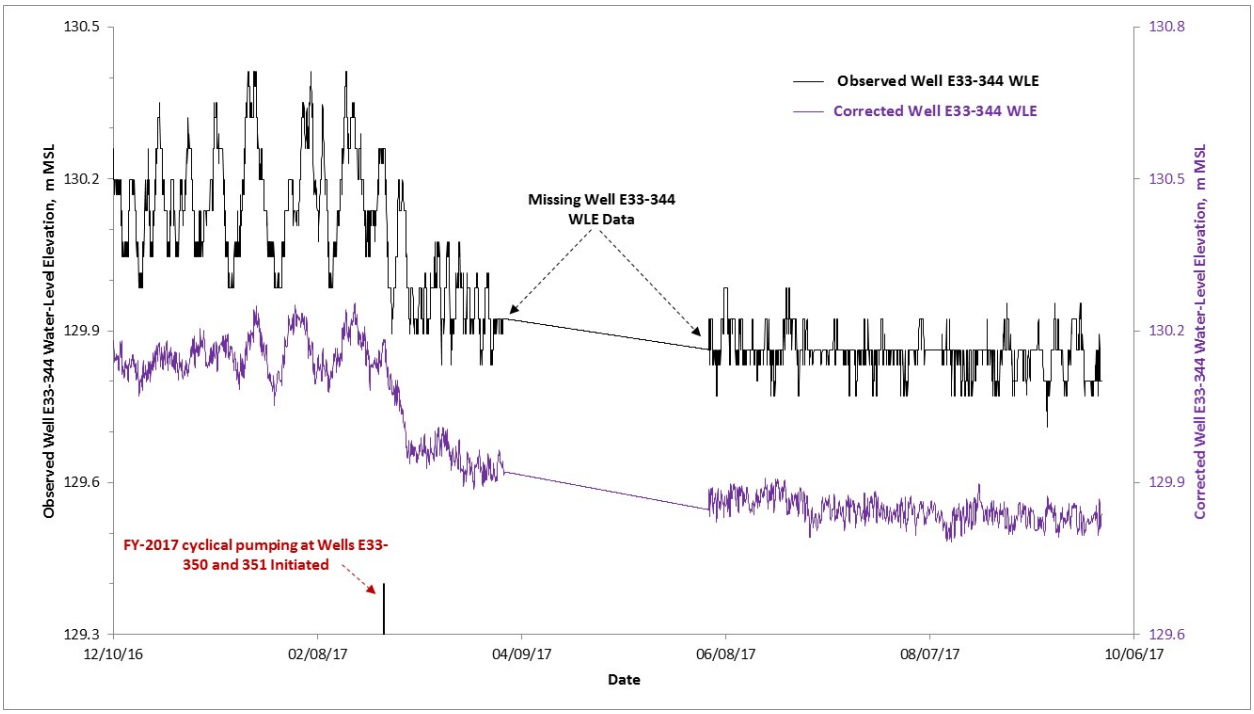

Figure B.20. Missing two-month observation Well 299-E33-344 water-level data period. This figure is FIO.

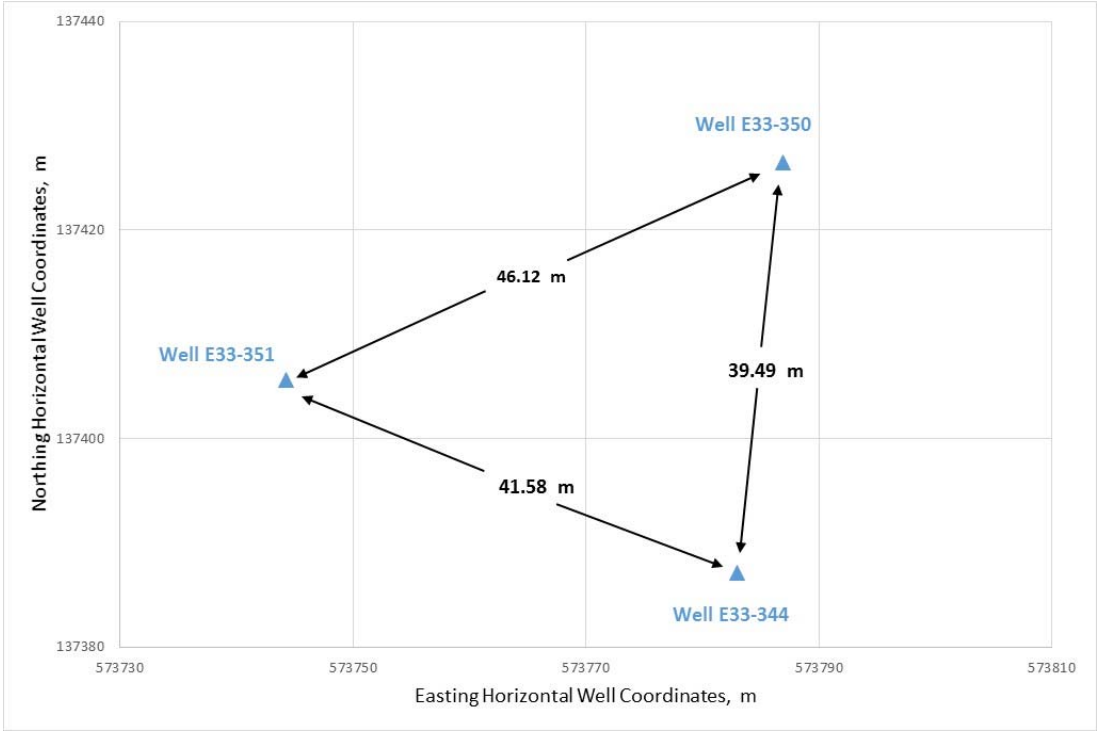

Figure B.21. Distance relationship between PWA test wells 299-E33-344, 299-E33-350, and 299-E33-351. This figure is FIO.

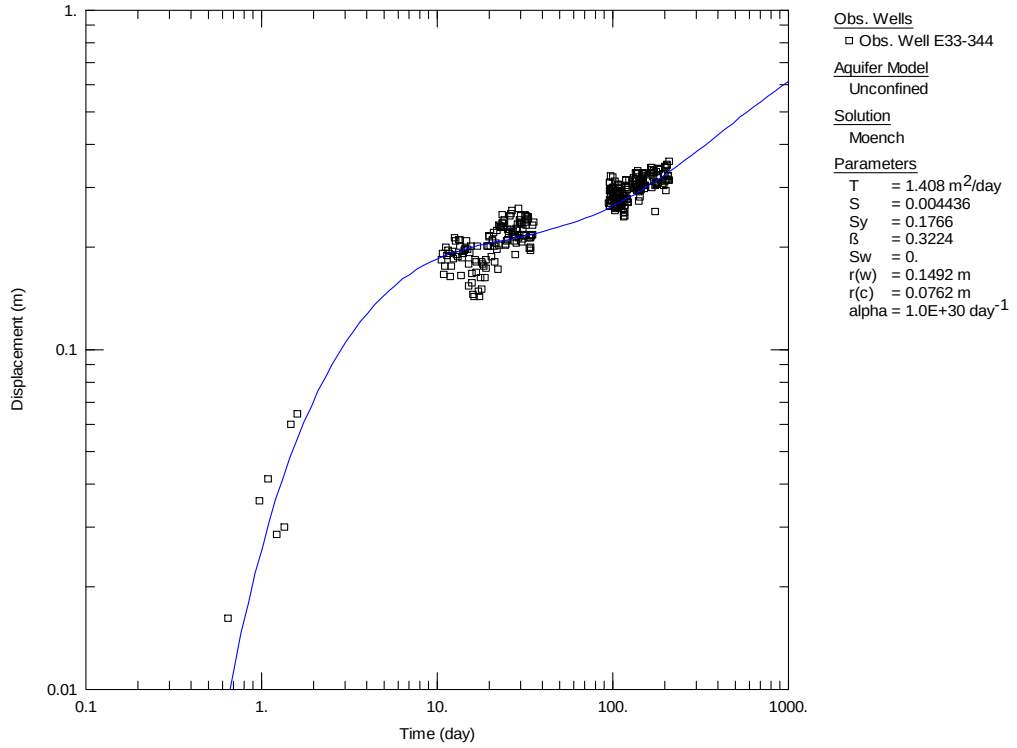

Figure B.22. Type-curve analysis of well 299-E33-344 corrected drawdown analysis: $K_D = 0.003$. This figure is FIO.

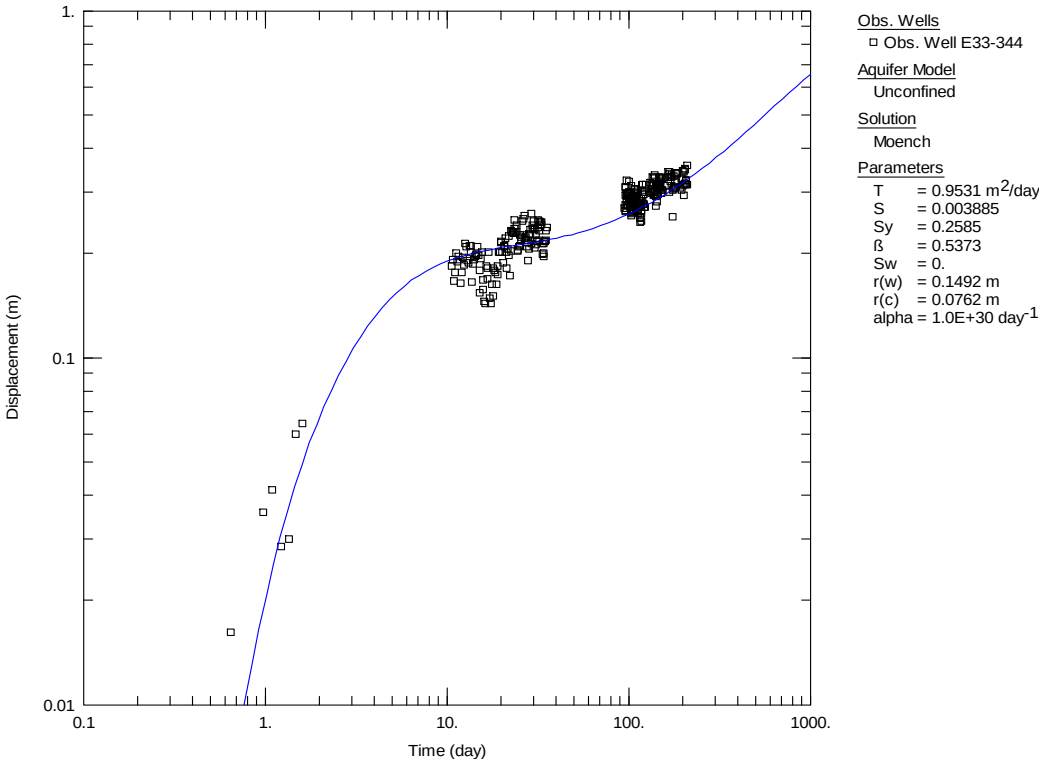

Figure B.23. Type-curve analysis of well 299-E33-344 corrected drawdown analysis: $K_D = 0.005$. This figure is FIO.

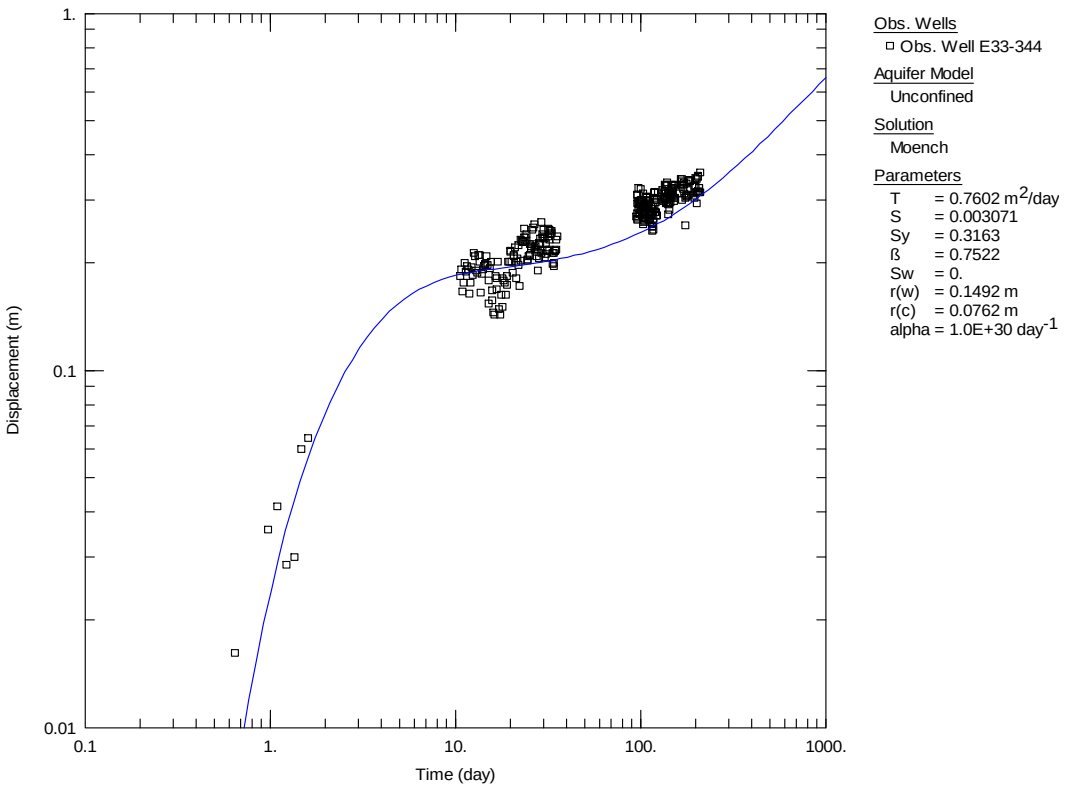

Figure B.24. Type-curve analysis of well 299-E33-344 corrected drawdown analysis: $K_D = 0.007$. This figure is FIO.

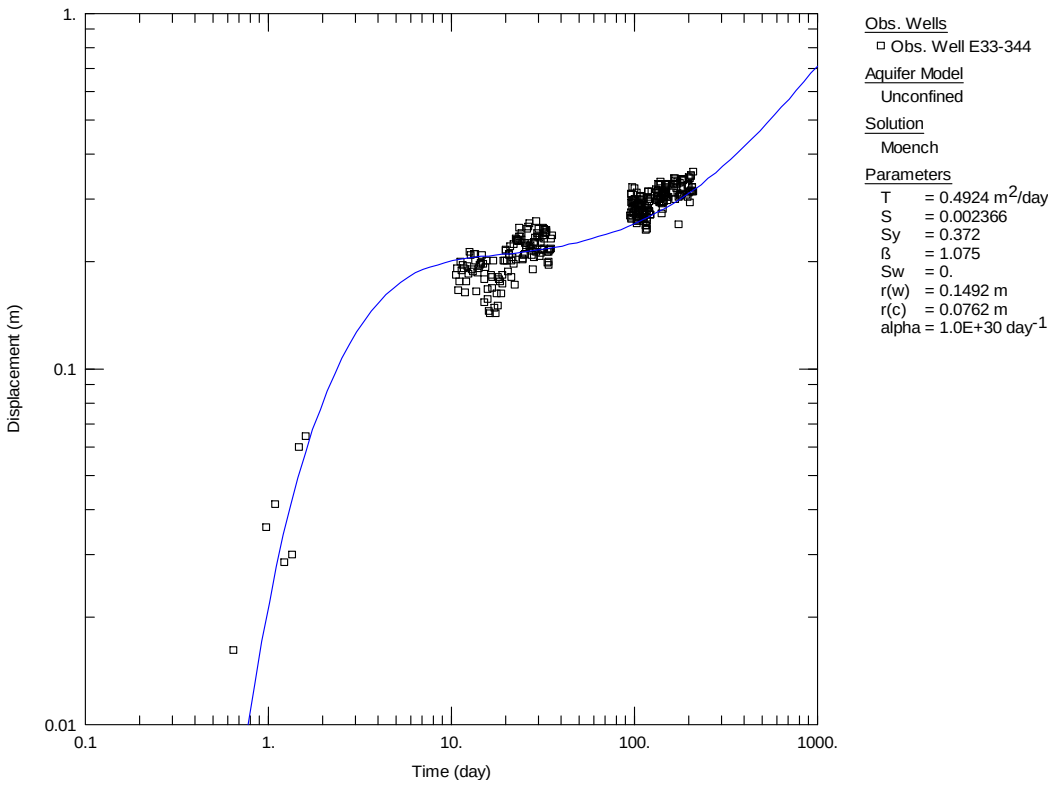

Figure B.25. Type-curve analysis of well 299-E33-344 corrected drawdown analysis: $K_D = 0.01$. This figure is FIO.

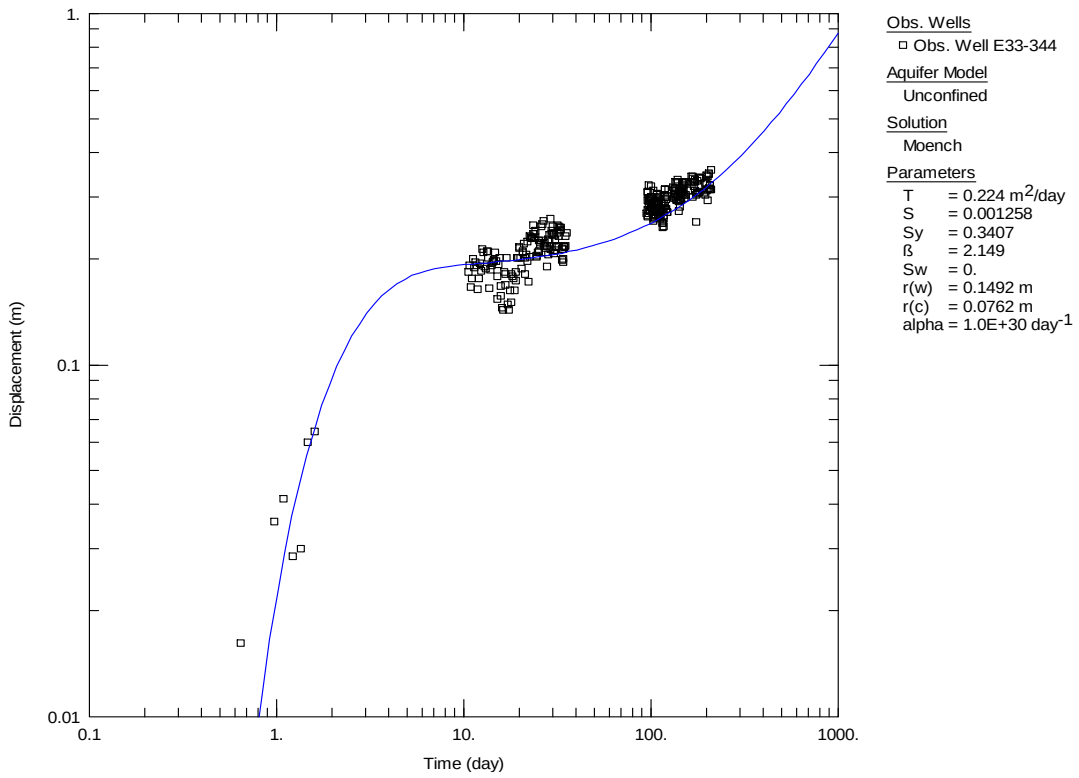

Figure B.26. Type-curve analysis of well 299-E33-344 corrected drawdown analysis: $K_D = 0.02$. This figure is FIO.

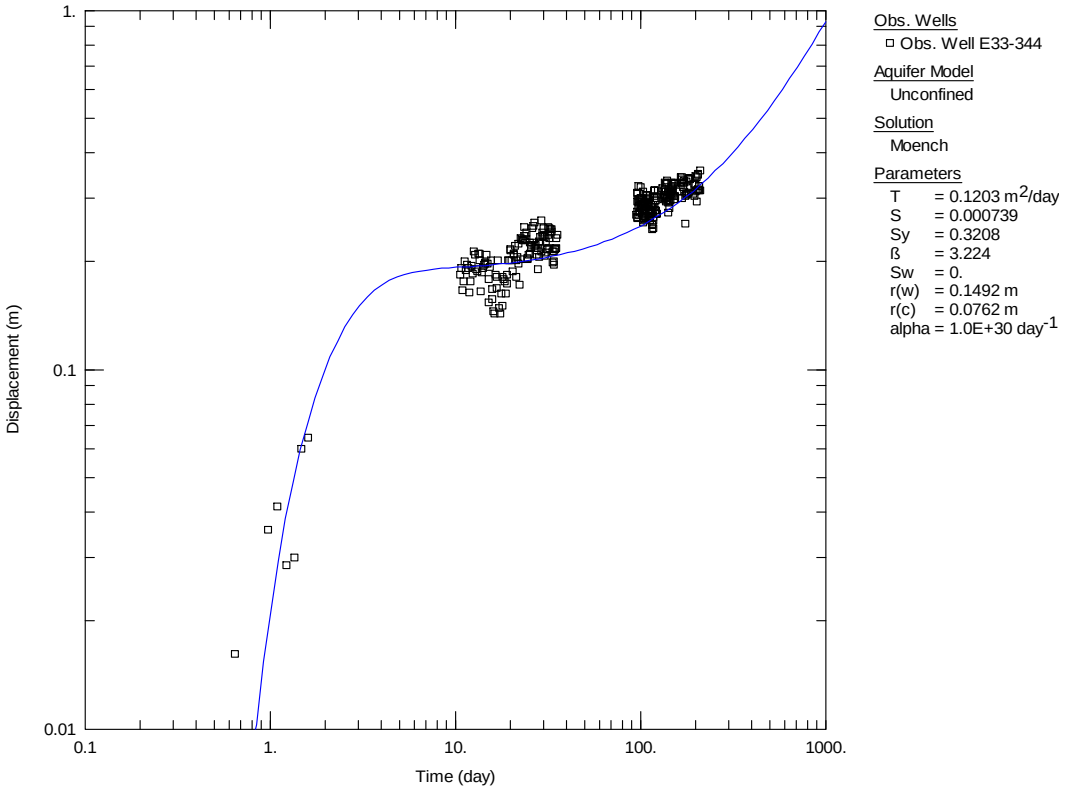

Figure B.27. Type-curve analysis of well 299-E33-344 corrected drawdown analysis: $K_D = 0.03$. This figure is FIO.

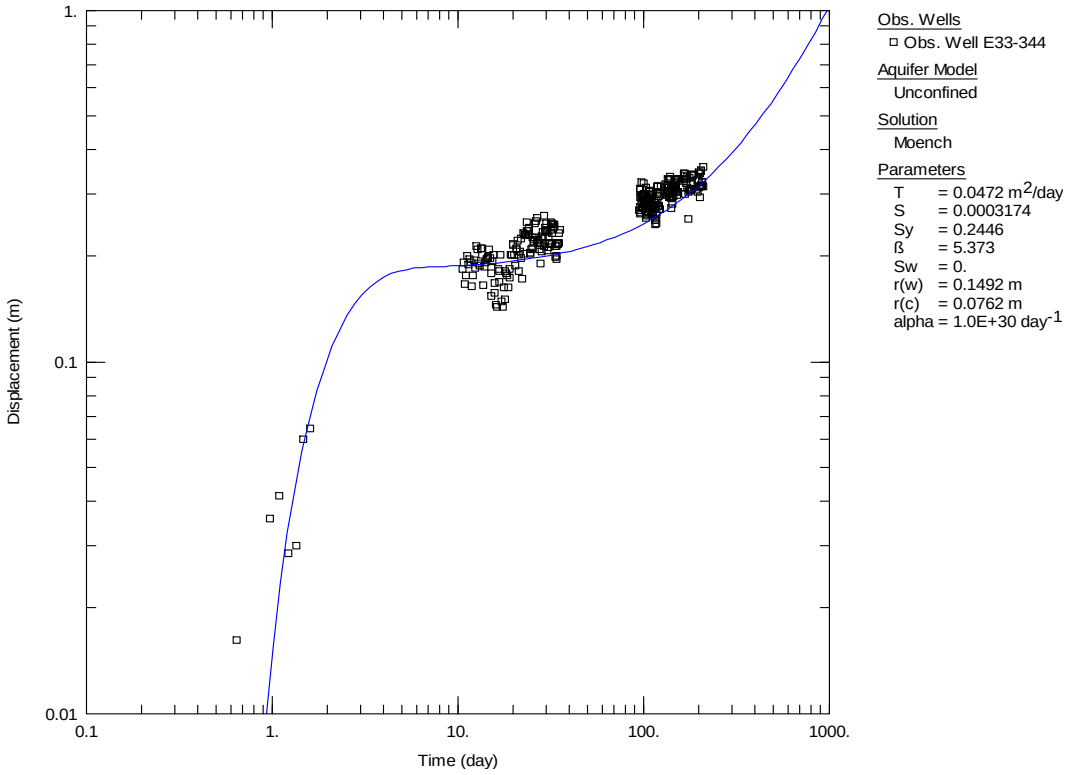

Figure B.28. Type-curve analysis of well 299-E33-344 corrected drawdown analysis: $K_D = 0.05$. This figure is FIO.

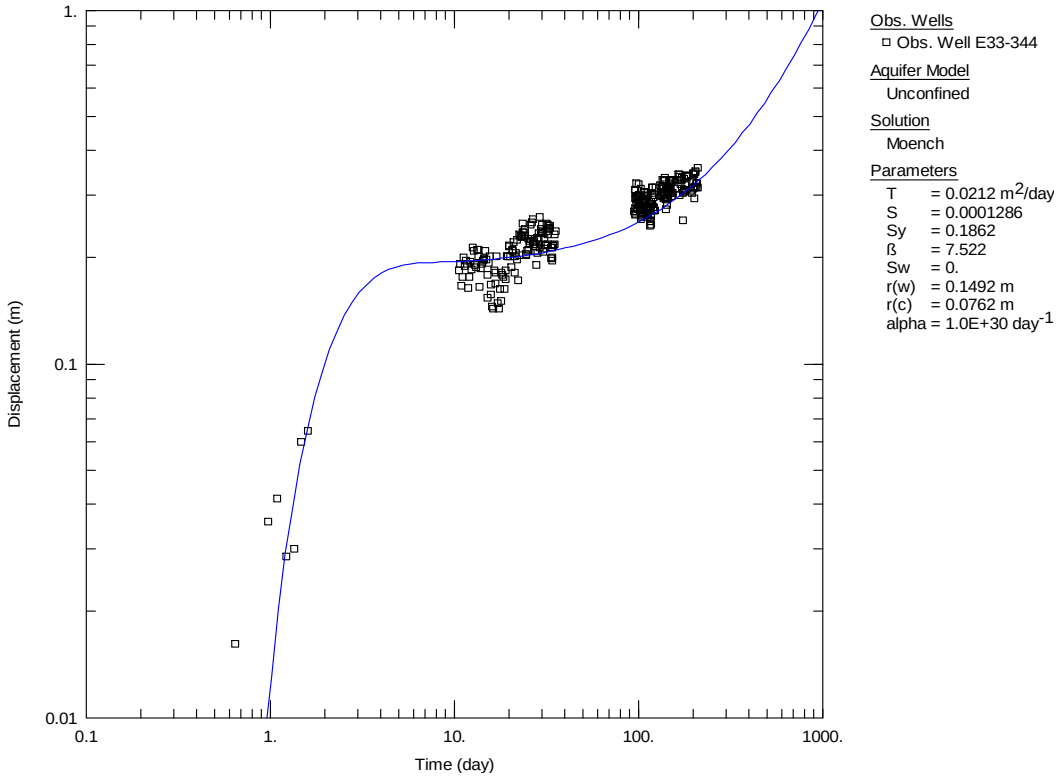

Figure B.29. Type-curve analysis of well 299-E33-344 corrected drawdown analysis: $K_D = 0.07$. This figure is FIO.

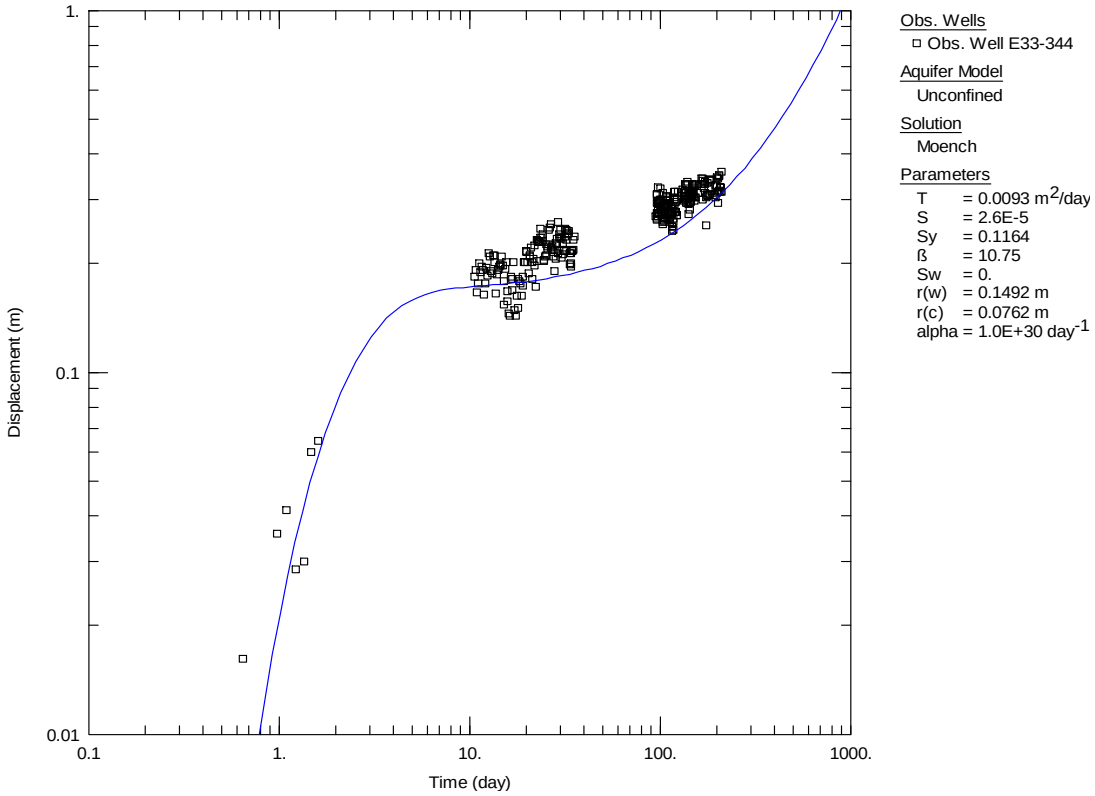

Figure B.30. Type-curve analysis of well 299-E33-344 corrected drawdown analysis: $K_D = 0.10$. This figure is FIO.

B.5 References

Bouwer H. 1989. "The Bouwer and Rice slug test – an update." *Ground Water* 27(3):304-309.

Bouwer H, and RC Rice. 1976. "A slug test for determining hydraulic conductivity of unconfined aquifers with completely or partially penetrating wells." *Water Resources Research* 12(3):423-428.

Butler JJ, Jr. 1998. *The Design, Performance, and Analysis of Slug Tests*. Lewis Publishers, CRC Press, Boca Raton, Florida.

DOE. 2016. Calendar Year 2016 Annual Summary Report for the 200-ZP-1 and 200-UP-1 Operable Unit Pump-and-Treat Operations. DOE/RL-2016-69, Rev. 0, prepared for U.S. Department of Energy by CH2M Hill, Richland, Washington.

Duffield, GM. 2007. *AQTESOLV for Windows Version 4.5 User's Guide*. HydroSOLVE, Inc., Reston, Virginia (http://www.aqtesolv.com).

Johnson AI. 1967. "Specific Yield – Compilation of Specific Yields for Various Materials." *Water-Supply Paper WSP 1662-D*. U.S. Geological Survey, Washington, D.C.

Liu WZ, and JJ Butler, Jr. 1995. *The KGS model for slug tests in partially penetrating wells (Version 3.0)*. Kansas Geological Survey Computer Series Report 95-1, Lawrence, Kansas.

Mackley RD, FA Spane, TC Pulsipher, and CH Allwardt. 2010. *Guide to using Multiple Regression in Excel (MRCX v.1.1) for Removal of River-Stage Effects from Well Water Levels*. PNNL-19482, Pacific Northwest National Laboratory, Richland, Washington.

Moench AF. 1997. "Flow to a well of finite diameter in a homogeneous, anisotropic water-table aquifer." *Water Resources Research* 33(6):1397–1407.

Neuman SP. 1972. "Theory of flow in unconfined aquifers considering delayed response of the water table." *Water Resources Research* 8(4):1031-1045.

Neuman SP. 1973. "Supplementary comments on 'Theory of flow in unconfined aquifers considering delayed response of the water table." *Water Resources Research* 9(4):1102-1103.

Neuman SP. 1974. "Effect of partial penetration on flow in unconfined aquifer considering delayed gravity response." *Water Resources Research* 10(2):303-312.

Neuman SP. 1975. "Analysis of pumping test data from anisotropic unconfined aquifers considering delayed gravity response." *Water Resources Research* 11(2):329-342.

Neuman SP. 1979. "Perspective on 'delayed yield'." *Water Resources Research* 15(4):899-908.

Newcomer DR. 2014. *Field-Derived Hydraulic Properties for Perched-Water Aquifer Wells 299-E33-350 and 299-E33-351, Hanford Site B-Complex Area*. PNNL-23380, Pacific Northwest National Laboratory, Richland, Washington.

Oostrom M, MJ Truex, KC Carroll, and GB Chronister, 2013. "Perched-water analysis related to deep vadose zone contaminant transport and impact to groundwater." *J. Hydrol.* 505:228-239.

Rasmussen TC and LA Crawford. 1997. "Identifying and Removing Barometric Pressure Effects in Confined and Unconfined Aquifers." *Ground Water* 35(3):502-511.

Reilly TE, OL Franke, and GD Bennett. 1987. "The Principle of Superposition and Its Application in Ground-Water Hydraulics." In *Techniques of Water-Resources Investigations*, Chapter B6, Applications of Hydraulics, U.S. Geological Survey, Denver, Colorado, pp. 28.

Spane FA, Jr. 1993. *Selected Hydraulic Test Analysis Techniques for Constant-Rate Discharge Tests*. PNL-8539, Pacific Northwest Laboratory, Richland, Washington.

Spane FA, Jr. 1999. *Effects of Barometric Fluctuations on Well Water-Level Measurements and Aquifer Test Data*. PNNL-13078, Pacific Northwest National Laboratory, Richland, Washington.

Spane FA 2002. "Considering Barometric Pressure in Groundwater-Flow Investigations." *Water Resources Research*, 38(6):10.1029

Spane FA and RD Mackley. 2011. "Removal of River-Stage Fluctuations from Well Response Using Multiple-Regression." *Ground Water* 49(6):794-807. doi:10.1111/j.1745-6584.2010.00780.x

Spane FA and DR Newcomer. 2009. *Field Test Report: Preliminary Aquifer Test Characterization Results for Well 299-W15-225: Supporting Phase 1 of the 200-ZP-1 Groundwater Operable Unit Remedial Design*. PNNL-18732, Pacific Northwest National Laboratory, Richland, Washington.

Spane FA, Jr., and SK Wurstner. 1993. "DERIV: A Program for Calculating Pressure Derivatives for use in Hydraulic Test Analysis." *Ground Water* 31(5):814-822.

Spane FA, Jr., PD Thorne, and DR Newcomer. 2001a. *Results of Detailed Hydrologic Characterization Tests – Fiscal Year 1999*. PNNL-13378, Pacific Northwest National Laboratory, Richland, Washington.

Spane FA, Jr., PD Thorne, and DR Newcomer. 2001b. *Results of Detailed Hydrologic Characterization Tests – Fiscal Year 2000*. PNNL-13514, Pacific Northwest National Laboratory, Richland, Washington.

Spane FA, Jr., PD Thorne, and DR Newcomer. 2002. *Results of Detailed Hydrologic Characterization Tests – Fiscal Year 2001*. PNNL-14113, Pacific Northwest National Laboratory, Richland, Washington.

Spane FA, Jr., PD Thorne, and DR Newcomer. 2003. *Results of Detailed Hydrologic Characterization Tests – Fiscal Year 2002*. PNNL-14186, Pacific Northwest National Laboratory, Richland, Washington.

Distribution

No. of Copies

1
CH2M Hill Plateau Remediation Company
Mark Byrnes

No. of Copies

Pacific Northwest National Laboratory

RE Clayton	(PDF)
I Demirkanli	(PDF)
DR Newcomer	(PDF)
MR Rockhold	(PDF)
DL Saunders	(PDF)
FA Spane	(PDF)
CJ Thompson	(PDF)
MJ Truex	(PDF)
MM Valenta-Snyder	(PDF)
TW Wietsma	(PDF)

Pacific Northwest
NATIONAL LABORATORY

www.pnnl.gov

902 Battelle Boulevard
P.O. Box 999
Richland, WA 99352
1-888-375-PNNL (7665)

U.S. DEPARTMENT OF
ENERGY